MODELING OF ARCHING UNREINFORCED MASONRY WALLS SUBJECTED TO BLAST LOADINGS

MODELING OF ARCHING UNREINFORCED MASONRY WALLS SUBJECTED TO BLAST LOADINGS

By

SEYEDEHSHADI SEYEDREZAI, B.E.

A Thesis

Submitted to the School of Graduate Studies

in Partial Fulfilment of the Requirements

for the Degree

Master of Applied Science

McMaster University

MASTER OF APPLIED SCIENCE (2011) McMaster University

(Civil Engineering) Hamilton, Ontario

TITLE: Modeling of Arching Unreinforced Masonry Walls Subjected to Blast Loadings

AUTHOR: Seyedehshadi Seyedrezai, B.E.

(McMaster University)

SUPERVISOR: Dr. Wael El-Dakhakhni

NUMBER OF PAGES: xiii, 131

Abstract

Masonry is one of the most commonly used materials in building construction throughout the world. Unreinforced masonry (URM) walls typically have very low flexural capacities and tend to posses brittle failure modes. Due to brittle nature of URM walls, it is critical to predict the behaviour of the wall when exposed to extreme out of plane loadings such as blast loads. An effective way to enhance the ability of unreinforced masonry walls to withstand blast loads and consequently to limit the amount of wall damage is imposing arching mechanism on the wall. Since carrying out physical experiments to study the response of URM walls subjected to blast load is both dangerous and expensive, finite element modeling has become more attractive to researchers. In this research, an unreinforced one-way arching wall is simulated using the finite element program LS-DYNA and its behaviour subjected blast loading is studied. The model is constructed based on the data recorded earlier during a physical blast experiment. Close agreement was observed between the numerical and experimental results which validated the developed model. A sensitivity study is then performed where the influence of variation of some input parameters such as mortar strength, coefficients of friction, scaled distance, boundary condition, wall height and the effect of two-way arching action on the wall's response is evaluated. The most influential parameters in this study found to be the scaled distance, wall height and two-way arching action. Smaller scaled distances result in high deflection and as the scaled distance increases the maximum deflection decreases. The wall height also significantly affect the wall's response to blast loads, i.e. the taller

the wall the larger the maximum displacement. It is also concluded that two-way arching action can significantly reduce the wall's maximum deflection.

Acknowledgements

I would like to thank my academic advisor, Dr. W. El-Dakhakhni for his guidance and support throughout this project. I specially appreciate his understanding during difficult times. His friendly advice and encouragement helped me get through the stressful situations.

I would also like to express my sincere gratitude to Dr. W. Mekky for his involvement, input and great assistance in building the finite element model. Without his help, learning the finite element software LS-DYNA would not have been possible. His extensive knowledge of the program, valuable comments and suggestions aided the completion of this research.

The financial support provided by my advisor and the Department of Civil Engineering at McMaster University is greatly acknowledged. I would like to acknowledge Livermore Software Technology Corporation for providing the LS-DYNA finite element software. Chris Galbraith of Metal Forming Analysis Corporation is also acknowledged for providing the license for using LS-DYNA.

I would like to thank Amr Nassr and Ahmed Mostafa for their help and encouragement during my graduate studies.

I would like to thank my parents and my brother for their endless love, support and encouragement throughout not only my academic career but in my entire life. Lastly, but most importantly, my deepest thank to the love of my life, Michael, for his love and support and for his constant confidence in me. To you I dedicate this thesis.

Table of Contents

List of Figures

List of Tables

List of Abbreviations and Symbols

b= wave front parameter

CMU= concrete masonry unit

COV= coefficient of friction

d= diameter

DC= exponential decay coefficient

D_e= peak displacements from experiment

D_f= peak displacements from finite element model

E_T= error between experimental and numerical peak displacement times

E_D= error between experimental and numerical peak displacements

E= total energy, error

FD= dynamic coefficient of friction

FE= finite element

FEM= finite element model

FS= static coefficient of friction

I_S^+= positive impulse

I_S^-= negative impulse

NFLS= normal failure stress

P_0= ambient pressure

P_S^+= peak over pressure

P_S^-= peak under pressure

R= standoff distance

RM= reinforced masonry

SDOF= single degree of freedom

SFLS= shear failure stress

t= time

t_a= arrival time

T_e= time of peal displacements from experiment

T_f= time peak displacements from finite element model

T^+= positive phase duration

T^-= negative phase duration

u_s= velocity of particles traveling behind the blast wave front

U_s= blast wave front velocity

URM= unreinforced masonry

V= volume

V_{rel} = relative velocity

W= charge mass

WGT= equivalent TNT mass

Z= scaled distance

λ= scale factor

σ_n= calculated normal stress

σ_s= calculated shear stress

1. Introduction

1.1. General

Many structures experience catastrophic damages due to aircraft crashes, petro-chemical explosions, nuclear leakage, etc. which result in large dynamic loads much greater than the structures' original design loads. In addition to the ever-present threat of these accidental extreme loading events, due to rapid development of conventional and non-conventional explosive materials, many government and military structures, as well as common and crowded public facilities, have been targeted by intentional blast events in the past few decades. Due to the threat from such extreme loading conditions, considerable attention has been brought to developing methods for the structures to be able to resist blast loads.

Masonry structures comprise a significant portion of the buildings worldwide most of which are constructed with unreinforced masonry blocks. Unreinforced masonry structures have low resistance to out of plane blast loading due to their low flexural capacity and as a result will experience brittle failure modes. Hence, masonry components in high risk facilities must be reinforced to withstand blast loads. Newly constructed buildings could be designed to resist blast loads. However, strengthening existing unreinforced masonry structures to enhance their blast-resistance capacity remains challenging. Enforcing arching action to unreinforced masonry walls is a cost effective technique which significantly improves their performance under blast loads. In order to test the arching mechanism, blast tests have been conducted over the past few

decades. However, performing these tests is not only costly and dangerous but also critical information is sometimes difficult to record even with the most sophisticated high speed cameras and gauges due to debris and dust resulting from the explosion. In addition, there are always some limitations involved regarding blast tests such as the charge weight or the standoff distance. Therefore, development of finite element models that could accurately capture the behaviour of the structure under blast has become imperative for predicting the failure mechanisms.

1.2. Objectives

The objectives of this research can be broken down into three major components:

- Development of a finite element model for studying the behaviour of one-way unreinforced masonry arching walls subjected to blast loads.
- Use the results from the blast test based on which the finite element model is constructed to verify the accuracy of the model's predictions.
- Perform an input sensitivity study to investigate the effects of variations of different parameters on the wall's blast response.

1.3. Scope and Methodology

The scope of this research includes the development of finite element model for a one-way unreinforced masonry arching wall that could accurately predict the wall's response subjected to blast loads. The model is based on the data from a field blast test (Abou-Zeid et al., 2010) and is constructed using an advanced general purpose finite element modeling program developed by Livermore Software Technology Corporation (LSTC)

called LS-DYNA (LSTC, 2006). The input file is created using finite element software ETA/VPG version 3.4 (ETA, 2011) as the pre-processor released by Engineering Technology Associates, Inc. (ETA) that comes with LS-DYNA software package. The input file created by ETA/VPG is analyzed using LS-DYNA solver and the produced results are then imported to LS-DYNA's advanced pre and post-processor LS-PrePost to generate fringe plots and response diagrams (LSTC, 2011). The finite element model is validated using the field test data. The comparisons between the numerical and experimental results are based on the mid-height displacements. Following the validation process a parametric study is conducted to investigate the influence of variations of some input parameters on the wall's displacement response. The parameters investigated within the scope of this study include mortar strength, coefficients of friction, scaled distance, boundary conditions, wall height as well as the effect of two-way arching. The sensitivity analysis is carried out by means of investigating the changes observed in the mid-height displacement response plots.

1.4. Thesis Organization

This thesis consists of 6 chapters. Chapter 1 identifies the objectives, scope, methodology and the organization of the dissertation. Chapter 2 is aimed to provide a literature review about the main topics on which this research is based: masonry (unreinforced masonry in particular), blast loading and finite element modeling. Chapter 3 is dedicated to the development of a finite element model based on an actual blast test. This chapter discusses all the components involved in the modeling process such as the units, geometry and dimensions, parts, material model selection, elements, hourglass, contact

surfaces, boundary conditions and loadings. In Chapter 4, the finite element model developed in Chapter 3 is validated by means of comparing its results to the results obtained experimentally. The comparison is based on the behaviour of the wall in terms of mid-height displacements. Once the validity of the finite element model is verified, a parametric study is performed in Chapter 5 where the model built in Chapter 3 is taken as the baseline model and the effects of variation of some input parameters on the behaviour of the wall is evaluated. Conclusions and recommendations are provided in Chapter 6.

2. Background and Literature Review

The current chapter aims to provide brief descriptions on different aspects of this study: Section 2.1 provides a brief background about masonry structures, general properties and their performance under loads. In Section 2.2 blast loads, properties of blast waves and structural response to blast waves are reviewed. Section 2.3 focuses on the behaviour of unreinforced masonry structures subjected to blast loading. Section 2.4 summarizes the common finite element approaches that have been developed in the past few decades to model unreinforced masonry structures under blast and the selected method in the current study.

2.1. Masonry Construction

One of the most commonly used construction materials is masonry. There is a wide range of variety for the application of masonry. It could be used for construction of load bearing walls, partition walls, or as infill in the exterior frames of building structures and many other applications. The most important characteristics of masonry include its simplicity, aesthetics, versatility, durability, low maintenance, sound absorption and fire protection.

2.1.1. General Properties

Masonry is a heterogeneous material composed of units and mortar joints that are typically arranged in a very regular manner. Bricks and concrete blocks are the most commonly used masonry units. Distinct directional properties of masonry are due to the arrangement of units and most importantly the mortar joints which act as planes of

weakness. This is the reason for typical crack initiation in mortar joints as opposed to the units.

2.1.2. Types of Masonry Construction

A masonry structure could be either unreinforced or reinforced. Masonry in general is strong in compression but weak in tension. Unreinforced masonry (URM) is commonly used in low-rise and medium rise buildings in areas with low seismic activities. Due to the absence of any kind of reinforcements in URM structures, the load resistance of the structures is solely dependent on the masonry strength. As mentioned earlier, in contrast to its impressive compressive strength, masonry's tensile strength is quite low. This means that in seismically active areas or in any other situation where the lateral loads could potentially increase and lead to the increase of tensile stresses, unreinforced masonry would not be adequate to use any longer. Therefore reinforced masonry (RM) must be used in which the reinforcement is incorporated in masonry in order to improve its tensile stress resistance. Reinforced masonry structures have higher ductility compared to unreinforced masonry structures. The use of reinforcement allows for designing much thinner walls. There are two types of reinforcements, vertical and horizontal.

When a masonry wall is under lateral load, masonry experiences tensile stresses. With the increase of lateral loads, flexural cracks develop near the base of the wall. In such situations, vertical reinforcement is used to help resisting the bending moment at the base of the wall. In the absence of vertical reinforcement, the tensile stress is resisted mainly by the resultant compressive force in masonry. However, when there are vertical

reinforcements, the tensile stress is resisted both by the resultant compressive force in the masonry and the tensile forces in reinforcements which explains why RM has higher ductility than URM. Reinforced and unreinforced masonry could be ungrouted, partially grouted, or fully grouted. Fully grouted reinforced masonry generally performs better in providing adequate strength and ductility.

Masonry walls may also need to be equipped with horizontal reinforcements. In case of high shear forces near the base of the wall, diagonal tension is produced in the masonry resulting in diagonal cracks. In such situations horizontal reinforcements must be used in order to prevent the diagonal tension in the masonry wall from exceeding the allowable value (Drysdale and Hamid, 2005).

2.1.3. Arching Action in Unreinforced Masonry

Unreinforced masonry has low tensile capacity. When reinforcements are incorporated in the masonry, the tensile failure would be characterized by yielding the vertical reinforcement which will result in a ductile and therefore a preferred mode of failure. In the contrast, when structures incorporating unreinforced masonry walls are subjected to extreme lateral loadings such as blast, catastrophic failures can be caused. In such situations a brittle non-ductile failure would occur where the masonry units break apart and enter the building with high velocities and potentially injure occupants. In order to prevent such catastrophic damages, improving the performance of unreinforced masonry structures during seismic or blast events are important to public safety (Drysdale and Hamid, 2005; Moradi et al., 2008). Arching action is an effective way of enhancing the out of plane capacity of unreinforced masonry walls. McDowell et al. (1956) carried out

the earliest in-depth investigation of the arching action of unreinforced masonry wall. McDowell et al. (1956) noted that under a certain condition where the walls were butted against supports that were essentially rigid, the masonry walls exhibited much larger load carrying capacity than those obtained by conventional bending analysis from simply supported walls. This theory assumes that after the development of cracks at the ends and the centre of the wall, the wall will be divided into two sections. These two sections will behave as rigid segments each rotating at its end (at the support) until either the masonry crushes at the support or the wall completely snaps in the middle. Figure 2-1 shows the typical arching mechanism.

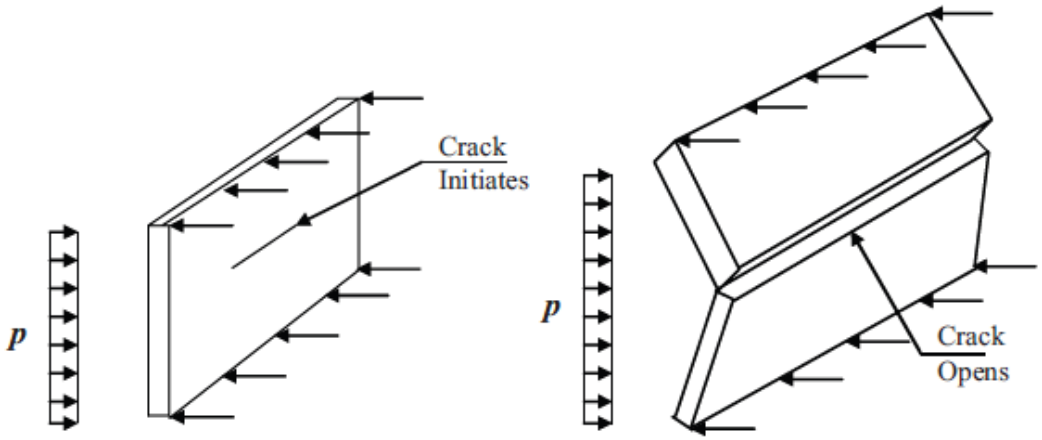

Figure 2-1. Arching mechanism (Moradi et al., 2008)

The advantage of arching behaviour in addition to resulting in smaller deflection is that if the wall collapses, it does not break into multiple high speed pieces and most likely only the two rigid sections will fall down. Also, since the fragment size is larger, the ejection

distance is much smaller as opposed to the cases where the wall shatters into many small fragments and hence there will be less potential damage to the occupants.

Following McDowell et al. (1956) proposed arching theory, many researchers have conducted different tests and validated the arching theory experimentally, analytically or numerically (Dawe and Seah, 1989; Gabrielsen et al., 1975; Henderson et al., 2003; Wilton and Gabrielsen, 1973).

2.2. Blast Loading

In the recent years blast resistant structures have drawn the attention of many designers. Blast resistance has become a highly valuable characteristic for some structures especially governmental buildings. The following sections aim to provide an overview of the history of explosives and describe the nature of explosions, formation of blast waves and blast wave parameters.

2.2.1. Explosions

There are many dictionary definitions for explosions such as:

- bursting noisily,
- a sudden loud violent release of energy,
- undergoing a rapid chemical or nuclear reaction with the production of noise, heat, and violent expansion of gases,
- bursting violently as a result of pressure within.

However, a more scientific definition of explosion can be quoted from Strehlow and Baker (Strehlow and Baker, 1976): “In general, an explosion is said to have occurred in

the atmosphere if energy is released over a sufficiently small time and in a sufficiently small volume so as to generate a pressure wave of finite amplitude traveling away from the source. This energy may have originally been stored in the system in a variety of forms; these include nuclear, chemical, electrical or pressure energy, for example. However, the release is not considered to be explosive unless it is rapid enough and concentrated enough to produce a pressure wave that one can hear. Even though many explosions damage their surroundings, it is not necessary that external damage be produced by the explosion. All that is necessary is that the explosion is capable of being heard."

It should be mentioned that the definition above refers to explosions in air. There are three types of explosions: physical, nuclear or chemical explosions. The most commonly used explosives are condensed. They could be solids or liquids. When an explosion occurs, the explosive violently decomposes which produces heat and gas. If the explosive is in contact with solid material the expansion of gas will generate shock pressures. However, if this expansion happens in a non-solid medium such as air, what it will generate is called blast waves (Mays and Smith, 1995)

2.2.2. Source Properties of Explosions

When a condensed high explosive detonates, hot gases in very high pressure and temperature are generated. As the results of violent expansion of these hot gases, the surrounding air is forced out of the volume it occupies. As a consequence a layer of compressed air (blast wave) is formed in front of the gas volume which contains the most energy released by the explosion (Hetherington and Smith, 1994). The properties of the

blast waves such as strength and duration, are strongly affected by the characteristics of the explosion source such as total energy (E), energy density (E/V, where V is the volume), and the rate of energy release, i.e., power. There are four explosions sources with high energy density and power that are usually referred to as *ideal* explosive sources. These four ideal explosion sources are point source, nuclear weapon, laser spark, and condensed phase explosives also known as high explosives. It has been found that the blast waves resulted from these ideal explosives are dependent only on a single parameter of the source and that is the total source energy. As was mentioned in the previous section most of the experimental work about blast loading is revolved about the use of high explosives. For this reason and also because the blast waves associated with high condensed phase explosives are ideal blast waves, high explosives are the main focus of researchers in studying blast loads. Most of the high explosives used for military or even commercial purposes are solid in the room temperature. The most commonly used type of solid high explosives is TNT which is used as the reference explosive in case of using sources of explosions other than TNT (Baker et al., 1983). This means that the mass of the charge used is converted into a TNT equivalent mass. In order to achieve this, the mass of the explosive is multiplied by a TNT conversion factor. TNT conversion factors are available for many of the explosives and are found by taking the ratio of the specific energies (Mays and Smith, 1995).

2.2.3. Blast Waves Properties

In order to be able to explain blast waves, some parameters need to be defined. Figure 2-2 shows the expected form of an ideal blast wave from a high explosive.

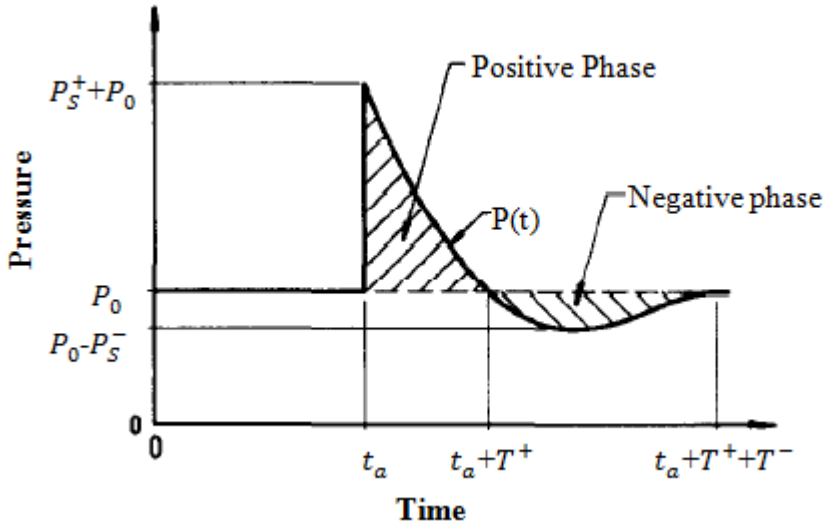

Figure 2-2. Ideal blast wave pressure-time profile (Baker, 1973)

The parameters in the pressure-time history in figure above are as follows:

- t_a: arrival time
- T^+: duration of the positive phase
- T^-: duration of the negative phase
- P_0 : ambient pressure
- P_S^+: peak side-on pressure (peak overpressure)
- P_S^-: peak under pressure

The blast wave produced by an explosion consists of a shock front in which the pressure rises abruptly from the ambient pressure to the peak value, followed by an expansion wave in which the pressure decays exponentially to the ambient pressure within a short time. Then as the air cools down, the pressure drops below the ambient pressure which causes suction. Eventually the pressure returns to the ambient pressure (Zalosh, 2003).

The portion of the time history where the pressure is higher than the ambient pressure (over pressure) is called positive phase and the portion where the pressure is below the ambient pressure is called negative or suction phase. Load intensity in this time-varying pressure loads is influenced by magnitude, shape and location of the detonation charge, explosive material, stand-off distance, and geometry and orientation of the target (Netherton and Stewart, 2009).

Another significant blast wave parameter is the specific impulse which is the area beneath the pressure-time curve. The following equations define the impulse for positive and negative impulses:

$$I_S^+ = \int_{t_a}^{t_a+T^+} [p(t) - P_0]dt \qquad \text{Eq. 1}$$

$$I_S^- = \int_{t_a+T^+}^{t_a+T^++T^-} [P_0 - p(t)]dt \qquad \text{Eq. 2}$$

The negative phase has a longer duration and its pressure has also lower intensity than the positive phase. Therefore, most of the times, the negative phase is ignored and only the parameters associated with the positive phase are considered. Thus, if in some cases there is not a positive or negative sign assigned to a parameter, it is referred to the positive value (Strehlow and Baker, 1976).

The blast wave generated by an explosion travels rapidly from the point of burst with a diminishing velocity $U_s$which is called the blast wave front velocity. The gas particles behind the blast wave front travel at lower velocities u_s, known as particle velocity.

These particle velocities are associated with dynamic pressure whose maximum value is denoted q_s (Mays and Smith, 1995).

One of the most important parameters that should also be included in the dictionary of the blast wave parameters is scaled distance. It is common to use scaled distance rather than the standoff distance when dealing with blast waves. Scaled distance, Z, is defined as (Baker, 1973):

$$Z = \frac{R}{W^{1/3}} \qquad \text{Eq. 3}$$

Where R is the standoff distance which is distance from the centre of the charge in meters and W is the charge mass expressed in kilograms of TNT.

There are so many figures in different references such as Figure 2-3 that are used to evaluate blast wave parameters as a function of scaled distance parameter.

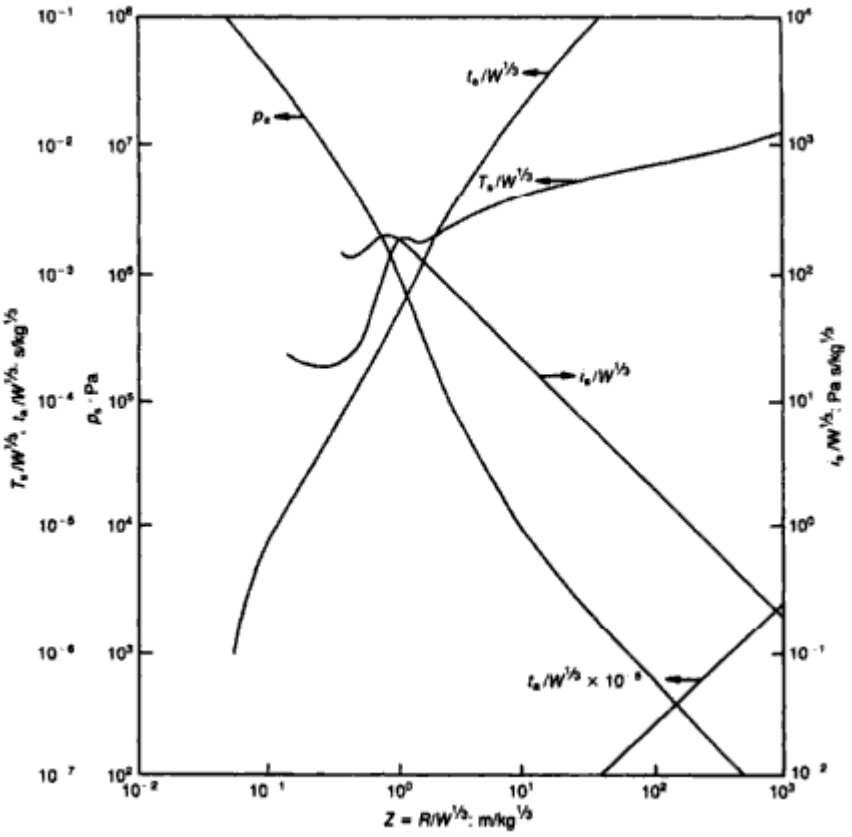

Figure 2-3. Side-on blast wave parameters for spherical charges of TNT (Mays and Smith, 1995)

2.2.4. Idealization of Pressure – Time Profile

Figure 2-2 in the previous section illustrated the typical form of the pressure-time history of a blast wave in which the pressure-time curve is often described by an exponential function. It was also mentioned that in most blast studies the negative phase is ignored. One of the most commonly used equations describing the exponential decay of the positive phase of the blast wave is Friedlander equation (Baker, 1973):

$$P(t) = P_0 + P_S^+ \left(1 - \frac{t}{T^+}\right) \exp\left(\frac{-bt}{T^+}\right) \qquad \text{Eq. 4}$$

In this equation t is measured after arrival time and b is the wave front parameter. For many purposes, even simpler approximations would produce satisfactory results. The simplest function assumes a linear decay of pressure creating a triangular blast wave shape, given by (Baker, 1973):

$$P(t) = P_0 + P_S^+ \left(1 - \frac{t}{T^+}\right), \quad 0 < t \leq T^+ \qquad \text{Eq. 5}$$

In this equation, t is again time after arrival shock. In the fitting of this form to data, the true value of the peak overpressure, P_S^+, is preserved while the positive phase duration, T^+, is adjusted so that the true value of impulse, I_S^+, is maintained.

2.2.5. Blast Wave Scaling Law

The most commonly used form of blast scaling law is Hopkinson scaling, also known as cube root scaling. This law states that two explosive charges of similar geometry and of same explosive in the same atmosphere but with different sizes will produce similar blast waves with identical peak overpressure at identical scaled distances (Baker et al., 1983). Hopkinson scaling law is presented graphically in Figure 2-4.

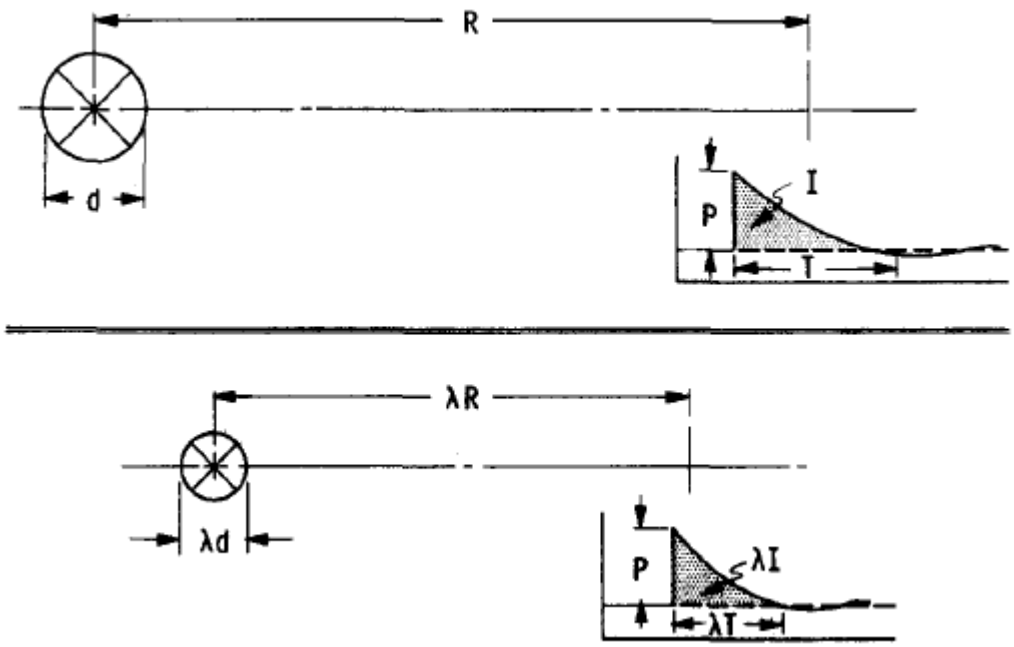

Figure 2-4. Hopkinson Blast Wave Scaling (Strehlow and Baker, 1976)

The formulation of Hopkinson scaling law for two charges in the same atmosphere with masses $W_1$and W_2 of same explosive with diameters d_1 and d_2 is (Mays and Smith, 1995):

$$\frac{d_1}{d_2} = \left(\frac{W_1}{W_2}\right)^{1/3} \quad \text{Eq. 6}$$

If the ratio of the two charge diameters is λ then at the scaled distance where the identical peak overpressure is generated, it can be proved that the ratio of the standoff distances would also be λ.

$$\frac{d_1}{d_2} = \lambda$$

Therefore from Equation 6:

$$\left(\frac{W_1}{W_2}\right)^{1/3} = \lambda$$

Using the definition of scaled distance:

$$\left(\frac{W_1}{W_2}\right)^{1/3} = \frac{R_1/Z_1}{R_2/Z_2}$$

Based on the Hopkinson law, the similar blast wave with identical peak overpressure is developed at the identical scaled distance, which means $Z_1 = Z_2$. Therefore:

$$\frac{R_1}{R_2} = \left(\frac{W_1}{W_2}\right)^{1/3} = \lambda \qquad \text{Eq. 7}$$

Similar relationships exist also for positive phase duration (T) and impulse (I) (Strehlow and Baker, 1976):

$$\frac{I_1}{I_2} = \frac{T_1}{T_2} = \frac{R_1}{R_2} = \left(\frac{W_1}{W_2}\right)^{1/3} = \lambda \qquad \text{Eq. 8}$$

2.2.6. Wave Reflection and Reflected Overpressure

When a blast wave hits an obstacle made of a denser medium than air such as ground surface or a structure, it will reflect from it. The induced reflected wave has a much greater pressure than the side-on over pressure.

The parameters described in previous section were all associated with the air burst explosion. Quoting from (UFC, 2008)"air burst explosion is an explosion which is located at a distance from and above the protective structure so that the ground reflections of the initial wave occur prior to the arrival of the blast wave at the protective structure. As used in this manual, an air burst is limited to an explosion which occurs at two to three times the height of a one or two-story building". From this description it is obvious that in order to have a realistic analysis, the effect of reflection must be taken into account for estimating the blast loads since in most studies the detonation is located close to or on the ground which is more similar to surface burst explosion's conditions in which the overpressure is amplified due to ground reflections. There are many figures like Figure 2-5 that can be used to evaluate side-on parameters such as side-on overpressure, P_S, or side-on impulse, I_S, as well as their corresponding reflected pressure, P_r, and reflected impulse, I_r as a function of scaled distance.

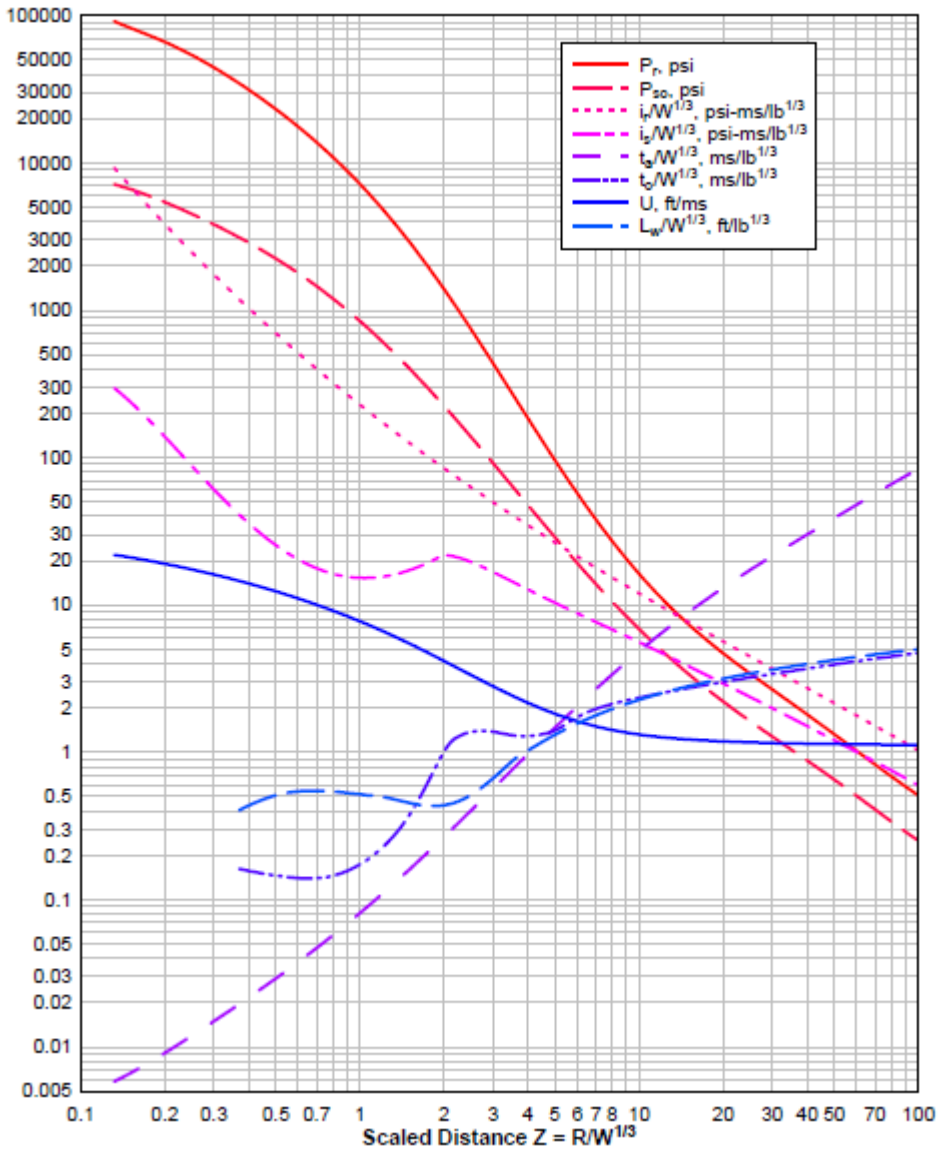

Figure 2-5. Side-on and reflected blast wave parameters for spherical charges of TNT (UFC, 2008)

2.2.7. Structural response to Blast Loading

In order to assess the behaviour of a structure subjected to blast load, calculations of final states such as maximum stresses, maximum strains, and maximum deflections become a lot more valuable to a designer than detailed time histories of the structure. The first step

in establishing the principles of such analysis is to identify the general response of the structure subjected to the blast loads. It has been found the structural response to blast loading is highly dependent on the ratio of the positive phase duration to the natural period of vibration of the structure. Depending on the magnitude of this ratio, there will be three possible loading regimes:

- Case 1: The duration of the load is much smaller than the natural period of the structure in which case the load acts on the structure very quickly even before the structure has time to respond significantly. This means that most deformations occur at times greater than the positive duration of the blast load. This is called impulsive loading which is represented below in Figure 2-6:

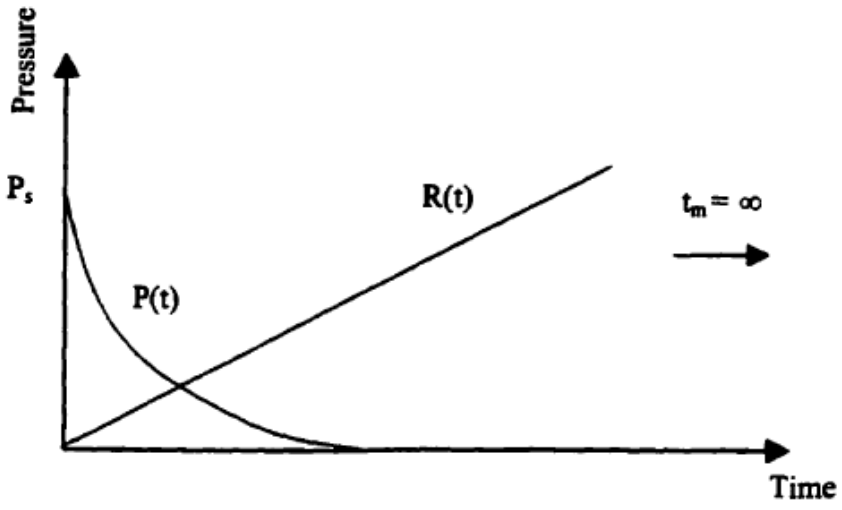

Figure 2-6. Impulsive loading (Tolba, 2001)

Where $R(t)$ represents the structure's resistance and $t_m$is the time to reach maximum dynamic displacement. In this loading regime the load drops to zero before the structure experiences any significant displacement. The response of the structure subjected to

impulsive loading is sensitive only to the associated impulse and insensitive to the peak pressure (Razaqpur et al., 2009; Shi et al., 2008).

- Case 2: The duration of the load is much longer than the natural period of the structure. This situation is referred to quasi-static or pressure loading. The structure in this loading regime experiences it maximum displacement before the load is decayed significantly (Hetherington and Smith, 1994). The structure's response under quasi-static loading is solely sensitive to the peak pressure and in contrast with impulsive regime it becomes insensitive to the impulse (Razaqpur et al., 2009; Shi et al., 2008). Figure 2-7 represents the quasi-static loading graphically.

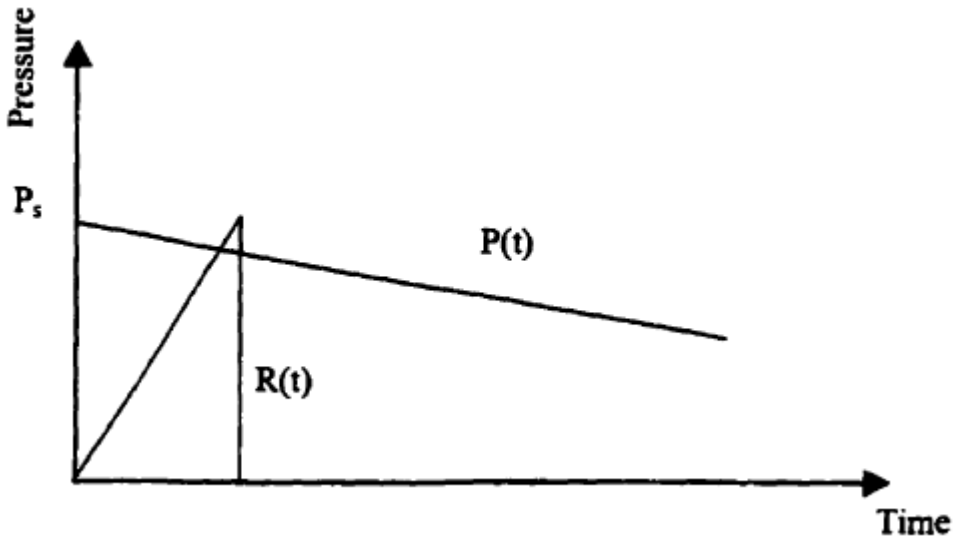

Figure 2-7. Quasi-static loading (Tolba, 2001)

- Case 3: In this case the duration of the load is approximately the same as the natural period of the structure. This case of loading is referred to as dynamic or

pressure-time loading. The assessment of the response of a structure subjected to dynamic loading is more complicated than the previous two cases and requires complete solution of the structure's equation of motion (Razaqpur et al., 2009; Shi et al., 2008). Figure 2-8 represents the dynamic loading graphically.

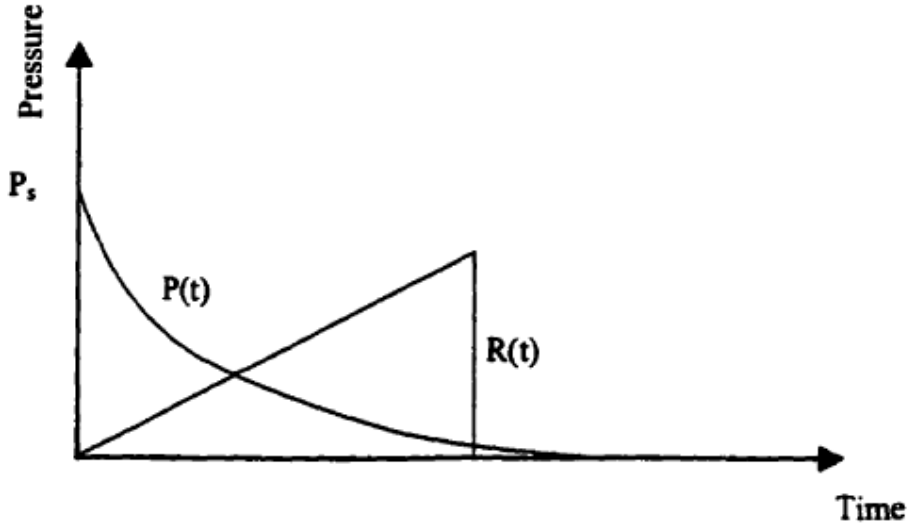

Figure 2-8. Dynamic loading (Tolba, 2001)

2.2.8. P –I Diagrams

Any blast wave form an explosion can cause damage to structures. There is a relatively simple way available in order to effectively correlate the blast wave properties with the damage they produce. This method is based on the concept that the damage is a function of peak over pressure (or force) and the applied impulse. Plotting the pressure and impulse combinations that wall cause a specific level of damage forms the pressure-impulse diagram (Strehlow and Baker, 1976). A pressure-Impulse (P-I) diagram for a particular structural component subjected to a particular blast loading time history is defined as an iso-damage curve. This means that, the same damage is produced for each

combination of pressure and impulse for the structural component of interest (Shi et al., 2008). Figure 2-9 shows a typical pressure-impulse diagram.

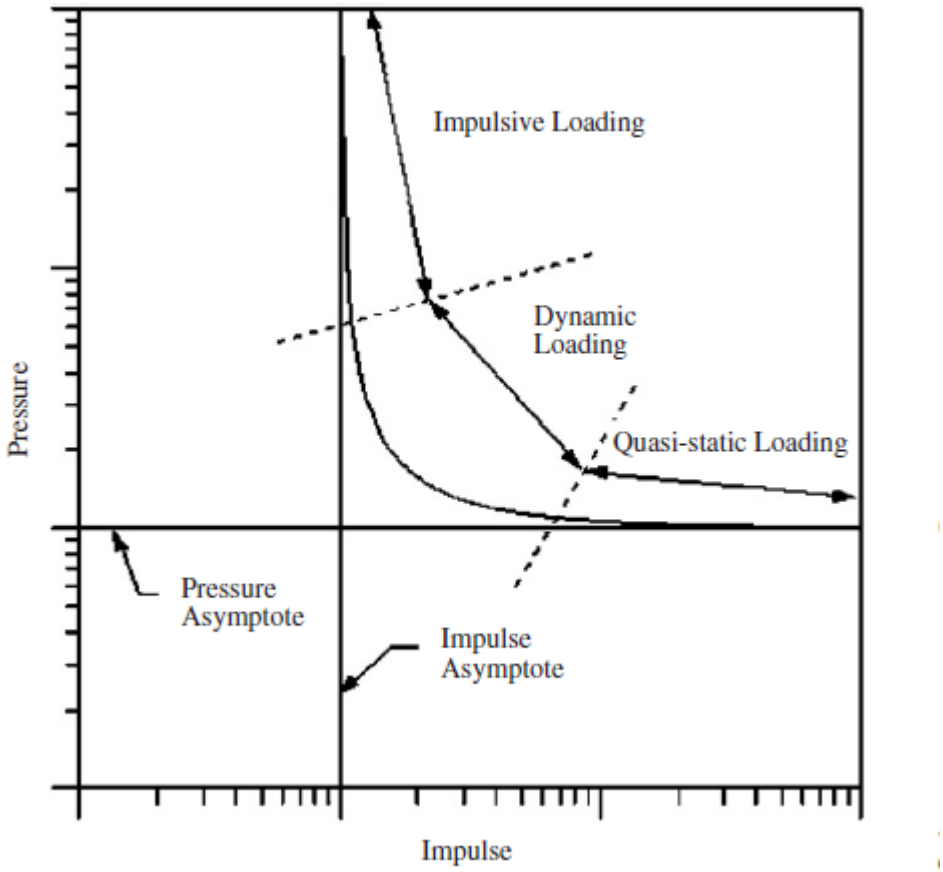

Figure 2-9. Typical pressure-impulse diagram (Shi et al., 2008)

As can be observed from the figure above, there are two asymptotes. The pressure asymptote which defines the limiting value for pressure by representing the minimum level of peak pressure required to reach the particular damage. And the impulse asymptote which defines the limiting value for impulse by representing the minimum impulse required to reach the specific damage. As was explained in the previous section,

the structure's response to quasi-static loading is insensitive to impulse but very sensitive to pressure. Therefore, as the load duration increases towards infinity, the response will be solely dependent on the pressure and therefore the creating a horizontal pressure asymptote. In the other hand, the response of the structure to impulsive loading is more sensitive to the impulse as opposed to the peak pressure. Thus, for loads with very short duration, the response will be solely dependent on the impulse which creates a vertical impulse asymptote. The assessment of the structure's response using P-I diagrams is quite easy. The curve indicates the combinations of pressures and impulses that cause failure based on the define damage level. Combinations of pressures and impulses that fall to the left or below of the curve will not cause failure (the damage is lower than the define damage level). Whereas, combinations of pressure and impulses fall above or to the right of the curve will induce failure (the damage level is exceeded) (Shi et al., 2008).

2.3. Behaviour of Unreinforced Masonry Structures under Blast

Masonry construction is one of the oldest building techniques that is still widely used in today's building industries. The exterior frame of most buildings is generally in-filled with masonry units. As explained in Sections 2.1.2 and 2.1.3, unreinforced masonry walls have low flexural capacity and exhibit brittle and non-ductile failure modes when subjected to extreme out of plane loadings such as blast load. Thus, evaluating the performance of the masonry structures subjected to blast loading and accurately predicting the damage is very important and of high interest.

The most common and direct approach to study masonry wall damage under blast is to conduct field blast tests. Many researchers have conducted blast tests on masonry structures to collect information on the behaviour of the structures.

A series of blast trials was done on twenty seven 3m×3m brick panel walls with different thickness by Varma et al. (1997). The reported blast test data included reflected pressure, reflected impulse, damage level and maximum deflection of the tested walls under blast loading of various magnitudes (Varma et al., 1997).

Forsen (1985) studied one-way response of masonry walls in various Swedish constructions. Forsen's test results compared favourably with pressure-impulse results obtained single degree of freedom analyses.

The U.S. Army Engineer Research and Development Centre (ERDC) conducted a series of blast experiments in order to study the response of one-way quarter-scale unreinforced masonry walls subjected to blast loads of various magnitudes were (Dennis et al., 2002).

Baylot et al. (2005) conducted blast tests to predict hazard levels associated with CMU walls. Nine ungrouted unreinforced quarter scaled masonry walls were tested three of which were retrofitted. The wall's hazard level was determined based on debris horizontal velocity. The results indicated that the retrofit techniques successfully reduced hazard levels (Baylot et al., 2005).

Wesevich and Oswald (2005) developed pressure-impulse diagrams for unretrofitted (unreinforced without arching, reinforced with arching and reinforced) and E-Glass retrofitted CMU walls subjected to blast loads based on the data from 236 open-air and shock tube tests. The blast tests were performed on conventional masonry walls with

different length, thickness, boundary condition and reinforcements. The damage assessments were based on predefined damage levels i.e. reuse, replace, collapse and blowout (Wesevich and Oswald, 2005).

Davidson et al. summarized the results from the tests on unreinforced masonry walls retrofitted with sprayed-on polymer subjected to blast loads that have been conducted by the Air Force Research Laboratory at Tyndall Air Force Base. The results clearly indicate that this method of retrofitting is an effective approach to strengthening unreinforced masonry walls against blast loads (Davidson, Porter et al., 2004).

2.4. Finite Element Modeling of Unreinforced Masonry Walls under Blast

As mentioned before, damage of masonry structures specially unreinforced masonry to explosive loadings could present a significant safety hazard to building occupants. Conducting conventional physical blast tests are often prohibited due to their high cost and safety considerations. In addition, some tests might not even be possible to be carried out due to limitations regarding the height, length, explosive weight, etc. Hence, in the past couple of decades other methods such as numerical simulations have become highly attractive to researches to predict the response of the masonry structures under blast loads. There are two common approaches when it comes to modeling masonry structures. One method is the discrete approach also known as micro modeling which involves separate modeling of masonry units and mortar and therefore the interaction between the units and mortar joints are included in the simulation. Several researches have used micro modeling approach in order to study the complex behaviour of masonry structures

Burnett et al. (2007) developed a discrete finite element modelling approach to model unreinforced brick work and block work masonry walls subjected to out of plane loading using finite element modeling software LS-DYNA. This approach involved using elastic solid elements for the units and contact interface model implemented in LS-DYNA for the mortar joint. The predicted response obtained by the simulation was compared with the response from the previously tested walls in the laboratory (Gilbert et al., 2002). It was found that the discrete model predicted the dynamic response of unreinforced masonry walls with reasonably accuracy (Burnett et al., 2007).

As discussed earlier, it is especially important to predict the structural response of unreinforced masonry walls subjected to extreme out of plane loading conditions such as blast. Wei and Stewart (2010) conducted numerical simulations to estimate the response and damage of 3m×3m brick masonry walls with different thickness under explosive loadings using finite element program LS-DYNA. Micro modeling approach was adopted to simulate the units and mortar joints. The blast load was modeled using ConWep (Hyde, 1991) which is implemented in LS-DYNA. The results obtained from the finite element model were compared with field test data carried out by Varma et al. (1997) in terms of the maximum deflection and good agreement was found (Wei and Stewart, 2010). Eamon et al. (2004) also used discrete modeling approach to simulate unreinforced masonry walls subjected to low, moderate or high blast pressures. However, in this research the thickness of the mortar was included in the CMU dimensions and the mortar was modeled as a zero-thickness contact surface. The software used in this study was DYNA3D. In terms of loading, it was assumed that the blast source was far enough

from the wall so that a uniform pressure is applied on the surface of the wall. Good agreement between the numerical and experimental results (Dennis et al., 2002) indicated that the model had the ability to predict walls' failure behaviour under blast (Eamon et al., 2004). Another study in micro modeling of unreinforced CMU walls under blast was done by Dennis et al. (2002). DYNA3D was used in this simulation. In this quarter scale model, each CMU was tied to the adjacent CMU by slide surfaces. The wall was subjected to blast loads with three different scaled distances. The comparisons of mid-height displacement responses between the simulation and experimental results indicated that the finite element model slightly under-predicted the maximum deflection (Dennis et al., 2002).

Davidson et al. (2004) also adopted a discrete finite element modeling approach to model polymer retrofitted CMU walls subjected to blast loading using LS-DYNA. The blocks are tied together using contact definitions in LS-DYNA. Contact surface was also used to represent contact between the unreinforced masonry wall and the thin membrane (Davidson, Sudame et al., 2004).

The second method is the continuous approach or continuum modeling also known as macro modeling in which the interaction between the units and mortar joints is excluded so the masonry and mortar joints are blended into a single continuum where equivalent properties of the homogenized composite material are used. Wei and Hao (2009) developed a brick masonry material model accounting for the strain rate effect using homogenization method. The equivalent properties were obtained by numerically simulating responses of a representative volume element (RVE) under different static and

dynamic stress states (Wei and Hao, 2009). Other researchers have also derived similar equivalent material properties for masonry using homogenization technique (Ma et al., 2001; Wu and Hao, 2006; Zucchini and Lourenço, 2004; Zucchini and Lourenço, 2009). These developed equivalent masonry material models and other similar ones are implemented in continuous modeling of masonry by other researchers to study the response of masonry structures subjected to extreme dynamic loads such as blast.

Hao (2009) used previously developed equivalent masonry material properties (Wei and Hao, 2009) in a macro modeling of a 2.88m×2.82m unreinforced brick masonry wall subjected to blast loads generated from TNT explosions with different scaled distances (1, 3, 5, and 7 $m/kg^{1/3}$) using AUTODYN. The midpoint displacement and velocity response as well as the wall's fragment distribution in each loading case was studied (Hao, 2009).

Wang et al. (2009) modeled a 1.92m×1.89m unreinforced brick masonry using both discrete and continuous finite element methods. In the micro model, distinctive brick and mortar material properties were used whereas in the macro model the homogenized material model developed by Wei and Hao (2009) was used. The response of the masonry wall was to blast loads with 2 $m/kg^{1/3}$ and 3 $m/kg^{1/3}$ scaled distances were studied. The results from both approaches found to be reasonably similar. However, since the distinctive model resulted in larger computational time it was concluded that the continuous approach is would save a lot of time in modeling large structures (Wang et al., 2009).

Wu and Hao (2007) used the computer program LS-DYNA3D to numerically simulate the damage of a one story, a two story and an eight story unreinforced masonry

reinforced concrete frame structures. The unreinforced masonry walls were modeled using a previously developed 3D homogenized material model (Wu and Hao, 2006). Contact surfaces were used to model the contact between the masonry wall and the RC frame. The response of each structure subjected to blast loads with various scaled distances was investigated using their displacement responses. The scaled distance less than 1.82 $m/kg^{1/3}$ found to resulted in the collapse of low rise (one and two story) masonry structures when a scaled distance less than 1.18 $m/kg^{1/3}$ resulted in collapse of medium rise (eight story) masonry structure (Wu and Hao, 2007).

The continuous approach has become more attractive to researchers since the discrete modeling method is very complex and computationally extensive especially for models simulating larger structures. However, since the failure in masonry structures often occurs in the weak joints (mortar bonds) micro modeling approach is a lot more capable of capturing all the possible failure modes than the macro modeling and as the result it can provide the best insight to behaviour of masonry structures. For this reason, if one could go through the effort of detailed distinctive modeling of units and mortar, more reliable predictions of the response of the masonry structure would be achieved. Hence, the discrete approach is adopted in developing the model of an unreinforced masonry wall subjected to blast loading in the current study for which the detailed process is described in Chapter 3.

3. Development of the Finite Element Model

The process of developing a finite element model (FEM) involves many steps before it can be trusted to be used for an accurate simulation. There are many parameters involved in each stage which makes it extremely difficult to achieve a finite element model useable for a complex problem. This is due to the fact that the smallest change in any of the parameters may significantly change the results. Therefore it is extremely important to understand each parameter and use it properly and accurately in construction of the finite element model.

This chapter describes development of the finite element model for an unreinforced masonry wall which is subjected to blast load. The model replicates an actual physical wall that was built and tested under blast loading (Abou-Zeid et al., 2010). Therefore, the basic inputs for the model are taken from the Abou-Zeid's experimental data in order to produce an accurate representative FEM. The experiment consisted of testing eight full-scale unreinforced masonry walls under blast loads. The walls were divided into three groups. The wall selected to be modeled was from the first group which contained five walls, each subjected to a single shot. The wall all had the same dimension and the same standoff distance. However, the size of the charge differed among the five walls. The purpose of testing the walls in this group was to study the arching action of the unreinforced masonry walls under blast load. The selected wall to be numerically modeled was the second wall, wall W2, which was subjected to blast load generated by the detonation of 100 Kg ANFO explosive charge located at a 15 m standoff distance (Abou-Zeid et al., 2010).

An advanced general purpose finite element modeling program LS-DYNA developed by Livermore Software Technology Corporation (LSTC) was used to develop the FEM in this research. LS-DYNA is a transient dynamic finite element program with a solver that works mainly based on explicit time integration methodology (LSTC, 2006). The finite element software ETA/VPG version 3.4 (ETA, 2011) released by Engineering Technology Associates, Inc. (ETA) was used as the pre-processor to develop the model and generate the input file for the LS-DYNA solver. ETA/VPG that comes with LS-DYNA software package allows for creation of advanced and accurate simulations. ETA/VPG incorporates a complete and direct LS-DYNA interface and writes all the LS-DYNA input cards and therefore the need for text editing of the LS-DYNA's input deck is mostly eliminated (ETA, 2004). The input file created by ETA/VPG is then analyzed using LS-DYNA solver. LS-DYNA's advanced pre and post-processor LS-PrePost is then used to post process the results produced by the solver and generate fringe plots and response diagrams (LSTC, 2011). The results from LS-PrePost are provided in Chapter 4.

The following sections provide detailed description of different stages involved in construction of the FE model.

3.1. Unit System

Table 3-1 below provides the measurement units used in all the analyses.

Table 3-1. Measurement units

Property	Measurement Unit
Length	millimetre
Time	second
Mass	tonne
Force	Newton

3.2. Dimensions and Geometry

The masonry wall structure involved in Abou-Zeid's explosive test is 2.5 block wide, 11 courses tall and one block thick. The standard 190 mm two-cell concrete blocks are used. The dimension of each concrete masonry unit (CMU) is 190 mm×190 mm×390 mm. The thickness of the mortar is assumed to be 10 mm. Considering the dimensions of the CMU blocks and the mortar joints, the modeled in LS-DYNA wall is 995 mm wide, 2190 mm tall and 190 mm thick.

Two 30 mm thick rigid plates are modeled at the top and bottom of the wall where the wall will be supported. The rigid boundaries restrain lateral translations of the wall at the top and bottom. There are no gaps considered between the blocks and the plates in the simulation in order to provide the one-way action of the wall's arching behaviour. The plates extend 30 mm beyond the edges of the top and bottom surfaces of the wall as well as covering 60 mm of the back of the wall (the side subjected to blast load is referred to as the front).

3.3. Parts

There are two parts defined in this model under *PART cards. Part1 represents the concrete masonry units and part2 represents the rigid plates. The mortar joints are not defined as separate parts. Mortar layers are designed as 10 mm gaps between the blocks and are modeled using contact surfaces which will be explained in details in Section 3.7. Each part card in LS-DYNA input deck includes section identification and material identification which are defined in *SECTION and *MAT sections respectively in the input file. *SECTION card contains element properties information and *MAT card contains material properties information.

3.4. Elements

LS-DYNA provides several element formulation options. The elements used in this FEM are 8-node solid elements and are included in *SECTION_SOLID card. The length, the width and height of each CMU is divided in to 26, 12 and 12 elements respectively which means the size of each element is 15 mm×15.83 mm×15.83 mm. Each side web of a CMU is divided into two elements and the middle web is divided into 4 elements. The face shells are also divided into two elements. The middle web of a block has been designed to be thicker than the side webs in order to facilitate adequate meshing of the half-blocks without having a very thin web on one side of the half-block, as well as maintaining the symmetric arrangement of the blocks. Similar technique has been employed in other studies for modeling hollow concrete blocks (Wu and Hao, 2008).

As the result of the meshing manner explained above, each CMU contains 2016 elements which results in a total number of 55440 elements in the whole wall.

The rigid plates on top and bottom of the wall are also made of 8-node solid elements. The thickness of the plate is divided into 2 elements and the long side of the surface is divided into 70 elements which make each plate contain 2520 15 mm×15 mm×15 mm solid elements. With the mesh fidelity for the entire model, the aspect ratio of all elements in the entire model is very close to one which is desirable in finite element mesh.

Figure 3-1 shows the model of one CMU and Figure 3-2 illustrates the entire wall.

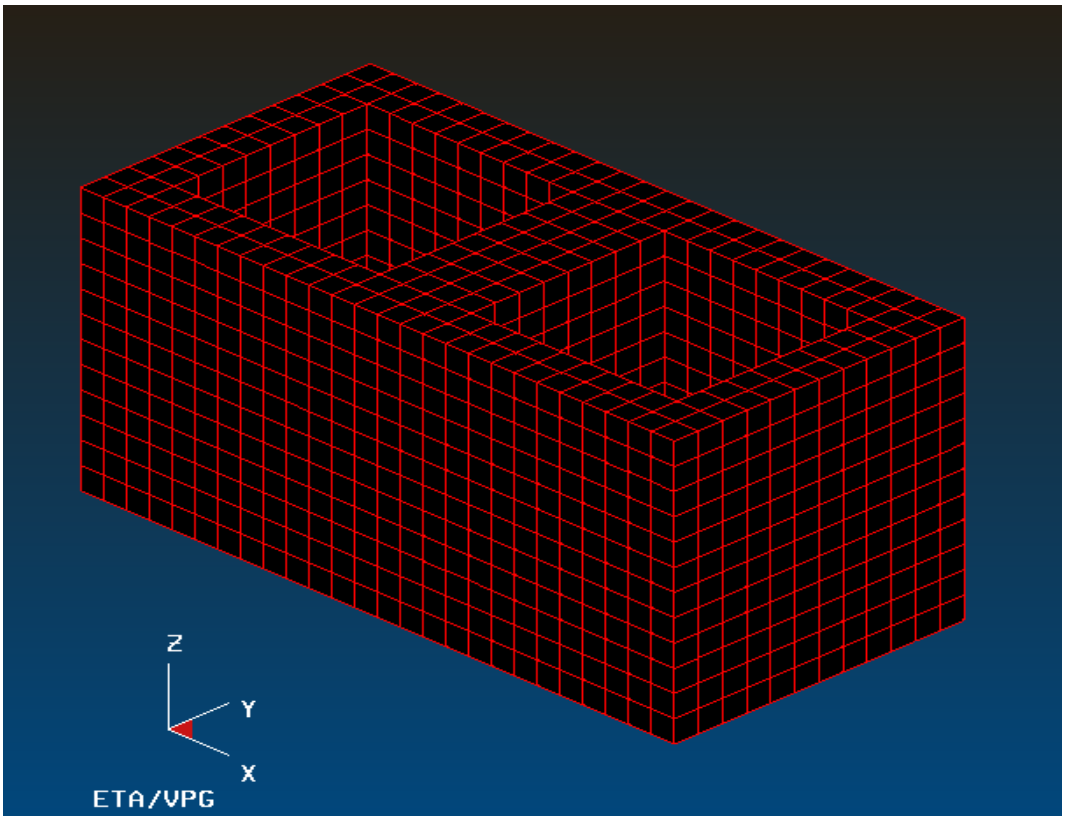

Figure 3-1. Concrete masonry unit mesh

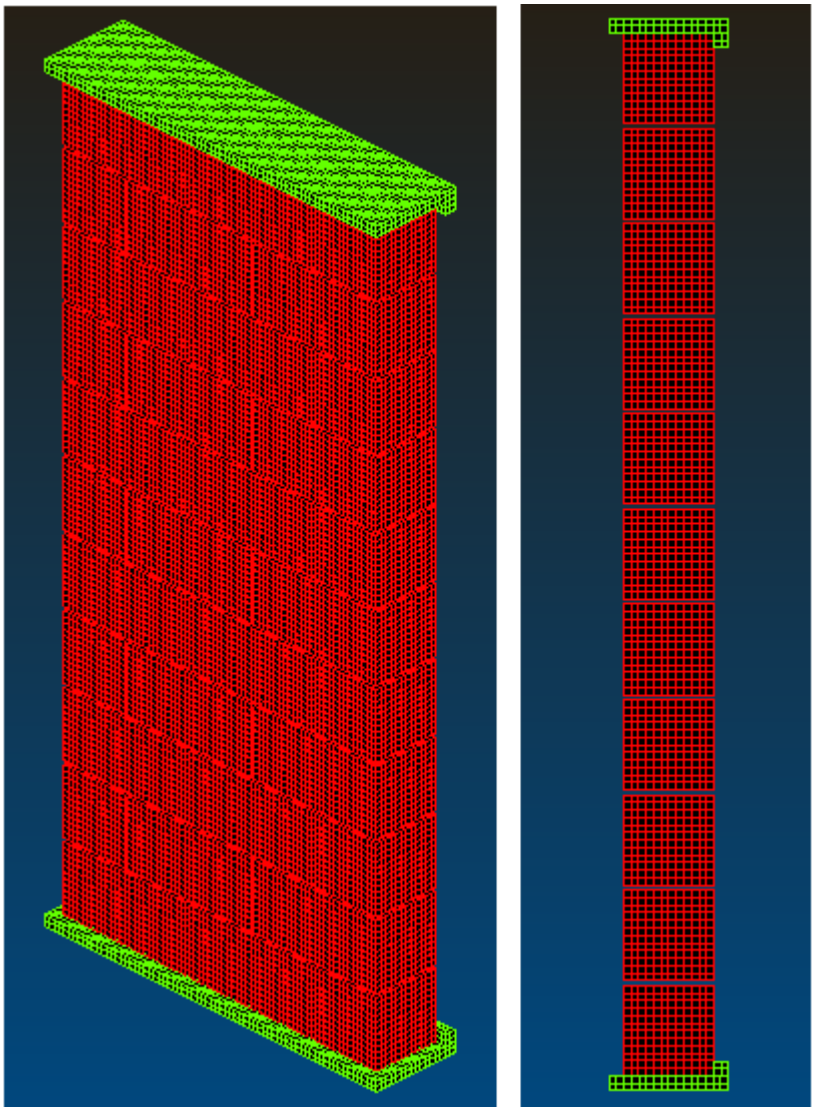

Figure 3-2. Finite element model of masonry wall. Left: Isometric view, Right: Side view

The elements used in this model are standard LS-DYNA's solid elements that are based on linear shape functions and use one point integration and hourglass control. The formulation of single point integrated constant stress solid elements (ELFORM=1) is very efficient since the CPU execution cost is relatively low compared to fully integrated elements while producing similar and comparable results. Under integrated solid

elements may develop zero energy deformations. In order to avoid these zero energy deformations hourglass control must be included in the simulation (LSTC, 2007). Hourglass is explained in details in Section 3.6.

3.5. Material Models

LS-DYNA offers a large selection of material models. Material constants for the selected material models are defined in *MAT section (LSTC, 2007).

3.5.1. Material model for Concrete Masonry Unit

The material model for part1, CMU, is *MAT_ELASTIC which is a simple elastic material model. The reason for choosing an elastic material model for the blocks is that when an unreinforced masonry walls fail due to blast load, the failure typically occurs at the mortar joints. The analysis this research is focused on this typical failure mode so the detailed behaviour of the CMUs is not of the interest in this research.

The required parameters in the material cards for *MAT_ELASTIC include mass density, Young's modulus and Poisson's ratio. Abou-Zeid performed a test on six prisms and obtained the average value of 22870 MPa with COV of 22.56% for elastic modulus. From Abou-Zeid's results and the values from literature, a value of 20000 MPa has been adapted for the simulation of CMU material model. For mass density and Poisson's ratio, typical values been extracted from literature (Abou-Zeid et al., 2010; Burnett et al., 2007; Gilbert et al., 2002; Voon and Ingham, 2006). Table 3-2 summarizes the material parameters for this simulation for the required parameters.

Table 3-2. Material properties of CMUs

Property	Value
Mass density (tonne/mm^3)	2.3E-9
Young's modulus (MPa)	20000
Poisson's ratio	0.3

3.5.2. Material model for Rigid Boundaries

LS-DYNA's material model *MAT_RIGID used to simulate the top and bottom rigid plates. Normally steel properties are used for this material model (Davidson, Sudame et al., 2004). LS-DYNA's manual provides the values for the required parameters which is presented in Table 3-3 (LSTC, 2007).

Table 3-3. Material properties of rigid plates

Property	Value
Mass density (tonne/mm^3)	7.85E-9
Young's modulus (MPa)	200000
Poisson's ratio (MPa)	0.3

3.6. Hourglass Control

Hourglass (HG) modes are non-physical, zero energy deformation modes that produce zero strain and no stress. As was mentioned in Section 3.4 hourglass modes may occur in under-integrated elements. Since the element used in the current simulation contain only

a single integration point, viscous hourglass control must be incorporated in the code under *HOURGLASS card to avoid the zero energy (hourglass) modes. There are several algorithms available in LS-DYNA for inhibiting hourglass modes. However, the default algorithm is the most effective while being computationally most economical. Thus, all the parameters in *HOURGLASS card which include hourglass and bulk viscosity properties are left as LS-DYNA's defaults (Davidson, Sudame et al., 2004; Dynasupport, 2011; LSTC, 2006; LSTC, 2007).

3.7. Contact Interfaces

As was mentioned earlier, 10 mm gaps are designed to represent the vertical and horizontal mortar layers which are basically the bonds between blocks. Contact is an effective way of treating interaction between disjoints parts of a model which makes it an ideal method to simulate mortar joints in this research. Contact surfaces are defined in *CONTACT cards in the input deck. LS-DYNA provides a large number of contact types. In this model each CMU block is attached to its neighbour block using *CONTACT_AUTOMATIC_SURFACE_TO_SURFACE_TIEBREAK contact type.

There are several parameters involved in contact definitions. Default values for contact parameters have evolved over time to work pretty well for most circumstances. Thus, in this simulation many of them are left as their default settings but some non-default values have been defined for key parameters to improve the behaviour of contacts for this specific model. The following sections review the user-defined parameters used in contact definitions (Davidson, Sudame et al., 2004; Dennis et al., 2002; LSTC, 2006; LSTC, 2007).

3.7.1. Master and Slave Surfaces

Each contact interface has two surfaces. One side of the interface is designated as the slave surface and the other is designated as the master surface. For modeling each contact interface, first the type of the slave and master surfaces must be identified. The parameters in *CONTACT card that allow to select the type are SSTYP and MSTYP for slave and master surfaces respectively. In this model, each slave and master surface is defined by a set of segments, called slave and master segments. The value of zero must be assigned to SSTYP and MSTYP parameters to represents segment sets as slave and master surface type. Abou-Zeid's test wall is face-shell mortar bedded. Therefore, the created segment sets along the horizontal mortar joints (bed joints) and the vertical mortar joints (head joints) were two-element wide to cover the face-shells. The segment sets are created in *SET_SEGMENT cards.

At each horizontal contact interface, the bottom segment set has been designated as the master set and the top segment set has been designated as the slave surface. For every vertical contact interface, the segment set on the left is set as master set and the one on the right is set as slave segment set. However, automatic contact treatment is symmetric and the definition of the slave and master surfaces is arbitrary since the same results will be produced either way. Another point that should be noted is that in contact definitions the contact segment normals must be oriented towards the contacting surface. But automatic contact types do not have orientation requirements and they can detect penetration from either side of the contact surface. For these reasons the automatic contact types are generally more robust than their non-automatic counterparts.

Once the type is selected, the slave and master segment set IDs must be specified through SSID and MSID. The identification numbers refer to corresponding segment sets that have already been defined in *SET_SEGMENT cards (Bala, 2001; Davidson, Sudame et al., 2004; LSTC, 2006; LSTC, 2007).

3.7.2. Friction

Friction is LS-DYNA is based on a Coulomb formulation. This formulation is based on static coefficient of friction (FS), dynamic coefficient of friction (FD), exponential decay coefficient (DC) and relative velocity between the surfaces involved in the contact (V_{rel}). The formula defining the coefficient of friction (μ) is:

$$\mu_C = FD + (FS - FD)e^{-DC|v_{rel}|} \quad \text{Eq. 9}$$

Friction is invoked by assigning non-zero values to static and dynamic coefficients of friction. In order to differentiate between static and dynamic FS must be greater than FD and DC must be set to a non-zero value for FD to have an effect (Bala, 2001; LSTC, 2006). In this model FS, FD and DC are taken as 0.6, 0.4 and 0.35 respectively (Davidson, Sudame et al., 2004; Dennis et al., 2002; Eamon et al., 2004).

3.7.3. Thickness Offsets

Contacts could be offset-based or non-offset based. The offset-based contacts incorporate element thickness in the contact definition. The thickness offsets are always included in automatic contact types. If solid elements are used, the contact thickness offset is controlled by the parameter SLDTHK which is the optional solid element thickness. A

non-zero positive value of SLDTHK activates the thickness offsets in the contact algorithm. Using the thickness offsets in this model is especially important since there are 10 mm gaps between the slave and master surfaces. In the treatment of thickness offsets, slave and master surfaces are both projected based on mid-surface normal projection vectors as shown in below (LSTC, 2006).

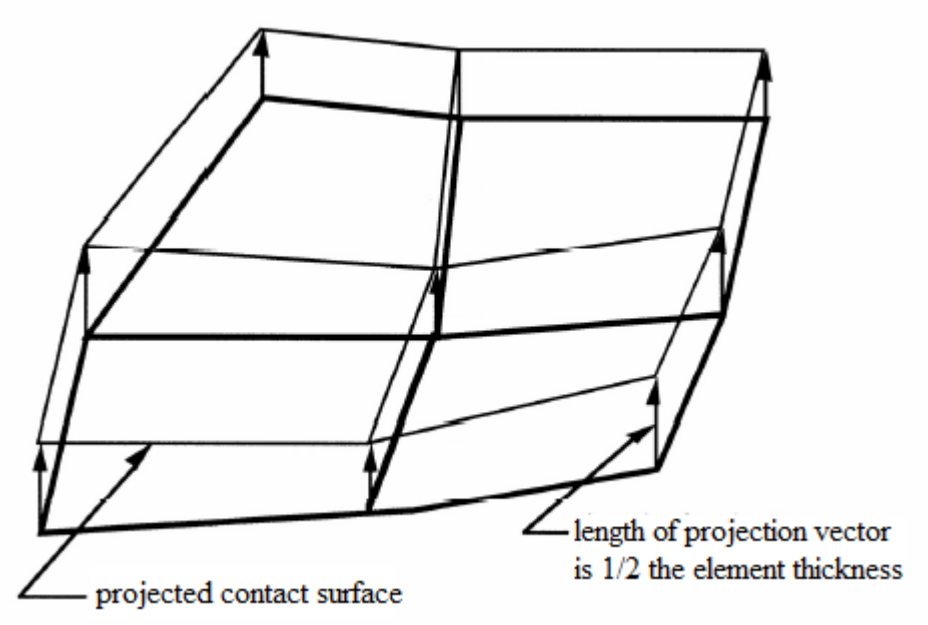

Figure 3-3. Contact surface based on mid-surface normal projection vectors

As the result, the slave and master surfaces are both offset by an amount equal to half of the element thickness that is by default the true thickness of solid element specified in *SECTION_SOLID equal to 15.83 mm. However, this value can be changed using previously mentioned parameter SLDTHK. Since the gap between the slave and master surfaces is 10 mm, SLDTHK is changed to 10 mm. This way the slave surface and master surface each is offset by 5 mm and the projected contact surfaces are in contact

halfway between the two surfaces (Bala, 2001; Davidson, Sudame et al., 2004; LSTC, 2006; LSTC, 2007).

3.7.4. Mortar Strength and Tiebreak

Tiebreak contacts are penalty based contact types that allow for the definition of failure parameters. Tiebreak option has been used in this simulation since the interfaces are basically representing the mortar bonds between the CMU blocks which have limited strength and will fail at some point after being subjected to the blast load. There are 9 options available for tiebreak in *CONTACT_AUTOMATIC-SURFACE-TO-SURFACE-TIEBREAK contact type. Option 6 which is for use with solid elements is selected. Based on this option, the tiebreak is active for all the nodes that are initially in contact. This applies perfectly to the nodes on slave surface and master surface of the interface which came to be in contact using mid-surface normal projection vectors explained in Section 3.7.3. For tiebreak to occur, first a failure criterion must be defined. Failure is based on stresses along normal (tensile) and shear directions and is formulated as follow:

$$\left(\frac{|\sigma_n|}{NFLS}\right)^2 + \left(\frac{|\sigma_s|}{SFLS}\right)^2 \geq 1 \qquad \text{Eq. 10}$$

Where σ_n is calculated normal stress, σ_s is calculated shear stress, NFLS is normal failure stress and SFLS is shear failure stress. NFLS and SFLS are taken as mortar's tensile strength and shear strength respectively. Mortar's tensile strength is 0.45 MPa and its shear strength is 0.63 MPa (Burnett et al., 2007; Dennis et al., 2002).

Once the tiebreak's stress failure criterion is met, damage initiates which is assumed to be a linear function of distance between points initially in contact (critical distance). The limit for critical distance is controlled by the parameter PARAM which is set to 10 mm. Once the distance is equal to PARAM damage is fully developed and the tiebreak failure occurs and this contact option will behave as a SURFACE_TO_SURFACE contact. At this point since the mortar joint is failed and there are no tensile or shear resistance at the interface, the contact between the surfaces is solely relied on frictional forces (Bala, 2001; Burnett et al., 2007; Davidson, Sudame et al., 2004; LSTC, 2007).

3.8. Boundary Condition

The wall in experiment was a one-way arching wall which was built in a steel container which acted as its reaction structure. The wall was fit snugly into the steel frame using two hollow rectangular steel sections welded to a steel plate at each end for the wall to be able to develop arching action. The sides of the wall were not tightly attached to the reaction structure and a gap was allowed such that it would be a one-way wall (Abou-Zeid et al., 2010).

In order to simulate the same boundary conditions in the finite element model, there are no gaps designed neither between the bottom-most block and the bottom rigid plate nor between the top-most block and the top rigid plate. This will enforce the arching action on the wall. The sides of the wall in the FEM are not restrained in order to simulate one-way action. As discussed in Section 2.1.3, during arching action tension cracks develop at the ends and the centre of the wall dividing the wall into two rigid segments. For this action to occur, the two rigid segments must be able to rotate at their ends (at the

supports) until either masonry crushes at the ends or the wall snaps at the centre. Hence, the boundary conditions applied in the simulation must allow for rotation at top and bottom of the wall while the rigid plates resist any lateral translation of the wall. In order to define such boundary conditions in LS-DYNA, two node sets are generated in *SET_NODE card. One is corresponding to the top surface of the top-most CMU block (under the top steel plate) and the other corresponding to the bottom surface of the bottom-most CMU block (above the bottom steel plate). The created node sets are then constrained under *BOUNDARY_SPC cards. Translational boundary constraints are imposed in x, y and z degrees of freedom by assigning a value of 1 to parameters DOFX, DOFY and DOFZ in the code. There are no rotational constraints since the nodes must be free to rotate. Thus, DOFRX, DOFRY and DOFRZ are set to zero (Davidson, Sudame et al., 2004; LSTC, 2006; LSTC, 2007).

3.9. Loading

The wall in this simulation is subjected to blast loading. Moreover, the gravity load on the wall has been also taken into consideration in order to produce more realistic results. The following sections describe how these loads are applied in details.

3.9.1. Gravity Load

There are a few ways to apply gravity load in LS-DYNA. In this model gravitational loads are added using *LOAD_BODY_Z command where z is the vertical axis. In this method, first a load curve is defined under *DEFINE_CURVE card. Since gravity is constant, the load curve is set as a constant equal to 1. In *LOAD_BODY_Z card,

parameter LCID assumes the identification number corresponding to the previously defined uniform load curve. The load curve is then scaled using the scaled factor parameter SF which is set to the gravitational acceleration constant equal to 9810 mm/s^2. It should be noted that positive body load in LS-DYNA acts in negative direction which is why a positive value for gravitational acceleration is used even though it acts in the negative z-direction (LSTC, 2007; Reid, 1998).

3.9.2. Blast Load

The wall in the experimental test was subjected to blast load which was generated by detonation of 100 Kg ANFO at a 15 m standoff distance from the wall. In the finite element simulation *LOAD_BLAST option was used to apply pressure loads to the wall due to explosion. The ConWep model (Hyde, 1991) is incorporated in LS-DYNA based on a study by Randers-Pehrson and Bannister (1997). The ConWep algorithms calculate the pressure values by taking into account the angle of incidence of the blast wave. *LOAD_BLAST must be used in conjunction with *LOAD_SEGMENT_SET where a segment set corresponding to the face of the wall on which the pressure will be applied is created. In *LOAD_SEGMENT_SET, the parameter LCID (load curve ID) must be input as -2 in order to call ConWep function algorithms to determine the pressure for the segment.

Once the segment set is created, properties of the explosive must be specified under *LOAD_BLAST card. The inputs include equivalent mass of TNT, detonation location, unit system and type of explosion. Table 3-4 summarizes all the parameters and their quantities used in this blast loading model.

Table 3-4. Blast load parameters

Parameter	Description	Value	Unit
WGT	equivalent TNT mass	0.08	tonne
XBO	x-coordinate of explosion point	497.5	mm
YBO	y-coordinate of explosion point	-15000	mm
ZBO	z-coordinate of explosion point	0	mm
IUNIT	unit conversion flag	5	tonne, mm, s, MPa
ISURF	type of busrt	1	

The explosive used in Abou-Zeid's test is ANFO. However, WGT must be input as TNT equivalent. The TNT equivalency factor for ANTO is taken as 0.8 (Chang and Young, 2010). Therefore, 100 Kg ANFO is equivalent to 80 Kg TNT. Since the charge is situated on the ground surface, a value of 1 is assigned to ISURF which defines the type of explosion as surface burst where the blast wave propagates with a hemispherical wave front. Assigning a value of 5 to IUNIT will allow converting the default units into LS-DYNA's units (Abou-Zeid et al., 2010; Adoum and Lapoujade, 2003; El-Dakhakhni et al., 2010; LSTC, 2007; Randers-Pehrson and Bannister, 1997).

4. Model Verification

In the previous chapter it was described in details how the finite element model of the unreinforced wall was constructed based on experimental data from field blast tests. The pre-processor software ETA/VPG was used to generate the input file for LS-DYNA solver. In this chapter the results produced by LS-DYNA solver are analyzed using LS-DYNA's advance pre and post-processor LS-PrePost and compared with the results obtained from the physical experiment. The objective in this Chapter is to verify the validity of the developed finite element model in order to confirm its reliability in future studies where the experimental data is not available due to the high costs and unsafe nature of blast loading tests. The comparison of the results is based on the midpoint displacement time histories and is provided in details in the following sections. The conclusion of the result of the verification process is explained in Section 4.4.

4.1. Experimental Results

The masonry wall on which the finite element model is based was subjected to 100 Kg ANFO at a 15 m standoff distance. In order to measure the displacements, three linear variable differential transformers (LVDTs) were located at 5^{th}, 6^{th} and 9^{th} course of the wall respectively. The maximum displacement occurs at the mid-height of the wall and the displacement time histories from all three LVDTs reported by Abou-Zeid et al. (2010) confirmed this fact as well. However, since only the maximum displacement response is of interest, the data from LVDT installed on the 6^{th} course is used in this research to be

compared with the numerical results. The displacement time history based on the 6th course LVDT data is plotted in Figure 4-1:

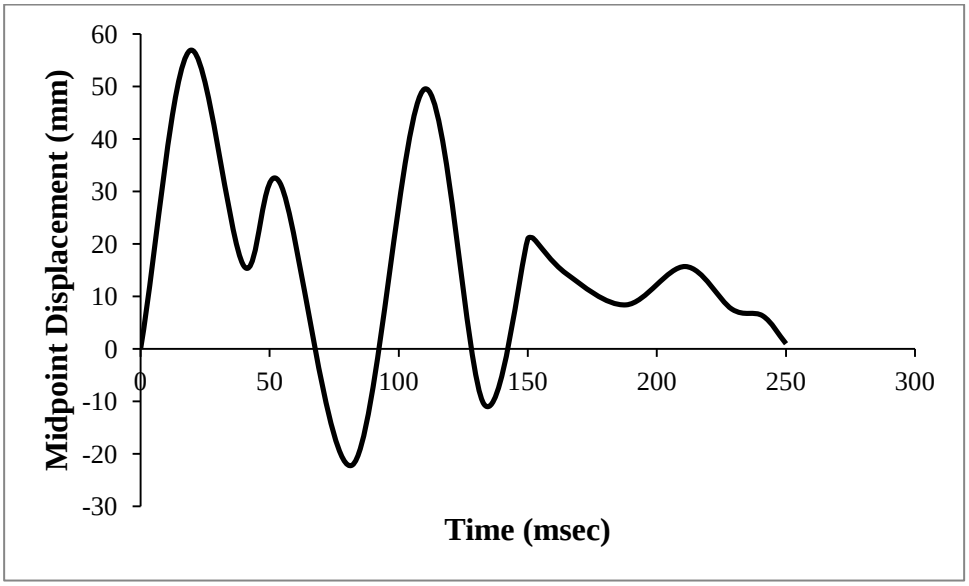

Figure 4-1. Experimental midpoint displacement time history

It can be observed from Figure 4-1 that the displacement response obtained by the data recorded in 250 msec has a more accurate and explainable behaviour within the first 150 msec. From 150 msec until the end of the recording range, the response does not maintain as accurate behaviour as the first 150 msec due to possible errors and inaccuracies involved the experimental work. However, the main expected behaviour is still apparent as the vibration tends to dissipate and the curve returns to zero.

4.2. Numerical Results

The process of developing the finite element model was described in details in Chapter 3. Table 4-1 summarizes LS-DYNA's input parameters used for the simulations.

Table 4-1. LS-DYNA input parameters

Parameter	Value	Unit
CMU's mass density	2.3E-9	tonne/mm^3
Young's Modulus	20000	MPa
Poisson's ratio	0.3	
Mortar's static coefficient of friction (FS)	0.6	
Mortar's dynamic coefficient of friction (FS)	0.4	
Exponential decay coefficient	0.35	
Solid element thickness for offset in contact definition	10	mm
Mortar's normal (tensile) failure stress	0.45	MPa
Mortar's shear failure stress	0.63	MPa
Equivalent TNT mass (WGT)	0.08	tonne
Standoff distance	15000	mm

The behaviour of the finite element model of the wall is described in this section in terms the mid-height centre displacement which corresponds to the displacement data recorded by the 6th course LVDT in the experiment. For this purpose, the D3Plots generated by LS-DYNA solver is opened in the LS-PrePost. A node at the center of the wall is selected where the 6th course LVDT would be located in the physical test and nodal displacement time history in y-direction is plotted. Figure 4-2 below illustrates the displacement response output by LS-PrePost:

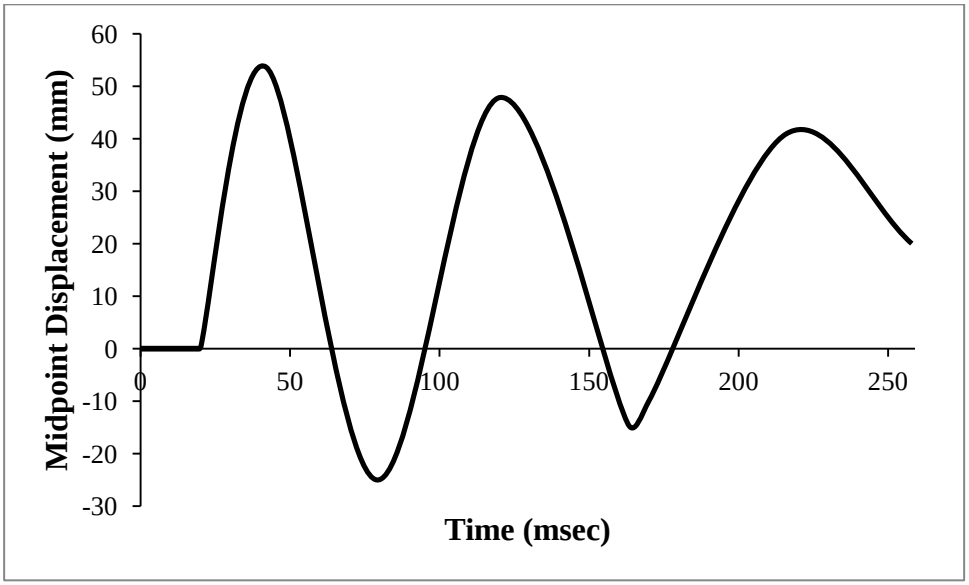

Figure 4-2. Numerical midpoint displacement time history

4.3. Comparison of Numerical and Experimental Results

In the previous sections the displacement at the mid-point of the wall in both the experiment and the finite element simulation was presented. In order to confirm the validity of the developed FEM, the results from the simulation are compared with the experimental results in this section. The main criterion on which the credibility of the FEM is judged is a close agreement of the maximum positive displacements (the first peak in the plots above) within 10% error. Other researchers have used limits for error larger than 10% (Burnett et al., 2007; Chaimoon and Attard, 2007; Dennis et al., 2002). Therefore, in the current study a smaller value for error (10%) is selected in order to increase the accuracy of the model. When a structure is subjected to blast which is a case of loading with an extremely short duration and a magnitude a lot larger than any other load that will be applied to the structure in its design life, then only the maximum positive

displacement becomes what is critical for the structure's survival. The subsequent vibrations matter only when the loads are repetitive. The first negative (rebound) displacement is also important however this value is most likely a lot less than the positive peak due to structure's damping. Therefore, the most important factor is the first maximum positive displacement at the wall's midpoint which is also the reason why typical failure criterion is often defined in terms of maximum midpoint displacement. Hence, the key element in the verification process is the accuracy of this value which is why a small amount of error is expected from the FEM predicted results.

Other criteria for assessing the accuracy of the FEM is the proximity of general shape of the displacement response, the values of the displacements and the times at which they occur to those of in experiment. It should be noted that magnitudes of displacements have higher priority than their times of occurrence since the different between times would be the matter of milliseconds which in reality does not change anything in terms of design or damage assessment. So in summary, as long as the first positive displacement in FEM closely matches the corresponding experimental value (10% error) while the general shape of the displacement response is captured by the simulation and the magnitudes of the rest of the peak displacements are preferably within 20% error from the experimental results, then the FEM is considered valid.

It can be observed from Figure 4-2, that the maximum positive displacement from the finite element simulation is 53.6 mm. This value is in extremely close agreement with the corresponding value obtained by experiment with only 5.63% error. The displacement response closely captures the shape of the response curve provided by experimental data.

The values of other peak displacements are in close agreements. However, in order to accurately implement the comparisons, the numerical displacement time history is superimposed on the experimental plot in Figure 4-3.

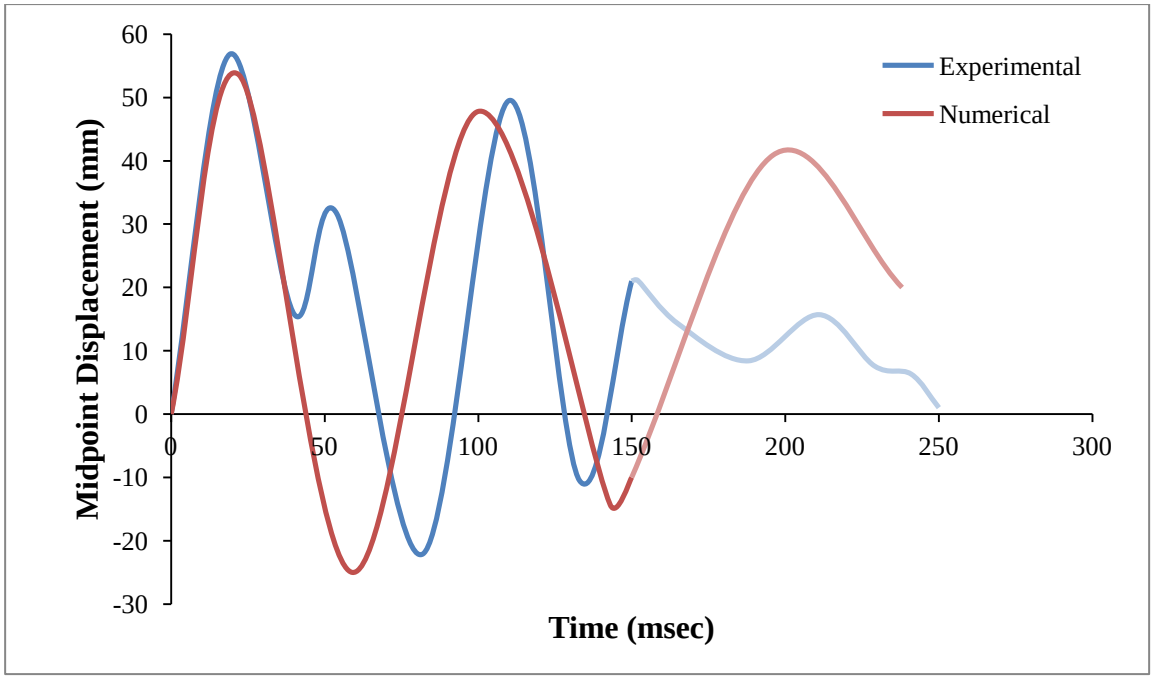

Figure 4-3. Experimental versus numerical midpoint displacement time histories

It should be noted that the arrival time in the numerical response plot is equal to 20 msec. This has been taken into consideration for superimposition by subtracting the 20 msec from the times in the numerically generated plot so that the superimposed plot would have zero arrival time which is identical to what have been assumed in the experimental curve.

Also due to the fact that based on the experimental results, only the first 150 milliseconds of the plot has a more reliable behaviour, the comparison between the experimental and numerical results is also is focused on the first 150 msec. However, it should be

mentioned that even after 150 msec, both response curves maintain the same trend as they eventually return to zero. Hence, the detailed point-to-point comparison is performed for only up to 150 msec of the response time history in the verification process which is why the plots in Figure 4-3 are drawn in paler colours are after 150 msec.

In order to be able to implement the comparison more accurately the detailed information is summarized in Table 4-2:

Table 4-2. Comparison between experimental and numerical peak midpoint displacements

Exp		FEM			Error (%)	
T_e	D_e	T_f	T_f-t_a	D_f	E_T	E_D
0	0	20	0	0	0	0
19	56.8	42	22	53.6	15.79	5.63
82	-22.1	79	59	-25.0	28.05	13.12
110	49.5	120	100	47.8	9.09	3.43
133	-10.5	163	143	-14.3	7.52	36.19

In the table above the T_e and T_f represent the time of occurrence of peak deflection in the experimental and numerical response curves respectively. t_a is the arrival time which is subtracted from T_f in order to eliminate the delay in the numerical response. E_T is the absolute error between the times at which the peak deflections occur. D_e and D_f are peak displacements in the experimental and numerical responses respectively. E_D represents

the absolute error between these two peak deflections. The column in Table 4-2 associated with E_D is the most important column for the FEM verification process.

The results from the finite element model are also in close agreement with the results obtained by Abou-Zeid using a single degree of freedom (SDOF) analysis which confirms the validity of the simulation results yet in another way. Figure 4-4 shows the displacement time histories obtained experimentally, numerically and analytically.

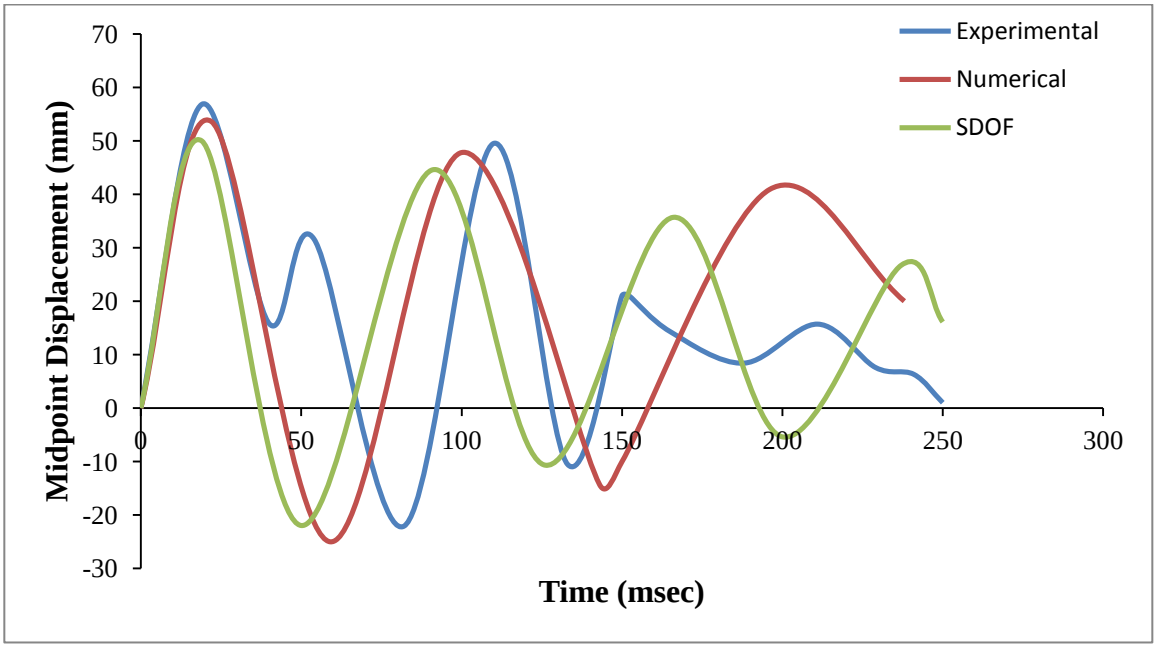

Figure 4-4. Displacement time histories from experimental, numerical and SDOF models

In addition to capturing correct midpoint displacement response, it is also important for the finite element simulation to be able to predict the correct deflected shape for the entire wall. Figure 4-5 illustrates the wall's deflected shape at the time of maximum displacement:

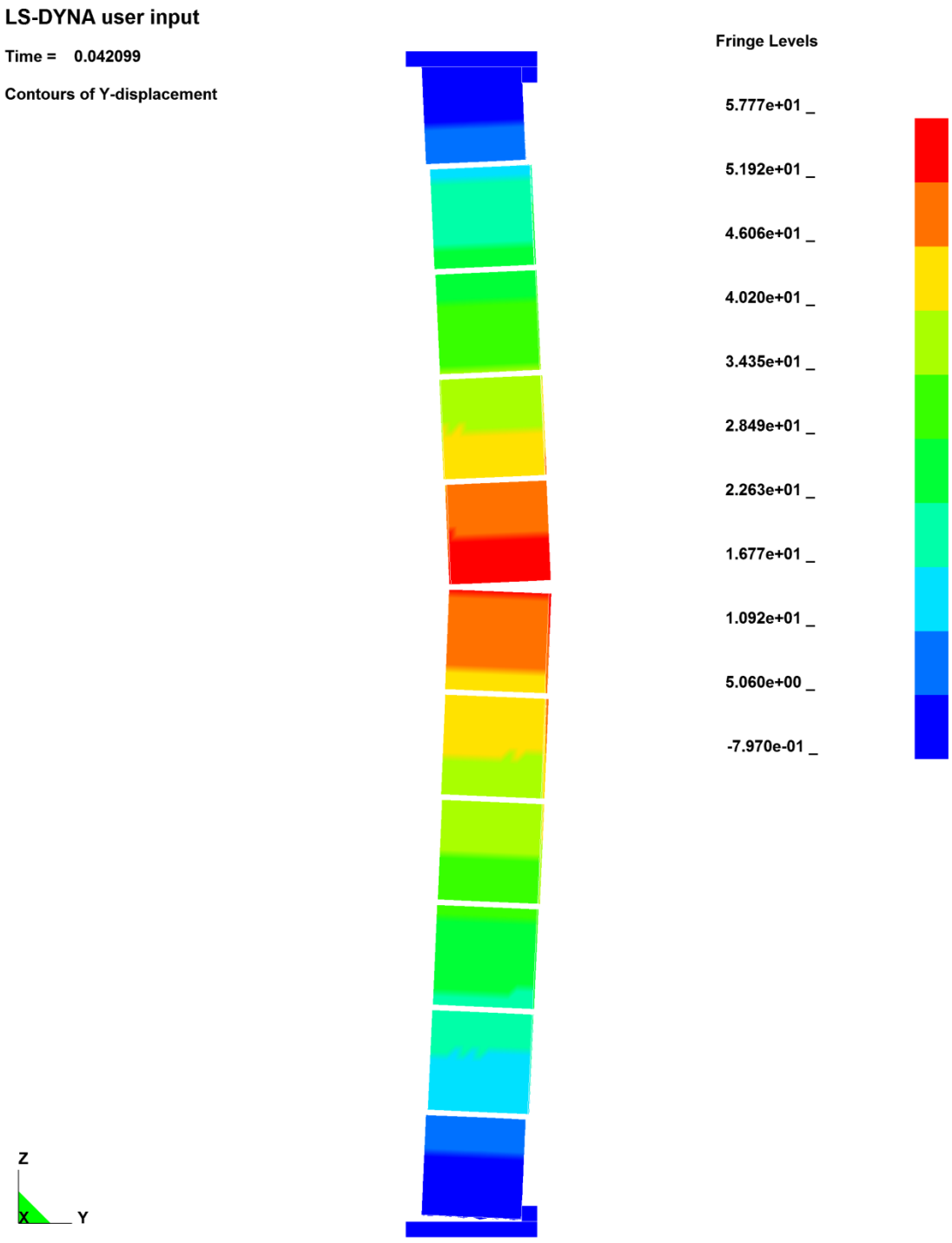

Figure 4-5. Wall behaviour at the time of maximum displacement

In addition to meeting the expectations on the wall's midpoint displacement response, the deflected shape also illustrates the predicted arching action of the wall which emphasizes on the accuracy of the developed finite element model in predicting the general behaviour of the wall. When the wall is subjected to the load, the top and bottom rigid boundaries resist the lateral movement of the wall which results in high shear forces at the top and bottom blocks which cause those blocks to tend to rotate. However, due to the absence of any space between the top and bottom blocks and the rigid boundaries, the vertical movement of the wall is also restricted which would have resulted in crushing the blocks, had an inelastic material properties been used, by the rigid plates and formation of arching action.

It is apparent that the blocks near the mid-height of the wall separate in tension and divided the wall into rigid sections. Theoretically, the gap opening should happen at the mid-height of the wall but since in this case the wall is eleven courses high, and the failure initiates at the a weak joints (mortar joint), then the wall separates at a mortar joint nearest to the mid-height of the wall. The reason for the separation occurring at this mortar joint and not the one below the middle block could be explained through the difference between pressures applied at these two locations. The ConWep function calculates the pressure applied on elements by taking the angle of incidence into account. The pressure applied to separated bond is slightly larger than the one applied to the joint below the middle block.

Since the separation occurs at a location higher than the mid-height of the wall, the amount of rotation at the supports are not equal. The top rigid section (the portion of the

wall above the opening) is one course shorter than the bottom rigid section (the portion of the wall below the opening). This will cause the angle of rotation at the top support to be larger than the angle of rotation at the bottom supports and as the result a smaller gap opening is visible at the top support in Figure 4-5.

As described before, the top and bottom sections behave as rigid bodies where the mortar bonds in the two sections remain intact however very small shear is detected at the top-most and bottom-most mortar joints which is due to same phenomenon explained earlier for the top-most and bottom-most blocks.

The deflected shape of the wall at center and bottom is illustrated in Figure 4-6:

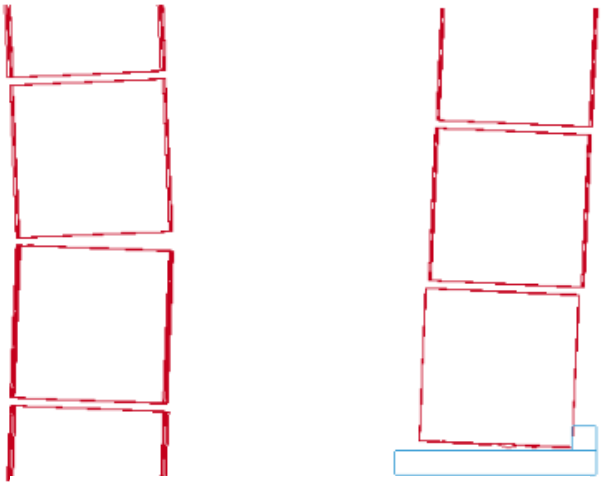

(a) (b)

Figure 4-6: Deflected shape of the wall (a) At the centre, (b) At the bottom

4.4. Conclusion

In this chapter the behaviour of an unreinforced masonry wall subjected to blast loading obtained both experimentally and numerically was described. The wall's behaviour was analyzed in terms of mid-height centre displacements. As discussed earlier the objective was to evaluate the accuracy of the constructed FEM and verify its validity. The evaluation process carried out by means of comparing the peak displacement values in the first 150 milliseconds of the displacement time histories. A few criteria must have been met before the FEM was considered acceptable. However, the one criterion that takes the priority over everything else was close agreement between the first maximum positive displacements within 10% error. The other criteria on which the validity of the FEM is judged are listed below in the order of their priority:

- Maintaining a general response shape close to the one obtained from experimental data.
- Matching the peak positive and negative displacements with experimental results (ideally within 20% error) and their time of occurrence up to 150 millisecons.
- Following the same trend as the experimental displacement response after 150 milliseconds.

From Table 4-2, it was observed that the maximum positive midpoint displacement from FEM is 53.6 with only 5.63% error from the experimental results.

Having met the first and most important criterion successfully, the FEM was evaluated based on the rest of the criteria listed earlier. In terms of the shape of the response plot, the simulation response curve again met the requirements. Especially up to 150 milliseconds the behaviour was very similar to the results from experiment, but even after 150 msec it still followed the same trend which was the eventual elimination of vibration and returning to zero.

As for the rest of the peak displacements, the limit was set to ideally 20% with respect to the values obtained from experimental data. According to Table 4-2, the first maximum rebound (negative) displacement was 13.12% higher than expected but it is still well within the allowable range. The next deflection peak was extremely close to the experimental value with only 3.43% error. The last peak before 150 msec, had the highest error (36.19%). However, this does not mean that the prediction is invalid for a few reasons. Firstly, the 20% error was set only as an ideal limit. Second, this peak was far from the first maximum displacement (at 143 msec) and the value is so much lower than the first maximum deflection that makes this deflection not very important. Moreover, despite the large error, the values are still not hugely different. Also, it should be kept in mind that even experimental results are not free of errors and there is always the chance that some of the experimental data is not accurate.

At this point it could be concluded that the finite element model's predictions are accurate based on the mid-point displacement response analysis. However, in addition to considering only the behaviour of the wall at the centre, in Section 4.3 the general

behaviour of the entire wall was analyzed as well. It was explained in detail how the simulation perfectly captured the true wall's arching behaviour.

It is concluded that the finite element model developed in this research satisfy the defined requirements and can produce accurate results.

5. Parametric Study

The parametric study provided in this chapter is essentially an input sensitivity analysis where the effect of some parameter variations in the model on the behaviour of the wall subjected to blast loading case described earlier is studied. Similar to the previous chapter, the aspect of wall behaviour that was used to study the influence the parameter variations is again the mid-height deflection time history. The previously developed FEM is taken as the baseline model and its displacement response presented in Figure 4-2 is used as the basis for comparisons carried out in the current chapter.

The parameters whose variations were investigated in the sensitivity analysis in this research are mortar strength, friction coefficients, boundary conditions, wall height as well as the influence of two-way arching action.

5.1. Influence of Key Contact Parameters

As previously discussed in Chapter 3, the mortar joints are modeled using contact surfaces defined under *CONTACT cards in LS-DYNA input deck. There are many parameters involved in contact definitions however there are a few which are expected to have higher impacts of the model behaviour. The values used for these certain parameters are varied in the following Sections 5.1.1and 5.1.2 in order to gain a better understanding about their influence on the wall's behaviour.

5.1.1. Influence of Mortar Strength

Obviously since the contact interfaces represent the mortar joints between the blocks, the effect of variation in bond strength is one of the most important aspects of contact

definition that needs to be evaluated. As discussed in Section 3.7.4, the failure of the mortar bond depends on mortar's tensile and shear strength which are defined by NFLS and SFLS in LS-DYNA's input file. NFLS and SFLS were taken as 0.45 MPa and 0.63 MPa respectively in the baseline model. In order to be able to detect the effect of each one of these two parameters systematically, Once NFLS is remained constant while SFLS is varied. Then SFLS is kept contact as NFLS is changed. At the end, both parameters are varied simultaneously. It should be noted that in this chapter just like the previous one, the behaviour of the wall is described in terms of mid-height center displacement and the arrival time delay (22 msec) is subtracted from the displacement times in all the response curves.

5.1.1.1. Tensile Strength

The effect of change in mortar bond's tensile strength is evaluated in this section. The bond's shear strength described by SFLS is remained the same as the value used in the baseline model (0.63 MPa) while the tensile strength described by NFLS is altered in the following cases. The values chosen for the tensile strength are all inspired by real mortar's tensile strengths in masonry structures. However, Case T1 and T5 are special cases since they do not reflect realistic situations. In Case T1, the mortar joints are assumed to have virtually no tensile strength and Case T5 represents a situation where tensile failure will never occur since the mortar bond has an extremely large tensile strength.

- Case T1: NFLS=1E-10 MPa, SFLS=0.63 MPa
- Case T2: NFLS= 0.40 MPa, SFLS= 0.63 MPa

- Case T3: NFLS= 0.55 MPa, SFLS= 0.63 MPa
- Case T4: NFLS= 1.00 MPa, SFLS= 0.63 MPa
- Case T5: NFLS= 1E+10 MPa, SFLS= 0.63 MPa

The mid-height displacement response curves for all cases above are plotted against the baseline model displacement response in Figure 5-1.

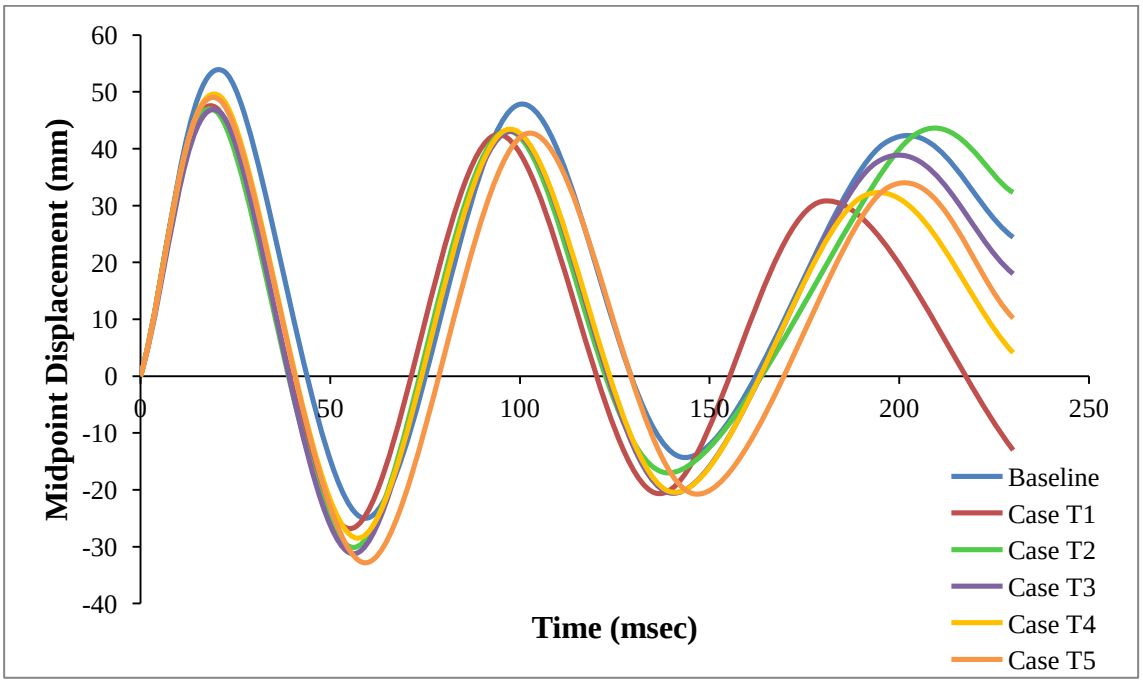

Figure 5-1. Effect of variation in mortar's tensile strength on displacement time history

It can be observed from the figure above that the displacement response produce by all the cases are pretty similar and are all comparable with the results from the baseline model.

Table 5-1 provides detailed point-to-point comparison for all the peak deflections where T is the time at which the peak displacement occurs in milliseconds, D is the peak

displacement in millimetres and E is the percentage error relative to the peak displacement values in the baseline model.

Table 5-1. Comparisons between peak deflections on displacement time histories when tensile strength is varied

Baseline		Case T1			Case T2			Case T3			Case T4			Case T5		
T	D	T	D	E	T	D	E	T	D	E	T	D	E	T	D	E
22	53.6	20	47.2	11.9	20	46.5	13.2	21	46.4	13.4	21	49.2	8.2	21	48.5	9.5
59	-25.0	55	-26.8	7.2	56	-30.1	20.4	56	-31.3	25.0	57	-28.5	14.0	59	-32.8	31.2
100	47.8	94	42.5	11.1	96	43.1	9.8	97	43	10.0	97	43.4	9.2	102	42.7	10.7
143	-14.3	136	-20.6	44.1	139	-17.0	18.9	140	-20.6	44.1	140	-20.4	42.7	146	-20.7	44.8
196	40.9	180	30.8	24.7	203	41.9	2.4	194	37.6	8.1	191	31.8	22.2	197	33.2	18.8

From Table 5-1 it is observed that the maximum displacement in none of the considered cases varies noticeably from the baseline model.

It was expected that by increasing the bond's tensile strength which leads to increasing the mortar strength, the maximum displacement would decrease. Therefore, it was expected to obtain larger maximum displacements in Cases T1 and T2 and smaller maximum displacements in Cases T3, T4 and T5 compared to the baseline model since in the first two cases the mortar bond strength was decreased and in the last three cases the mortar strength was increased. Contemplating the results of the five cases studied above, it was observed that Cases T3, T4 and T5 followed the expected trend since the maximum displacement in these cases are reduced when their bond strength were increased. However, no linearity was detected in the correlation between the increase in bond strength and decrease in maximum displacement. In Case T3 the tensile strength was increased by 22% and as the results the maximum mid-height deflection decrease by 13.4% from the baseline model. In Case T4, the tensile strength was increased by 122% nevertheless the decrease in maximum deflection was only 8.2% which is less than Case T3. Similar situation was observed in Case T5 where despite having maximum tensile strength, the maximum displacement is decreased by only 9.5% which is still higher than Case T4 but not higher than Case T3.

Cases T1 and T2, do not follow the expected trend since by decreasing the tensile strength which results in lower bond strength, the maximum displacement in both cases still decreases compared to the baseline model. Zero tensile strength in Case T1 means that the bond must fail in shear.

Not having larger displacements in Cases T1 and T4, not observing a linear trend in Cases T3, T4, and T5, as well as producing very similar results in all cases regardless of increasing or decreasing the mortar strength suggest that the maximum displacement under such huge blast load with 3.5 $m/Kg^{1/3}$ scaled distance, is not really sensitive to variation in mortar strength.

It should be mentioned that the wall's deflected shape in all the cases is the same, similar to the baseline model presented in Figure 4-5 which means the mortar joint between the 6^{th} and 7^{th} course which is subjected to the highest pressure resulted by the blast load, fails due to the bocks separation at that location. Therefore, complete tiebreak failure occurs no matter what the mortar strength is since the loading is so much more than what even the strongest mortar could handle. As explained in Section 3.7.4, the first stage for the tiebreak failure to occur is meeting the stress failure criterion defined in Equation10. Once the stress criterion is met, the failure will be completed only when the critical distance (distance between the points initially in contact) becomes larger than the critical distance defined by PARAM. It is obvious from Figure 4-5, that this distance in the 6^{th} mortar layer has become much larger than 10 mm that was assigned to PARAM which means that the tiebreak failure has been fully developed. Therefore, the behaviour of the wall at mid-height which is half a block below the separation point is not sensitive to variations in mortar strength. In other words, having higher or lower mortar strength will not keep the 6^{th} layer of mortar joint from failing when subjected to a blast load with 3.5 $m/Kg^{1/3}$ scaled distance that applies much larger stresses to the mortar bond than its failure stresses (NFLS and SFLS) and therefore the displacement at half block below the

failed mortar joint is not influenced by the mortar's strength. This is the reason why even in Case T5 where the mortar's tensile strength was extremely large, the bond still failed because the shear strength was too small to resist the huge stress applied to it by the blast load.

5.1.1.2. Shear Strength

In this section the impact of variation in mortar's shear strength is evaluated. In the following cases, the mortar's tensile strength described by NFLS remains unchanged with respect to the value used in the baseline model (0.45 MPa) while the shear strength is altered. Similar to the previous section, the values used for the shear strength are all inspired by the true mortar properties in masonry structure with exceptions of Cases S1 and S5. Case S1 represents a situation where the mortar joints have virtually no shear strength. In Case S5 an extremely large value is assigned to SFLS which means the mortar will fail only in tension and shear failure will not govern.

- CaseS1: NFLS= 0.45 MPa, SFLS= 1E-10 MPa
- Case S2: NFLS= 0.45 MPa, SFLS= 0.50 Mpa
- Case S3: NFLS= 0.45 MPa, SFLS= 0.70 MPa
- Case S4: NFLS= 0.45 MPa, SFLS= 1.5 MPa
- Case S5: NFLS= 0.45 MPa, SFLS= 1E+10 MPa

All the above cases except Case S5 produce similar displacement response curves that are all superimpose on the displacement time history from the baseline model illustrated in Figure 5-2.

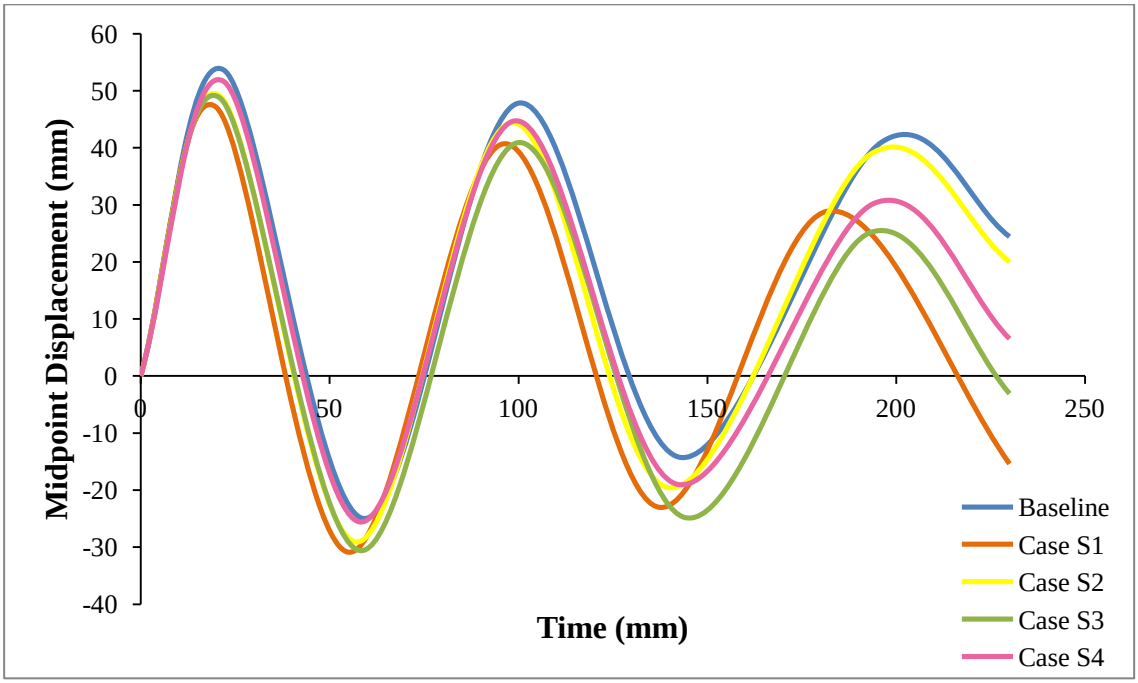

Figure 5-2. Effect of variation in mortar's shear strength on displacement time history

In Case S5 the wall fails completely when the pressure resulted from the blast load applies on the wall and the blocks fly away. Therefore, the plot in Figure 5-3 mainly shows the displacement time history of the middle block rather than the wall's midpoint displacement since the wall has obviously failed by the time it reached 190 mm displacement (Drysdale and Hamid, 2005).

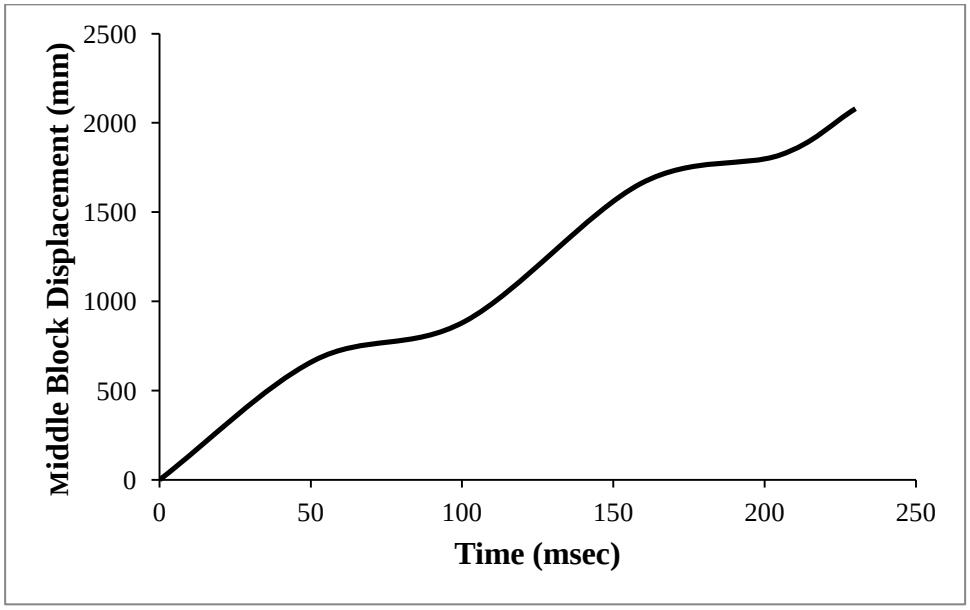

Figure 5-3. Displacement time history for Case S5

Table 5-2 summarizes the comparisons between the peak displacements in first four cases (S1-S4) and the baseline model.

Table 5-2. Comparisons between peak deflections on displacement time histories when normal strength is varied

Baseline		Case S1			Case S2			Case S3			Case S4		
T	D	T	D	E	T	D	E	T	D	E	T	D	E
22	53.6	20	47.1	12.1	21	49.1	8.4	21	48.7	9.1	22	51.6	3.7
59	-25.0	55	-30.9	23.6	57	-29.1	16.4	58	-30.6	22.4	58	-25.6	2.4
100	47.8	96	40.7	14.9	98	44.4	7.1	100	40.9	14.4	99	44.7	6.5
143	-14.3	137	-23.0	60.8	140	-19.6	37.1	144	-24.8	73.4	142	-19.0	32.9
196	40.9	182	28.9	29.3	193	38.8	5.1	193	25.1	38.6	194	30.2	26.2

Most what was discussed in the previous section applies in this section as well. In Cases S1 and S2, the mortar bond's shear strength was reduced while the tensile strength was remained unchanged which leads to an overall weaker mortar bond. In Cases S3, S4 and S5, the shear strength was increased which means the mortar bond was stronger compared to the baseline model. In the last three cases, it was expected to have smaller maximum deflections than the base model. The results of maximum displacements in these three cases met the expectations in terms of the general trend. However, just like previous section, no linearity was observed. In Cases S3, the shear strength was increased by 11.1% and as the result the maximum displacement at mid-height was reduced by 9.1% whereas in Case S4, despite of increasing the mortar's bond shear strength by 138%, the maximum deflection was reduced by only 3.7%. In other words, the mortar strength in Case S4 was stronger than in Case S3 nevertheless larger maximum displacement was obtained in Case S4. In Case S5, an extremely large value was assigned to the bond's shear strength. As a result not only the 6^{th} layer of mortar joint failed but the whole wall collapsed. Case T5 from previous section has the reverse conditions of Case S5. In case T5 where the bond has maximum tensile strength and a shear strength of 0.63 MPa, only the 6^{th} mortar bond failed and the rest of the wall remained intact. The reason for Case S5 to collapse unlike Case T5 could be due to the bond having smaller tensile strength (0.45 MPa) than bond's shear strength in Case T5 (0.63 MPa). However, more research must be done to be able to determine exactly what happened in this case.

In Cases S1 and S2 the mortar strength was decreased so it was expected to obtain larger maximum displacements than the one from the base model. The results however were

counterintuitive since in both cases the maximum deflections were smaller than the value from the baseline model.

Overall as discussed earlier in Section 5.1.1.1, what is consistent among all the cases (except S5) is that the midpoint displacement response seems insensitive to variations of mortar strength because the load is large enough that no matter how strong the mortar is, the mortar joint subjected to highest pressure (the 6^{th} layer) would definitely fail and therefore the maximum displacement at half a block below that mortar layer would not be influenced by the mortar strength.

5.1.1.3. Combined Tensile Strength and Shear Strength

In Sections 5.1.1.1 and 5.1.1.2 the effect of variations in mortar's tensile strength and shear strength on the behaviour of the wall was examined. Change in either tensile or shear strength separately did not seem to have significant effects. Therefore, in this section both contributing parameters in mortar joint bond strength are changed through the following three cases. In Case TS1, both parameters are dramatically decreased simulating a situation where the mortar joints contain basically no bond strength. In Case TS2, both NFLS and SFLS decreased from the baseline model representing a weaker mortar bond. Case TS3, has a stronger mortar bond than the baseline model due to increasing both NFLS and SFLS. In Case TS4, both parameters are dramatically increased to very large values to simulate an extremely strong mortar bond.

- Case TS1: NFLS= 1E-10 MPa, SFLS= 1E-10 MPa
- Case TS2: NFLS= 0.4 MPa, TS3= 0.5 MPa
- Case TS3: NFLS= 1.0 MPa, SFLS= 1.5 MPa

- Case TS4: NFLS= 1E+3 MPa, SFLS= 1E+3 MPa

Figure 5-4 shows the displacement response plots against the displacement time history obtained by the baseline model.

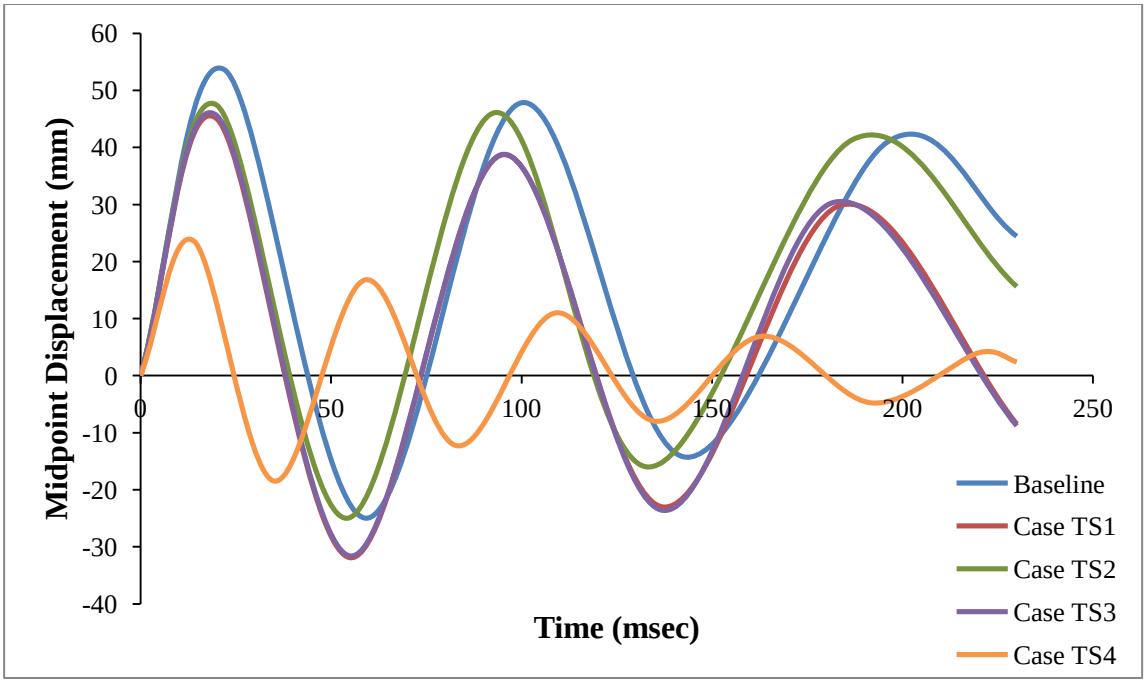

Figure 5-4. Effect of variation in mortar's strength on displacement time history

From figure above it can be observed that Cases TS1, TS2, and TS3 produce results comparable to the base model. Case TS4 on the other hand, illustrates much smaller maximum displacement which is what expected since the mortar strength was extremely large. The maximum mid-height displacement in Case TS4 is 23.6 mm which is 56% smaller than the maximum deflection obtained by the baseline model.

Table 5-3 summarizes the point to point comparisons between the peak displacements for Cases TS1, TS2 and TS3. Case TS4 is not included in the table since the values are quite different than the others so the close comparison is not required.

Table 5-3. Comparisons between peak deflections on displacement time histories when mortar strength is varied

Baseline		Case TS1			Case TS2			Case TS3		
T	D	T	D	E	T	D	E	T	D	E
22	53.6	20	45.0	16.0	20	47.4	11.6	20	45.6	14.9
59	-25.0	55	-31.9	27.6	54	-25.0	0	55	-31.6	26.4
100	47.8	95	38.7	19.0	93	46.1	3.6	95	38.8	18.8
143	-14.3	137	-23.0	60.8	133	-16	11.9	137	-23.6	65.0
196	40.9	184	29.9	26.9	187	41.4	1.2	182	30.4	25.7

In Case TS2, mortar bond was stronger than in Case TS1 nevertheless the maximum displacement was 5.3% higher than Case TS1's displacement. The bond strength in Case TS2 was still lower than what it was in the baseline model but it resulted in lower displacement than that in the base model by 11.6%. The results from Case TS3 followed the expectations. The mortar strength was increased in this case compared to both Case TS2 and baseline model and the maximum deflection obtained by Case TS3 was lower than that in other two cases. Maximum displacement was 14.9% less than that in the base model and 3.8% lower than that in Case TS2. In case TS1 when the mortar bond has

basically no strength almost the same displacement is obtained compared to other cases where certain strength is assigned to the mortar bond.

From all above it is yet again concluded that despite obtaining some counterintuitive results in some cases, overall the mid-height maximum displacement of this wall subjected to such large blast load is not really influenced by mortar strength. The only time that major difference in the maximum deflection was detected was in a case where the mortar was unrealistically strong.

To summarize, in Sections 5.1.1.1, 5.1.1.2, 5.1.1.3 the effect of different mortar strengths on the behaviour of the masonry wall in terms of midpoint maximum displacement when the wall was subjected to a blast load resulted from 80 Kg ANFO at a 15 metre distance (3.5 m/$Kg^{1/3}$ scaled distance) was examined.

First, five cases (T1-T5) were considered in which the shear strength of the bond was remained the same as that in the base model while the tensile strength was altered. The maximum displacement results from these cases were all very close to each other and the result from the main model. Such results suggested that the mortar bond which was defined by tiebreaks in contact surfaces in LS-DYNA between the 6^{th} and 7^{th} course of the wall failed. Hence, the maximum displacement at the wall's mid-height which was only half a block below this failed mortar layer remained unaffected by the mortar strength.

In the second stage of this sensitivity analysis, another five cases (S1-S5) were considered. This time the mortar strength was altered by changing the bond's shear strength when the tensile strength remained constant. The results from the first four cases

(S1-S4) were again very similar and matched the results from the previously considered five cases (T1-T5) which suggested the same conclusion. However, in Case S5, the wall's behaviour was extremely different since it entirely failed and all the blocks got unattached and flew apart. This was a quite unexpected result since the mortar bond in this case was much stronger than the bond in the baseline model so perhaps more tests must be done in order to be able to explain such behaviour.

In the last stage in the parametric study, the mortar strength of altered by simultaneous change of bond' both tensile and shear strengths. Four cases (TS1-TS4) were considered for which the results were yet again in consistency with the other cases studied in the first and second stages. In the first three cases, the displacement time histories were again almost in close agreement with the displacement response from the main model. The last case however resulted in much smaller deflection which was due to its extremely strong mortar bond which allows it to resist higher stresses compared to other cases.

Based the results of this parametric study it is concluded that the wall's behaviour subjected to this large blast load is not affected by the mortar strength. As described in Section 3.7.4, the mortar bond is defined by tiebreak in contact surfaces in LS-DYNA. For the tiebreak failure to occur, first the stress failure criterion defined by Equation 10 must be met. Since the stresses from the blast load that are applied to the mid-height mortar joint (between 6^{th} and 7^{th} layer) are much higher than the bond's failure stresses, the stress failure criterion defined by Equation 10 is always met. Once this criterion is met, the tiebreak failure is not complete until the distance between the points initially in contact becomes larger than the critical distance defined by PARAM which was set to 10

mm. It is obvious from that gap opening is larger than 10 mm (the original mortar bond thickness). Hence, it is clear that since all the criteria are met, the tiebreak failure fully develops at the 6th layer mortar joint. Once the tiebreak failure happens, frictional forces are what the surfaces rely on to remain in contact. So it is concluded that when the wall is subjected to such a blast load, the 6th layer mortar joint fails (tiebreak fails) no matter how strong the mortar bond is. Hence, the maximum displacement at the mid-height which is only half a block below the failed mortar joint is not sensitive to mortar strength which is the reason for obtaining very similar displacement time histories in all the cases considered above.

5.1.2. Influence of Friction Parameters

In this section is concentrated on the effects of friction between the CMU blocks on the behaviour of the wall subjected to blast loads. Friction was defined through contact surface cards in LS-DYNA input deck. As discussed previously in Section 3.7.2, the coefficient of friction is formulated based on which depends on static coefficient of friction, dynamic coefficient of friction, decay coefficient and the relative velocity between the CMU bocks in contact. The parametric study conducted in this section aims to capture a better understanding about the influence of static and dynamic coefficients of friction in particular.

5.1.2.1. Static Coefficient of Friction

The static coefficient of friction (FS), dynamic coefficient of friction (FD) and decay coefficient (DC) in the base model was taken as 0.6, 0.4 and 0.35 respectively. In order

to examine how the variation of static coefficient would affect the wall's behaviour four case studies are considered in which the FD and DC are kept the same as in the base model while FS is changed.

- Case 1: FS= 0.4, FD= 0.4, DC= 0.35
- Case 2: FS= 0.5, FD= 0.4, DC= 0.35
- Case 3: FS= 0.7, FD= 0.4, DC= 0.35
- Case 4: FS= 0.8, FD= 0.4, DC= 0.35

The displacement time histories of the case studies above are plotted in Figure 5-5 to be compared with the baseline model's results.

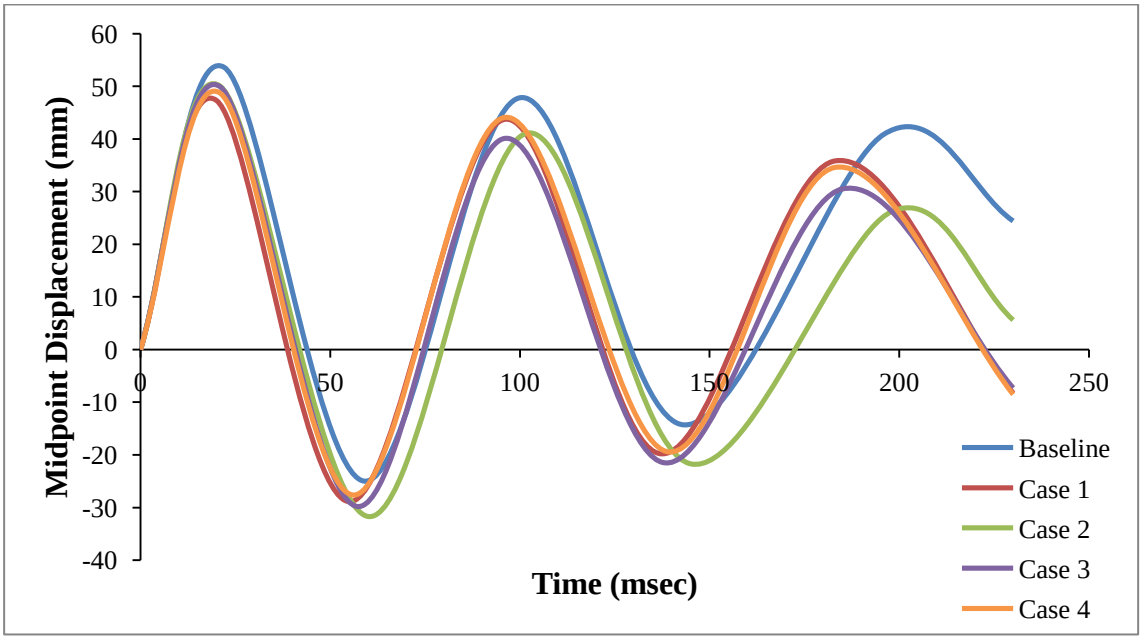

Figure 5-5. Displacement response curves for walls with different static coefficients of friction

It can be observed from the graphs above that all the displacement results match closely which implies that the maximum displacement is not sensitive to changes in static coefficient of friction as long as a non-zero value between 0.4 and 0.8 is selected. Table 5-4 summarizes the detailed peak displacement comparisons.

Table 5-4. Comparison between peak displacements when FS is varied

Baseline		Case1: FS=0.4			Case2: FS=0.5			Case 3: FS=0.7			Case 4:FS=0.8		
T	D	T	D	E	T	D	E	T	D	E	T	D	E
22	53.6	20	47.3	1.2	21	50.0	6.7	21	49.9	6.9	21	48.7	9.1
59	-25.0	55	-28.9	1.6	60	-31.7	26.8	57	-29.8	19.2	56	-27.6	10.4
100	47.8	96	43.7	0.9	102	41.1	14.0	96	40.1	16.1	96	44.1	7.7
143	-14.3	137	-19.8	3.8	145	-21.7	51.8	138	-21.5	50.3	139	-19.4	35.7
196	40.9	183	35.8	1.2	198	26.2	35.9	185	30.5	25.4	183	34.6	15.4

In the first two cases FS is decreased relative to the value in the base model when in the last two cases this value is increased which did not agree with what was expected. Since the only parameter that is being varied is FS, it is expected from Equation 9 that by decreasing FS, coefficient of friction would also decrease (assuming the relative velocity remains the same) which will result in larger displacements. On the other hand the results from Cases 3 and 4 not only agreed with the expectations, i.e. the larger the static coefficient of friction the smaller the maximum displacement. FS was increased by 16.7% and 33.3% in Cases 3 and 4 respectively which resulted in decrease of maximum displacement by 6.9% and 9.1% respectively. However, it should be noted that despite obtaining counterintuitive results in Cases 1 and 2, the difference between maximum displacements is very small. Hence, the original conclusion remains valid: the maximum displacement of the wall subjected to the blast load is not sensitive to small variations of static coefficient of friction and as long as FS assumes a non-zero positive value between 0.4 and 0.7, similar maximum deflections would be obtained.

5.1.2.2. Dynamic Coefficient of Friction

In contrast with previous section, here the effect of variation in dynamic coefficient of friction on the behaviour of the wall is studied. For this purpose four cases are considered where FS and DC are kept unchanged relative to the base model and only FD is varied.

- Case 1: FS= 0.6, FD= 0, DC= 0.35
- Case 2: FS= 0.6, FD= 0.3, DC= 0.35
- Case 3: FS= 0.6, FD= 0.5, DC= 0.35
- Case 4: FS= 0.6, FD= 0.6, DC= 0.35

The results from these cases indicate that the wall completely fails when the dynamic coefficient of friction is less than 0.4. In fact in Case 1 where FD is considered zero, the wall fails as the result of applied blast pressure. Therefore, the plot in Figure 5-6 is mainly representing the displacement time history of the middle block rather than the wall's midpoint displacement since the wall clearly has already failed once it reached 190 mm displacement (Drysdale and Hamid, 2005).

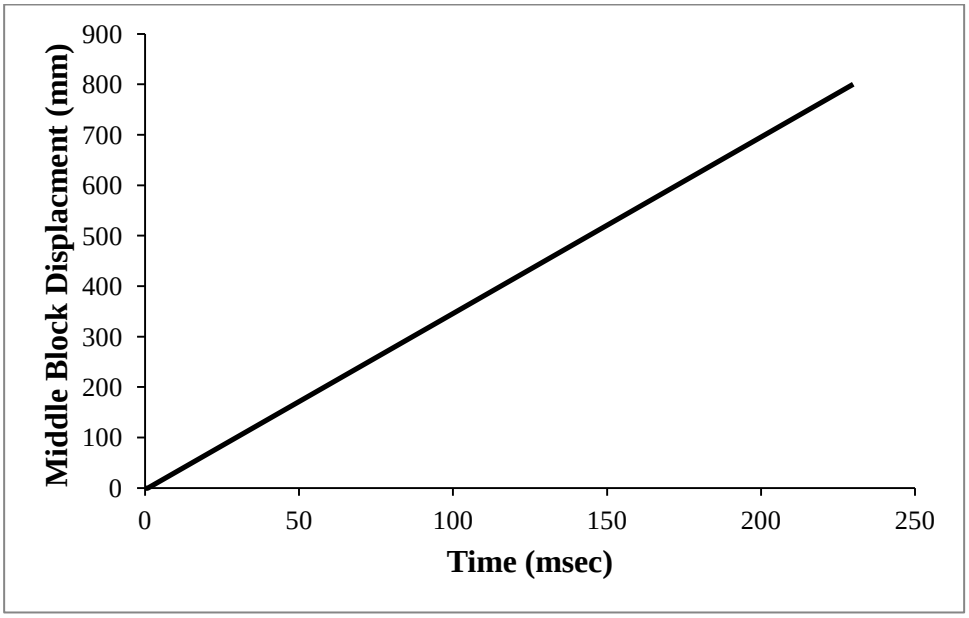

Figure 5-6. Displacement time history for Case 1 (FD=0)

The results from Cases 2, 3 and 4 are presented in Figure 5-7 below:

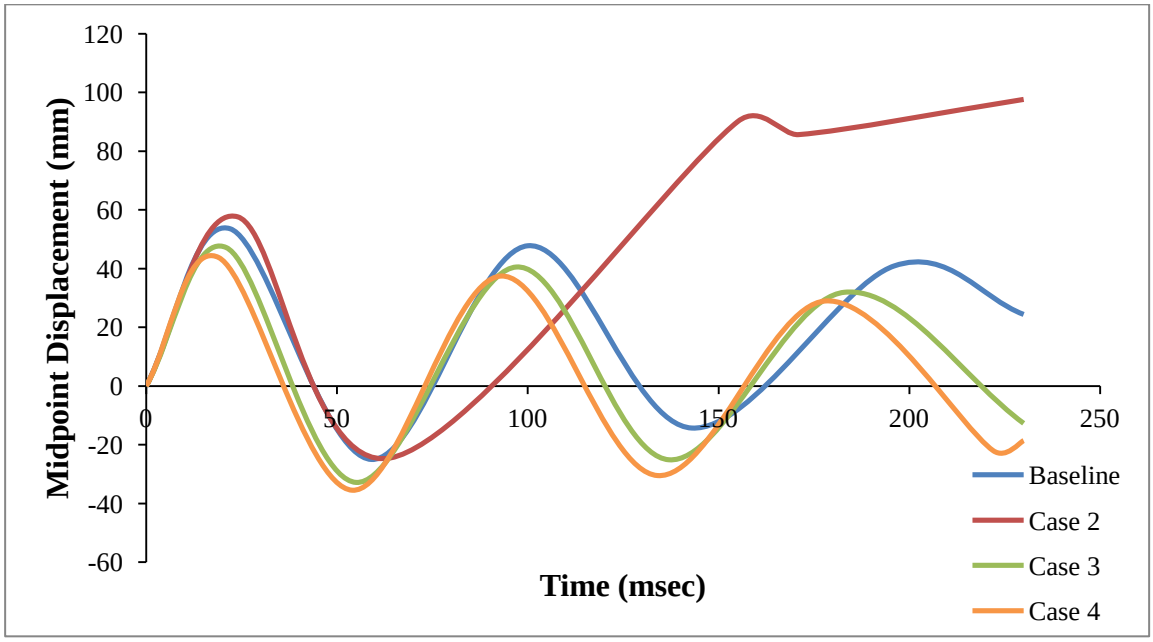

Figure 5-7. Displacement response curves for walls with different dynamic coefficients of friction

As explained in Section 3.7.4, when the blast pressure is applied if the mortar joint fails and the tiebreak failure occurs, frictional forces come into play in order to keep the surfaces in contact. If the coefficient of friction (μ_C) which is calculated using Equation 9 is not large enough then the frictional forces would also fail holding the blocks together and the wall collapses. The results from the parametric study in this section indicate that dynamic coefficients smaller than 0.4 will result in insufficient coefficient of friction which leads to insufficient frictional force in order to resist the blast load. In an extreme case like Case 1, the absence of dynamic coefficient will results in a non-ductile failure of the wall. However, this case cannot be considered a representative case since in reality dynamic friction always exists between the blocks. Considering this case in the research emphasizes the importance of including this parameter in simulations of this sort. FD in

Case 2 is not zero but still very small. The displacement response curve indicates that the wall is still not capable of resisting the blast pressure but the failure is more ductile than the case with zero dynamic coefficient of friction. In Cases 3 and 4, FD was increased compared to that in the base model by 25% and 50% respectively which resulted in decrease in the maximum displacement by 12.1% and 18.3% respectively. It should be mentioned that not only the results from Cases 3 and 4 agree with the general expectation of producing less displacement than the base model (due to higher coefficient of friction) but the results between the two cases alone were also intuitive. In Case 4 since the dynamic and static coefficients of friction are the same (0.6) the second term in Equation 9 will be eliminated and therefore the coefficient of friction would be equal to dynamic coefficient of friction. In Case 3 in the other hand, if the relative velocity is equal to zero then the coefficient of friction will be equal to the static coefficient of friction which is again equal to 0.6 which would be the highest possible $\mu_C$that could be produced in this case. Thus, only in a situation where relative velocity is zero both Cases 3 and 4 have the same coefficient of friction and with any other value for relative velocity, Case 3 will have a smaller $\mu_C$than Case 4 which implies that it would have less resistance and therefore would be susceptible to larger displacements and the results from parametric study conducted above shows that maximum deflection in Case 3 is larger than that in Case 4.

Detailed peak displacement comparisons for Cases 3 and 4 against the baseline model are provided Table 5-5:

Table 5-5. Comparison between peak displacements when FD is varied

Baseline		Case3: FD=0.5			Case4: FD=0.6		
T	D	T	D	E	T	D	E
22	53.6	21	47.1	12.1	19	43.8	18.3
59	-25.0	55	-32.8	31.2	54	-35.5	42
100	47.8	97	40.5	15.3	93	37.5	21.6
143	-14.3	137	-25.1	75.5	134	-30.5	113.0
196	40.9	183	31.9	22.0	178	29.0	29.1

Overall in can be concluded that there is an inverse correlation between the maximum deflection and dynamic coefficient of friction, i.e. with the increase of FD maximum displacement is decrease. Also by comparing the results from this section and Section 5.1.2.1, it can be concluded that the behaviour of the wall is more influenced by variations in dynamic coefficient of friction as opposed to static coefficient of friction. However, the difference between the FS and FD plays an important role since the second term in Equation 9 is highly dependent on it.

5.1.2.3. Exponential Decay Coefficient

The last friction parameter whose influence on the wall behaviour is studied in this parametric study is the decay coefficient (DC). In order to examine the impact of decay coefficient on the coefficient of friction and therefore the displacement three cases are considered in which FS and FD are remained the same as before while DC is varied.

- Case 1: FS= 0.6, FD= 0.4, DC= 0

- Case 2: FS= 0.6, FD= 0.4, DC= 0.25
- Case 3: FS= 0.6, FD= 0.4, DC= 0.45

The displacement response curves at wall's mid-height in these three cases are plotted in Figure 5-8 below:

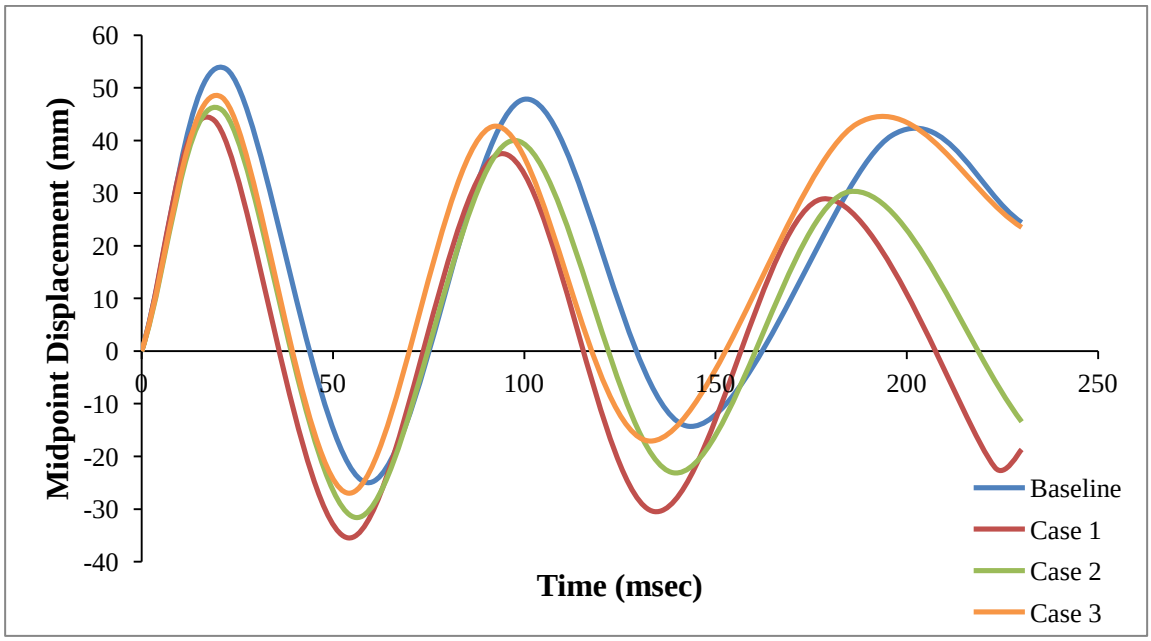

Figure 5-8. Displacement response curves for walls with different Decay coefficients

The displacement results from all the three cases are very similar and comparable to the base model. The detailed point-to-point comparisons of the peak deflections are provided in Table 5-6.

Table 5-6. Comparison between peak displacements when DC is varied

Baseline		Case 1: DC=0			Case 2: DC=0.25			Case 3: DC=0.45		
T	D	T	D	E	T	D	E	T	D	E
22	53.6	19	43.8	18.3	21	45.8	14.6	21	48.2	10.1
59	-25.0	54	-35.5	42.0	56	-31.6	26.4	54	-27.0	8.0
100	47.8	94	37.5	21.5	97	40.0	16.3	92	42.7	10.7
143	-14.3	134	-30.5	113.3	139	-23.1	61.5	133	-17.1	19.6
196	40.9	178	28.9	29.3	185	30.3	25.9	187	43.2	5.6

It can be observed from the results that by increasing the decay coefficient the displacement is increased due to decreasing the coefficient of friction μ_C. In Case 1, DC was reduced to zero and as the result maximum displacement was reduced by 18.3% compared to the base line model. Case 1 has the highest coefficient of friction since $\mu_C$in this case is always 0.6 and not dependent on FS and relative velocity. In Cases 2, 3 and in the base model, maximum μ_C would be 0.6 corresponding to a situation with zero relative velocity between the surfaces in contact. If relative velocity is anything but zero, Case 2 would have the highest μ_C, then the baseline model and Case 3 would have the smallest value (assuming relative velocity is the same in all cases). In Case 2, DC is decreased from the value in the baseline model by 28.6% and as the result the maximum deflection is reduced by 14.6% which matches the expectations since the coefficient of friction in this case is higher than that in the base model. Also, as expected, the deflection in Case 2 exceeds the value in Case 1 due to having lower μ_C. Case 3, has a 28.6% higher decay

coefficient than the base model. The maximum deflection in this case found to be 48.2 mm. This shows that the maximum deflection in Case 3 is 10% lower than the baseline model which is counterintuitive since the coefficient of friction in this case is smaller than that in the base model. However, with respect to Case 2, it still has a higher deflection with agrees with the expectations since the coefficient of friction was smaller than in Case 2. However, it should be noted that all the comparisons between the μ_C in different cases were based on the assumption of having the same relative velocity which could easily not be the case. Hence, it cannot be said with confidence whether or not Case 3 has smaller μ_C than the baseline model.

Overall from the results of the parametric study in this section it can be concluded that the maximum displacement tend to increase with the increase of decay coefficient.

5.2. Influence of Scaled Distance

In the baseline model the blast load was generated by detonation of 100 Kg ANFO equivalent to 80 Kg TNT at a standoff distance of 15 m. Therefore, the scaled distance (Z) found by Equation 3 would be 3.5 m/kg$^{1/3}$. In this section the effect of change in scaled distance on the wall's response is investigated. For this purpose eight cases are considered:

- Case 1: Z= 1.0 m/kg$^{1/3}$
- Case 2: Z= 2.0 m/kg$^{1/3}$
- Case 3: Z= 2.5 m/kg$^{1/3}$
- Case 4: Z= 3.0 m/kg$^{1/3}$
- Case 5: Z= 4.0 m/kg$^{1/3}$

- Case 6: Z= 5.0 m/kg$^{1/3}$
- Case 7: Z= 6.0 m/kg$^{1/3}$
- Case 8: Z= 7.0 m/kg$^{1/3}$

Mid-height displacement response curves of the cases above are plotted against the baseline displacement time history in Figure 5-10. However, the response curve for Case 1 which is provided in Figure 5-9 is mainly representing the displacement time history of the middle block rather than the wall's midpoint displacement due to the fact that the wall has already failed once it reached 190 mm displacement (Drysdale and Hamid, 2005).

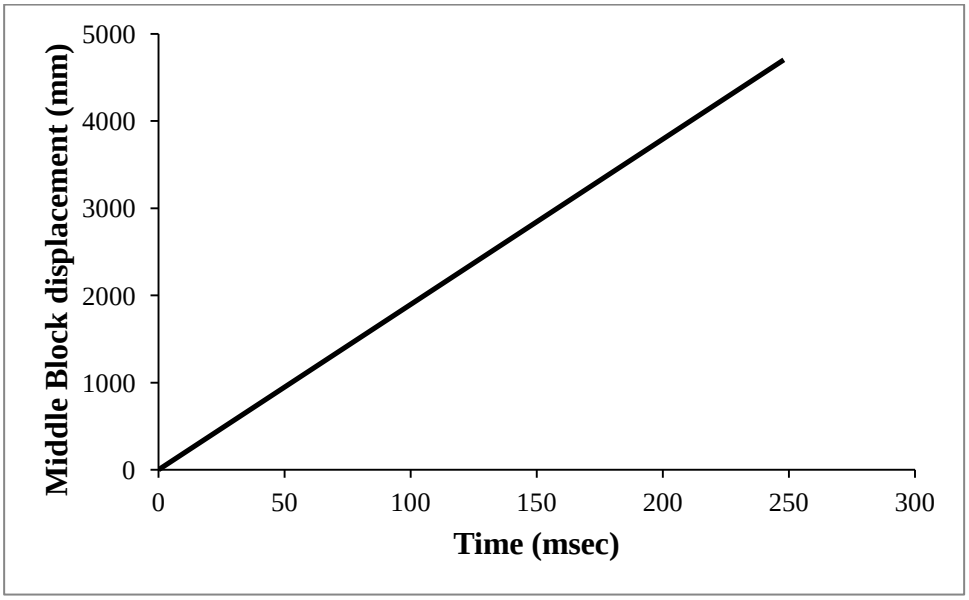

Figure 5-9. Displacement time history for Case 1

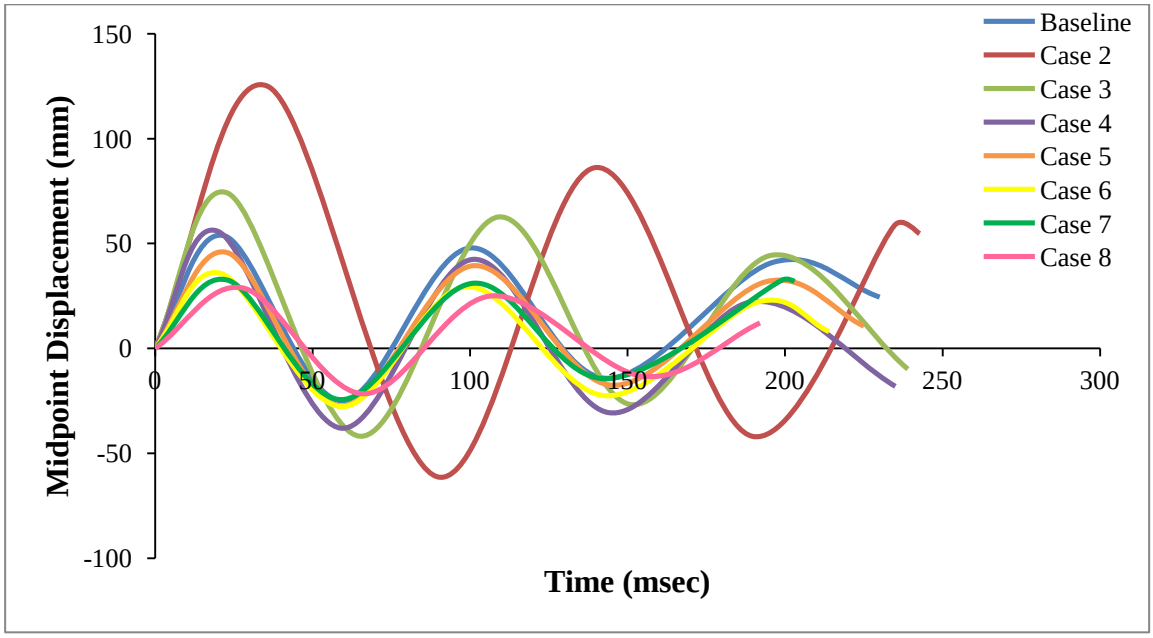

Figure 5-10. Midpoint displacement time histories for walls subjected to blast loads with different Z

The arrival times are subtracted from the times in the plots above. However, due to having a different arrival time in each case due to various scaled distances, the curves do not end at similar times even though the run time for all the cases have been the same. It can be observed from figure above that the peak displacement decreases with the increase of scaled distance. In Case 1 when the scaled distance is very small (Z=1 m/kg$^{1/3}$) the wall is not able to resist the applied blast load and collapsed completely. The blast wave arrival time in this case is the shortest of all cases and the blast pressure on the wall is the highest. As Z increase in Cases 2, 3 and 4, the peak displacement decreases but since in these cases scaled distance is still smaller than that in the baseline model, the corresponding maximum displacements are still larger than in the baseline model (53.6 mm). In Cases 5, 6, 7 and 8 scaled distance keeps increasing and as the result the peak displacements keep decreasing and because in these cases Z is larger than in the base

model, the corresponding maximum displacements are smaller than 53.6. It should be mentioned that the results indicate that smaller values for scaled distance have stronger effects on the maximum deflection than larger values. Figure 5-11 shows the peak displacement for various scaled distances.

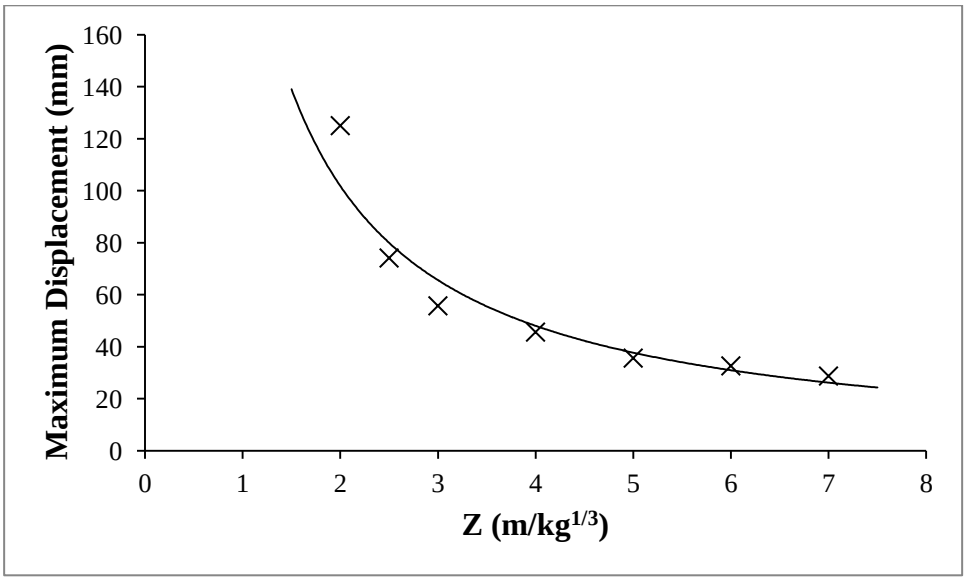

Figure 5-11. Maximum displacements resulted from various scaled distances

It is concluded that variations in scaled has noticeable influence on the wall's behaviour under blast. In fact an inverse correlation was found between maximum displacement and scaled distance i.e. as the scaled distance increases the peak displacement decreases.

5.3. Influence of Boundary Conditions

The wall in the base model was modeled in a way that nodes at top and bottom ends of the wall were free to rotate so that the wall could have an arching action. Thus, the boundary condition imposed on the wall in the base model simulated hinges at top and

bottom ends of the wall where translational constraints were imposed in x, y and z direction but no rotational constraints were applied.

In this section the influence of different boundary conditions on the behaviour of the wall is studied. In addition to the baseline model where only translational constraints were applied three other cases are considered. Table 5-7 shows the details of boundary conditions in each case:

Table 5-7. Bottom and top boundary conditions

Case	Bottom constraints	Top constraints
1	rotational and translational	translational
2	rotational and translational	rotational and translational
3	translational	rotational and translational

The displacement time history from all these three cases turn out to be identical to the baseline model. This might be attributed to the fact that fixing the top and bottom blocks would not result in appreciable fixation of other wall blocks as the mortar cracks would form immediately above or immediately below the bottom and top boundary blocks, respectively; in essence, reducing the wall height to nine courses. So even in cases where there are rotational constraints on the boundary blocks, the other wall blocks have freedom to rotate.

5.4. Influence of Wall Height

In this section the effect of wall height on the wall's behaviour subjected to blast load is analyzed. For this purpose six cases are considered in which the width of the wall is remained constant (995 mm) while the height is altered. The first three cases consider walls shorter than that in baseline model (2190 mm) and the last three cases assume heights taller than the original height. Table 5-8 summarizes the details of each case:

Table 5-8. Walls with different heights

Case	Number of courses	Wall height (mm)
1	3	590
2	5	990
3	7	1390
4	13	2590
5	15	2990
6	17	3390

In Case 6 the blast load results in complete collapse of the wall. Therefore, the plot in Figure 5-12 mainly shows the wall's middle block displacement time history rather than the wall's midpoint displacement since the walls has already failed by the time it reached 190 mm displacement (Drysdale and Hamid, 2005).

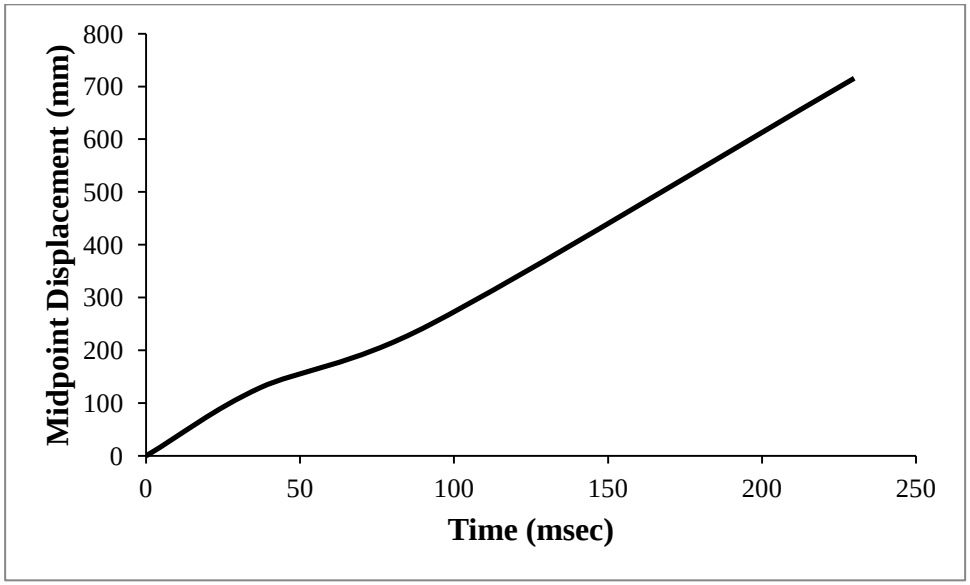

Figure 5-12. Displacement time history for Case 6

The midpoint displacement time histories corresponding to the other five cases are plotted against the baseline model's displacement response curve in Figure 5-13:

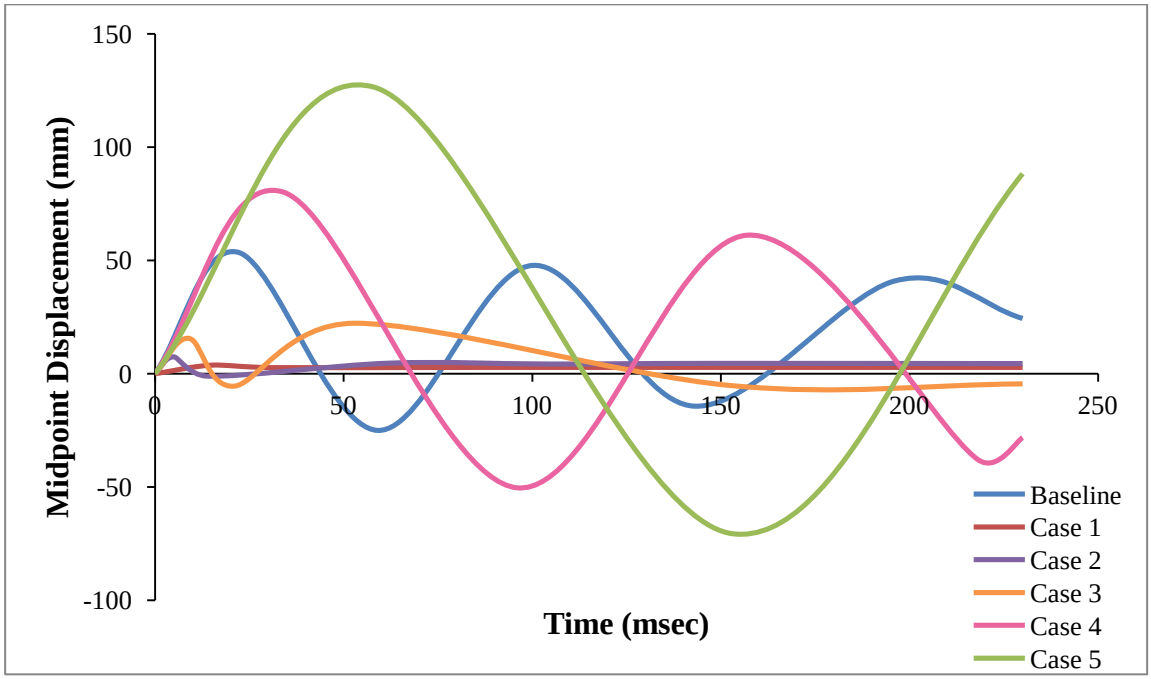

Figure 5-13. Midpoint displacement time histories for walls with different heights

The displacement responses from all the cases above indicate that there is a direct correlation between the height of the wall and the maximum displacement, i.e. the taller the wall the larger the peak displacement. Figure 5-14 shows the peak displacement for walls with various heights.

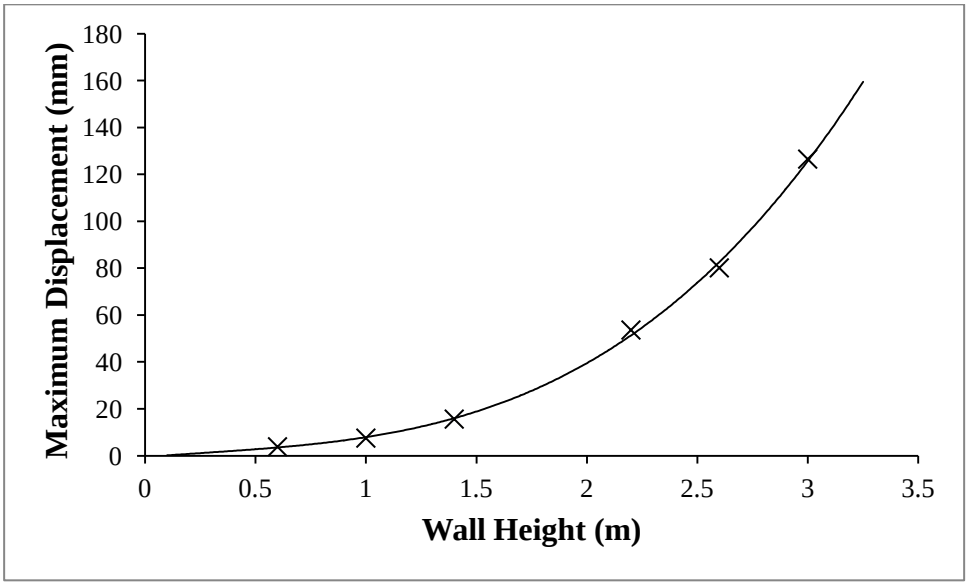

Figure 5-14. Maximum displacement for walls with different heights

The maximum displacement in Cases 1 and 2 where the height was less than 1 m was 3.8 mm and 7.5 mm, respectively, which is almost negligible. The peak displacement increased to 15.6 mm, 80.1 mm and 126.5 mm in Cases 3, 4 and 5 respectively. The wall in Case 6 which was 3.4 m failed completely under the subjected blast load. It is concluded that the wall's behaviour in terms of maximum displacement is highly sensitive to the height. Shorter walls are found to be less susceptible to larger displacements which is due to increase in their stiffness which leads into higher resistance against blast loads.

It should be noted that this is only a virtual parametric study with the goal of identifying the effect of a parameter (wall height) on the wall behaviour and of course such short walls in Cases 2 and 3 are not really practical to use in many structures and they have been included in this study only for completeness.

5.5. One-way Versus Two-way Arching Action

In the model developed in Chapter 3, boundary conditions were applied only to the top and bottom ends of the wall in order to simulate a one-way action. In this section, the left and right edges of the wall are restrained in addition to top and bottom to simulate a two-way behaviour. No gap is provided between the left and right boundaries in order to maintain the arching effect in a two-way manner. As explained before, in one-way arching action the wall will snap at the middle and essentially will be divided into two rigid segments about the wall's horizontal axis. For this mechanism to occur, both rigid segments must be able to rotate at the connection to the top and bottom supports which is the reason for applying a pin-pin boundary condition to the baseline model. In a two-way action, similar mechanism happens except that the wall is divided into two segments about its vertical axis. This implies that the two rigid segments must be free to rotate at the left and right ends of the wall. In order to achieve this, a node set on each side of the wall is defined. Similar to the boundary condition at top and bottom of the wall, translational constraints in x, y and z direction are applied to the nodes while no rotational constraints are imposed.

The mid-height displacement time history is plotted against the displacement response curve from the baseline model in Figure 5-15:

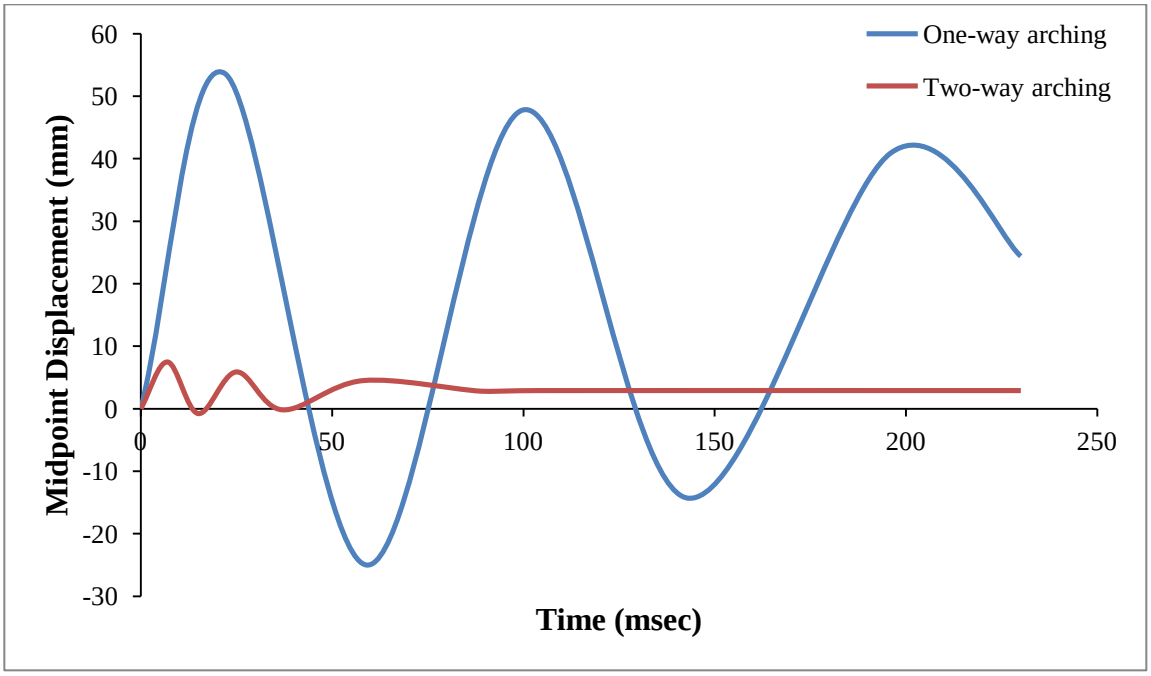

Figure 5-15. One-way versus two-way arching action midpoint displacement time histories

It is obvious from the plot above that there is a considerable difference between the displacement responses of one-way and two-way arching walls. The maximum displacement in the two-way action has been reduced significantly to a value of 7.5 mm which so small relative to the thickness of the wall that it can almost be ignored. In fact the deflected shape of the wall looked identical to its state prior to the blast load applications.

Although two-way arching was shown to exist for walls with aspect ratios more than 2.0 (Drysdale and Hamid, 2005), one can rationalize the low value of the maximum deflection by considering the two-way wall to act essentially as a one-way arching wall in the short direction. This is also justified by the fact that the 7.5 mm deflection of the two-way arching wall corresponds well with the deflection of Case 2 in Table 5-8.

6. Conclusions

6.1. Summary and conclusions

In this thesis a finite element model was developed to evaluate the behaviour of a one-way unreinforced masonry arching wall subjected to blast load using an advanced finite element modeling program LS-DYNA. The wall which was modeled based on a physical blast test was 2.5 blocks wide and 11 courses tall and was subjected to a blast load from detonation of 100 Kg ANFO at a 15 m standoff distance. The main objective of this research was to develop a finite element model whose results are accurate and reliable. In order to validate the model, the results from the simulation were compared with the experimental results in terms of wall's mid-height displacement response. The simulation results found to be in close agreement with experimental results. Therefore, it was concluded that developed finite element model was valid and reliable to predict the true response of the wall subjected to such blast loads. This model was then selected as a baseline model on which an input sensitivity study was conducted. In the parametric study, some parameters of the baseline model were systematically altered and the effects of such variation on the wall's displacement response were studied. The input parameters considered included mortar strength, friction parameters, boundary conditions, wall's aspect ratio and two-way arching. It was concluded that in this particular loading case, the wall's response is not affected by variations of mortar strength. The reason seemed to be that the failure of the mortar joint at the mid-height of the wall (where is susceptible to

largest blast pressure) will fail when the wall is subjected to such high blast pressures and therefore slightly higher or lower bond strength does not have a significant effect.

In order to study the effects of friction, static coefficient of friction, dynamic coefficient of friction and decay coefficient was varied. It was concluded that variations in friction parameters did not result in major changes to the wall's response. However, the absence of coefficient of friction (FD in particular) will result in total collapse as there will be nothing to hold the wall intact since the mortar bond always fail before frictional forces come to play.

Scaled distance found to have noticeable effect on the wall's response. Inverse correlation was observed between scaled distance and maximum displacement. Small scaled distances resulted in very large deflections and as Z increased maximum deflection decreased.

The effects of different boundary conditions were also examined. However, since in this particular case, the presence of rigid brackets at both ends of the wall with no gap considered, the rotation was limited. As a result, changing the boundary conditions from only translational constraints to both translational and rotational constraints did not influence the response.

The effect of change in wall height on the response was also studied. It was concluded that as the wall height increases the mid-height deflection also increase. It was observed that the maximum deflection for walls with heights less than 1 m was negligible.

Finally the effect of two-way versus on-way arching was examined. For this purpose, similar boundary conditions to top and bottom of the wall (translational constraints) were

applied on the left and right sides of the wall to simulate two-way arching. The results showed that two-way arching action can significantly reduce the deflection. The two-way arching mechanism enabled the wall to almost completely resist the applied blast load.

6.2. Recommendations for Future Work

In order to conduct a more accurate finite element analysis and hence have a better representation of the physical problem, the following recommendations for further research are proposed:

- Additional parameters such as wall thickness, blocks' material strength, strain rate effects, etc. should be included in parametric study in order to provide better insight into the influence of dominant parameters on wall's response.
- Pressure-impulse diagrams could be generated for the wall modeled in this thesis. This can be done by defining a certain level of damage and then applying different blast loads on the wall. This process could be very time consuming but once enough data points are created, the P-I diagram can be plotted by connecting the points that has the same damage as the damage criteria. Therefore, P-I diagram indicates the combinations of pressures and impulses that produce failure. This can be done to obtain several P-I diagrams associated with different damage levels which would be extremely useful in terms of predicting structural damage caused by a certain loading case. Such numerically produced P-I diagrams are incredibly valuable since it is extremely difficult to collect all the required data to generate P-I diagrams experimentally.

Bibliography

Abou-Zeid, Badr M., El-Dakhakhni, Wael W., Razaqpur, Ghani A., and Foo, S. "Response of Arching Unreinforced Concrete Masonry Walls to Blast Loading." *Journal of Structural Engineering* (2010).

Adoum, Melissa, and Lapoujade, Vincent. "Examples Manual for *User_Loading Option." In *4th European LS-DYNA Users Conference*. Germany, 2003.

Baker, W. E. *Explosions in Air*. Austin: University of Texas Press, 1973.

Baker, W.E., Cox, P.A., Westine, P.S., Kulesz, J.J., and Strehlow, R.A. *Explosion Hazards and Evaluation* Fundamental Studies in Engineering: Elsevier Scientific Publishing Company, 1983.

Bala, S. "Contact Modeling in Ls-Dyna." *FEA Information International News* (2001).

Baylot, James T., Bullock, Billy, Slawson, Thomas R., and Woodson, Stanley C. "Blast Response of Lightly Attached Concrete Masonry Unit Walls." *Journal of Structural Engineering* 131, no. 8 (2005): 1186-1193.

Burnett, S., Gilbert, M., Molyneaux, T., Beattie, G., and Hobbs, B. "The Performance of Unreinforced Masonry Walls Subjected to Low-Velocity Impacts: Finite Element Analysis." *International Journal of Impact Engineering* 34, no. 8 (2007): 1433-1450.

Chaimoon, Krit, and Attard, Mario M. "Modeling of Unreinforced Masonry Walls under Shear and Compression." *Engineering Structures* 29, no. 9 (2007): 2056-2068.

Chang, David B., and Young, Carl S. "Probabilistic Estimates of Vulnerability to Explosive Overpressures and Impulses." *Journal of Physical Security* (2010).

Davidson, James S., Porter, Jonathan R., Dinan, Robert J. , Hammons, Michael I., and Connell, James D. "Explosive Testing of Polymer Retrofit Masonry Walls " *Journal of Performance of Constructed Facilities* 18, no. 2 (2004): 100-106.

Davidson, James S., Sudame, Sushant, and Dinan, Robert J. *Development of Computational Models and Input Sensitivity Study of Polymer Reinforced Concrete Masonry Walls Subjected to Blast*. Birmingham: University of Alabama at Birmingham, 2004.

Dawe, J. L. , and Seah, C. K. . "Out-of-Plane Resistance of Concrete Masonry Infilled Panels." *Canadian Journal of Civil Engineering* 16, no. 6 (1989): 854-864.

Dennis, Scott T., Baylot, James T., and Woodson, Stanley C. "Response of 1/4-Scale Concrete Masonry Unit (Cmu) Walls to Blast." *Journal of Engineering Mechanics* 128, no. 2 (2002): 134-142.

Drysdale, Robert G., and Hamid, Ahmad A. *Masonry Structures Behaviour and Design*. Mississauga, Ontario: Canada Masonry Design Centre, 2005.

Dynasupport, LS-DYNA Support. *Hourglass* 2011, accessed July 22, 2011 http://www.dynasupport.com/howtos/element/hourglass.

Eamon, Christopher D., Baylot, James T., and O'Daniel, James L. "Modeling Concrete Masonry Walls Subjected to Explosive Loads." *Journal of Engineering Mechanics* 130, no. 9 (2004): 1098-1106.

El-Dakhakhni, W. W., Mekky, W. F., and Rezaei, S. H. Changiz. "Validity of SDOF Models for Analyzing Two-Way Reinforced Concrete Panels under Blast Loading." *Journal of Performance of Constructed Facilities* 24, no. 4 (2010): 311-325.

ETA, Engineering Technology Associates, Inc. "eta/Vpg User's Manual, a Mechanical System Simulation Software " (2004).

ETA, Engineering Technology Associates, Inc., Concept to Product. *eta/VPG Version 3.4* 2011, accessed July 18, 2011 http://www.eta.com/index.php/software/vpg.

Forsen, R. "Airblast Loading of Wall Panels." *FOA Rep. C 20586-D6.* National Defence Research Institute, Stockholm, Sweden (1985).

Gabrielsen, Bernard L., Wilton, C., and Kaplan, Kenneth. *Response of Arching Walls and Debris from Interior Walls Caused by Blast Loading*. San Mateo, California: URS Research Co., 1975.

Gilbert, M., Hobbs, B., and Molyneaux, T. C. K. "The Performance of Unreinforced Masonry Walls Subjected to Low-Velocity Impacts: Experiments." *International Journal of Impact Engineering* 27, no. 3 (2002): 231-251.

Hao, Hong. "Numerical Modelling of Masonry Wall Response to Blast Loads.(Technical Report)." *Australian Journal of Structural Engineering* 10, no. 1 (2009): 37(17).

Henderson, R. C. , Fricke, K. E., Beavers, J. E. , and Bennett, R. M. . "Summary of a Large- and Small-Scale Unreinforced Masonry Infill Test Program." *Journal of Structural Engineering* 129, no. 12 (2003): 1667-1675.

Hetherington, J. G., and Smith, P. D. *Blast and Ballistic Loading of Structures* Butterworth-Heinemann, 1994.

Hyde, D. W. "Conwep-Conventional Weapons Effects Computer Code." *US Army Engineer Waterways Experimental Station* (1991).

LSTC, Livermore Software Technology Corporation. *Ls-Dyna Theory Manual*. Livermore, California, 2006.

LSTC, Livermore Software Technology Corporation. *Ls-Dyna Keyword User's Manual-Version 971* Livermore, California, 2007.

LSTC, Livermore Software Technology Corporation. *Ls-Prepost Online Documentation: About Ls-Prepost* Livermore, California: 2011, accessed July 18, 2011 http://www.lstc.com/lspp/.

Ma, Guowei, Hao, Hong, and Lu, Yong. "Homogenization of Masonry Using Numerical Simulations." *Journal of Engineering Mechanics* 127, no. 5 (2001): 421-431.

Mays, G. C., and Smith, P. D. *Blastt Effects on Buildings*, 1995.

McDowell, E. L., McKee, K. E., and Sevin, E. "Arching Action Theory of Masonry Walls." *Journal of the Structural Division: Proceedings of the American Society of Civil Engineers* 82, no. 2 (1956): 1-8.

Moradi, Lee G., Davidson, James S., and Dinan, Robert J. "Resistance of Membrane Retrofit Concrete Masonry Walls to Lateral Pressure." *Journal of Performance of Constructed Facilities* 22, no. 3 (2008): 131-142.

Netherton, Michael D., and Stewart, Mark G. "The Effects of Explosive Blast Load Variability on Safety Hazard and Damage Risks for Monolithic Window Glazing." *International Journal of Impact Engineering* 36, no. 12 (2009): 1346-1354.

Randers-Pehrson, Glenn , and Bannister, Kenneth A. "Airblast Loading Model for Dyna2d and Dyna3d." *Army Research Laboratory* (1997).

Razaqpur, G., Mekky, W., and Foo, S. "Fundamental Concepts in Blast Resistance Evaluation of Structures." *Canadian Journal of Civil Engineering* 36, no. 8 (2009): 1292-1304.

Reid, John D. *Ls-Dyna Examples Manual* Livermore Software Technology Corporation LSTC, 1998.

Shi, Yanchao, Hao, Hong, and Li, Zhong-Xian. "Numerical Derivation of Pressure-Impulse Diagrams for Prediction of Rc Column Damage to Blast Loads." *International Journal of Impact Engineering* 35, no. 11 (2008): 1213-1227.

Strehlow, Roger A., and Baker, Wilfred E. "The Characterization and Evaluation of Accidental Explosions." *Progress in Energy and Combustion Science* 2, no. 1 (1976): 27-60.

Tolba, Ahmed Fahmy Farag. "Response of Frp-Retrofitted Reinforced Concrete Panels to Blast Loading." Carleton University, 2001.

UFC, Unified Facilities Criteria. *Structures to Resist the Effects of Accidental Explosions* United States of America: Department of Defence, 2008.

Varma, R. K., Tomar, C. P. S., Parkash, S., and Sethi, V. S. "Damage to Brick Masonry Panel Walls under Hight Explosive Detonations." *Structures Under Extreme Loading Conditions, AMSE* 351 (1997).

Voon, K. C., and Ingham, J. M. "Experimental in-Plane Shear Strength Investigation of Reinforced Concrete Masonry Walls." *Journal of Structural Engineering* 132, no. 3 (2006): 400-408.

Wang, Ming, Hao, Hong, Ding, Yang, and Li, Zhong-Xian. "Prediction of Fragment Size and Ejection Distance of Masonry Wall under Blast Load Using Homogenized Masonry Material Properties." *International Journal of Impact Engineering* 36, no. 6 (2009): 808-820.

Wei, Xueying, and Hao, Hong. "Numerical Derivation of Homogenized Dynamic Masonry Material Properties with Strain Rate Effects." *International Journal of Impact Engineering* 36, no. 3 (2009): 522-536.

Wei, Xueying, and Stewart, Mark G. "Model Validation and Parametric Study on the Blast Response of Unreinforced Brick Masonry Walls." *International Journal of Impact Engineering* 37, no. 11 (2010): 1150-1159.

Wesevich, J. W., and Oswald, C. J. "Empirical Based Concrete Masonry Pressure-Impulse Diagrams for Varying Degrees of Damage." 171, 207-207. New York, New York: ASCE, 2005.

Wilton, C., and Gabrielsen, Bernard L. *Shock Tunnel Tests of Preloaded and Arched Wall Panels*. San Mateo, California: URS Research Co., 1973.

Wu, Chengqing, and Hao, Hong. "Safe Scaled Distance for Masonry Infilled Rc Frame Structures Subjected to Airblast Loads." *Journal of Performance of Constructed Facilities* 21, no. 6 (2007): 422-431.

Wu, Chengqing, and Hao, Hong. "Numerical Derivation of Averaged Material Properties of Hollow Concrete Block Masonry." *Engineering Structures* 30, no. 3 (2008): 870-883.

Wu, Chengqing., and Hao, Hong. "Derivation of 3d Masonry Properties Using Numerical Homogenization Technique." *International Journal for Numerical Methods in Engineering* 66, no. 11 (2006): 1717-1737.

Zalosh, Robert G. *Industial Fire Protection Engineering*. West Sussex, England: Wiley, 2003.

Zucchini, A., and Lourenço, P. B. "A Coupled Homogenisation-Damage Model for Masonry Cracking." *Computers & Structures* 82, no. 11-12 (2004): 917-929.

Zucchini, A., and Lourenço, P. B. "A Micro-Mechanical Homogenisation Model for Masonry: Application to Shear Walls." *International Journal of Solids and Structures* 46, no. 3-4 (2009): 871-886.

Appendix - LS-DYNA Input Deck for the Baseline Model

```
$---+----1----+----2----+----3----+----4----+----5----+----6----+----7----+----8
$ LS-DYNA(971) DECK WAS WRITTEN BY: eta/VPG VERSION 3.4
$
$ ENGINEER:
$  PROJECT:
$    UNITS:  MM, TON,  SEC,  N
$     DATE:  Jul 13, 2011 at 12:04:40
$
$    NOTES:
$
$---+----1----+----2----+----3----+----4----+----5----+----6----+----7----+----8
$ VIEWING INFORMATION
$ -.563750E+020.105138E+04-.171663E+030.361663E+03
$ 0.100000E+010.000000E+000.000000E+00
$ 0.000000E+000.100000E+010.000000E+00
$ 0.000000E+000.000000E+000.100000E+01
$---+----1----+----2----+----3----+----4----+----5----+----6----+----7----+----8
*KEYWORD
$---+----1----+----2----+----3----+----4----+----5----+----6----+----7----+----8
*TITLE

$---+----1----+----2----+----3----+----4----+----5----+----6----+----7----+----8
*CONTROL_TERMINATION
$   endtim    endcyc     dtmin    endeng    endmas
   0.25000         0       0.0       0.0       0.0
$---+----1----+----2----+----3----+----4----+----5----+----6----+----7----+----8
*DATABASE_BINARY_D3PLOT
$  dt/cycl      lcdt      beam     npltc
  .1000E-3         0         0         0
$    ioopt
         0
$---+----1----+----2----+----3----+----4----+----5----+----6----+----7----+----8
*PART
Concrete Block
$      pid     secid       mid     eosid      hgid      grav    adpopt      tmid
         1         1         1         0         0         0         0         0
*PART
Rigid Plates
         2         2         2         0         0         0         0         0
$---+----1----+----2----+----3----+----4----+----5----+----6----+----7----+----8
*SECTION_SOLID_TITLE
Concrete Blocks
$    secid    elform       aet
         1         1         0
*SECTION_SOLID_TITLE
Rigid Plates
$    secid    elform       aet
         2         1         0
$---+----1----+----2----+----3----+----4----+----5----+----6----+----7----+----8
*MAT_ELASTIC_TITLE
CMU
$      mid        ro         e        pr        da        db
         1 .23000E-8  20000.00   0.30000       0.0       0.0
*MAT_RIGID_TITLE
Rigid plates
$      mid        ro         e        pr         n    couple         m     alias
         2 .78500E-8  200000.0   0.30000       0.0       0.0       0.0       0.0
$      cmo      con1      con2
       0.0         0         0
$       a1        a2        a3        v1        v2        v3
```

```
       0.0       0.0       0.0       0.0       0.0       0.0
$---+----1----+----2----+----3----+----4----+----5----+----6----+----7----+----8
*HOURGLASS_TITLE

$     hgid       ihq        qm       ibq        q1        q2    qb/vdc        qw
         1         1   0.10000         0     1.500   0.06000       0.0       0.0
$---+----1----+----2----+----3----+----4----+----5----+----6----+----7----+----8
*SET_NODE_LIST_TITLE
Bottom Surface
$      sid       da1       da2       da3       da4
         1
$     nid1      nid2      nid3      nid4      nid5      nid6      nid7      nid8
         1         2         3         4         5         6         7         8
         9        10        11        12        13        14        15        16
        17        18        19        20        21        22        23        24
        25        26        27        28        29        30        31        32
        33        34        35        36        37        38        39        40
        41        42        43        44        45        46        47        48
        49        50        51        52        53        54        55        56
        57        58        59        60        61        62        63        64
        65        66        67        68        69        70        71        72
        73        74        75        76        77        78        79        80
        81        82        83        84        85        86        87        88
        89        90        91        92        93        94        95        96
        97        98        99       100       101       102       103       104
       105       106       107       108       109       110       111       112
       113       114       115       116       117       118       119       120
       121       122       123       124       125       126       127       128
.
.
.
.
      6411      6412      6415      6416      6419      6420      6423      6424
      6427      6428      6431      6432      6435      6437      6439      6441
      6442      6445      6447      6449      6451      6453      6455      6457
      6459      6461      6463      6465
*SET_NODE_LIST_TITLE
Top Surface
$      sid       da1       da2       da3       da4
         2
$     nid1      nid2      nid3      nid4      nid5      nid6      nid7      nid8
     81389     81390     81391     81392     81393     81394     81395     81396
     81397     81398     81399     81400     81401     81402     81403     81404
     81405     81406     81407     81408     81409     81410     81411     81412
     81413     81414     81415     81416     81417     81418     81419     81420
     81421     81422     81423     81424     81425     81426     81427     81428
.
.
.
.

     86345     86346     86347     86348     86349     86350     86351     86352
     86353     86354     86355     86356     86357     86358     86359     86360
     86361     86362     86363     86364     86365     86366     86367     86368
     86369     86370     86371     86372
*SET_NODE_LIST_TITLE
NODE SET_21
$      sid       da1       da2       da3       da4
        21
$     nid1      nid2      nid3      nid4      nid5      nid6      nid7      nid8
```

```
         6         7         8        19        20        21        32        33
        34        94       107       119       120       121       133       146
       207       219       220       221       233      3128      3132      3133
      3136      3172      3308      3312      3313      3316      3346      3370
      3372      3374      3398      3538      3539      3570      3572      3574
      6236      6239      6240      6244      6279      6415      6416      6419
      6420      6423      6424      6451      6453      6455
*SET_NODE_LIST_TITLE
NODE SET_22
$      sid       da1       da2       da3       da4
        22
$     nid1      nid2      nid3      nid4      nid5      nid6      nid7      nid8
     81399     81400     81401     81402     81403     81404     81420     81421
     81422     81491     81492     81507     81508     81509     81521     81534
     81602     81604     81605     81606     81621     84506     84508     84509
     84510     84528     84596     84598     84599     84600     84615     84627
     84628     84629     84641     84711     84712     84727     84728     84729
     86258     86259     86260     86262     86279     86347     86348     86349
     86350     86351     86352     86365     86366     86367
$---+----1----+----2----+----3----+----4----+----5----+----6----+----7----+----8
*SET_SEGMENT_TITLE
R1
$      sid       da1       da2       da3       da4
         2
$       N1        N2        N3        N4
      2869      2882      2883      2870
      2870      2883      2884      2871
      2882      2895      2896      2883
      2883      2896      2897      2884
      2895      2908      2909      2896
.
.
.
.
      7812      7818      7819      7813
      7817      7837      7838      7818
      7818      7838      7839      7819
      7837      7850      7851      7838
      7838      7851      7852      7839
*SET_SEGMENT_TITLE
R1-1
$      sid       da1       da2       da3       da4
         3
$       N1        N2        N3        N4
      7856      7855      7854      7853
      7862      7861      7855      7856
      7855      7906      7905      7854
      7861      7909      7906      7855
      7906      7932      7931      7905
.
.
.
.
     13005     13046     13044     13004
     13008     13048     13046     13005
     13046     13072     13070     13044
     13048     13074     13072     13046
*SET_SEGMENT_TITLE
R2
$      sid       da1       da2       da3       da4
```

```
         4
$       N1        N2        N3        N4
      9365      9366      9367      9368
      9368      9367      9369      9370
      9366      9391      9392      9367
      9367      9392      9393      9369
.
.
.
.
     15663     15669     15670     15664
     15664     15670     15671     15665
     15669     15689     15690     15670
     15670     15690     15691     15671
     15689     15702     15703     15690
     15690     15703     15704     15691
*SET_SEGMENT_TITLE
R2-2
$      sid       da1       da2       da3       da4
         5
$       N1        N2        N3        N4
     15708     15707     15706     15705
     15714     15713     15707     15708
     15707     15758     15757     15706
     15713     15761     15758     15707
.
.
.
.
     22091     22103     22100     22088
     22100     22141     22139     22099
     22103     22143     22141     22100
     22141     22167     22165     22139
     22143     22169     22167     22141
*SET_SEGMENT_TITLE
R3
$      sid       da1       da2       da3       da4
         6
$       N1        N2        N3        N4
     18573     18574     18575     18576
     18576     18575     18577     18578
     18574     18599     18600     18575
.
.
.
.
     23522     23542     23543     23523
     23541     23554     23555     23542
     23542     23555     23556     23543
*SET_SEGMENT_TITLE
R3-3
$      sid       da1       da2       da3       da4
         7
$       N1        N2        N3        N4
     23560     23559     23558     23557
     23566     23565     23559     23560
.
.
.
.
```

```
     28750     28776     28774     28748
     28752     28778     28776     28750
*SET_SEGMENT_TITLE
R4
$      sid       da1       da2       da3       da4
         8
$       N1        N2        N3        N4
     25069     25070     25071     25072
     25072     25071     25073     25074
     25070     25095     25096     25071
.
.
.
.
     31374     31394     31395     31375
     31393     31406     31407     31394
     31394     31407     31408     31395
*SET_SEGMENT_TITLE
R4-4
$      sid       da1       da2       da3       da4
         9
$       N1        N2        N3        N4
     31412     31411     31410     31409
     31418     31417     31411     31412
     31411     31462     31461     31410
.
.
.
.
     37807     37847     37845     37804
     37845     37871     37869     37843
     37847     37873     37871     37845
*SET_SEGMENT_TITLE
R5
$      sid       da1       da2       da3       da4
        10
$       N1        N2        N3        N4
     34277     34278     34279     34280
     34280     34279     34281     34282
     34278     34303     34304     34279
.
.
.
.
     39225     39245     39246     39226
     39226     39246     39247     39227
     39245     39258     39259     39246
     39246     39259     39260     39247
*SET_SEGMENT_TITLE
R5-5
$      sid       da1       da2       da3       da4
        11
$       N1        N2        N3        N4
     39264     39263     39262     39261
     39270     39269     39263     39264
     39263     39314     39313     39262
.
.
.
.
```

```
     44413     44454     44452     44412
     44416     44456     44454     44413
     44454     44480     44478     44452
     44456     44482     44480     44454
*SET_SEGMENT_TITLE
R6
$      sid       da1       da2       da3       da4
        12
$       N1        N2        N3        N4
     40773     40774     40775     40776
     40776     40775     40777     40778
.
.
.
.
     47077     47097     47098     47078
     47078     47098     47099     47079
     47097     47110     47111     47098
     47098     47111     47112     47099
*SET_SEGMENT_TITLE
R6-6
$      sid       da1       da2       da3       da4
        13
$       N1        N2        N3        N4
     47116     47115     47114     47113
     47122     47121     47115     47116
     47115     47166     47165     47114
.
.
.
.
     53511     53551     53549     53508
     53549     53575     53573     53547
     53551     53577     53575     53549
*SET_SEGMENT_TITLE
R7
$      sid       da1       da2       da3       da4
        14
$       N1        N2        N3        N4
     49981     49982     49983     49984
     49984     49983     49985     49986
     49982     50007     50008     49983
.
.
.
.
     54930     54950     54951     54931
     54949     54962     54963     54950
     54950     54963     54964     54951
*SET_SEGMENT_TITLE
R7-7
$      sid       da1       da2       da3       da4
        15
$       N1        N2        N3        N4
     54968     54967     54966     54965
     54974     54973     54967     54968
     54967     55018     55017     54966
.
.
.
```

```
.
     60120     60160     60158     60117
     60158     60184     60182     60156
     60160     60186     60184     60158
*SET_SEGMENT_TITLE
R8
$      sid       da1       da2       da3       da4
        16
$       N1        N2        N3        N4
     56477     56478     56479     56480
     56480     56479     56481     56482
     56478     56503     56504     56479
.
.
.
.
     62782     62802     62803     62783
     62801     62814     62815     62802
     62802     62815     62816     62803
*SET_SEGMENT_TITLE
R8-8
$      sid       da1       da2       da3       da4
        17
$       N1        N2        N3        N4
     62820     62819     62818     62817
     62826     62825     62819     62820
.
.
.
.
     69212     69253     69251     69211
     69215     69255     69253     69212
     69253     69279     69277     69251
     69255     69281     69279     69253
*SET_SEGMENT_TITLE
R9
$      sid       da1       da2       da3       da4
        18
$       N1        N2        N3        N4
     65685     65686     65687     65688
     65688     65687     65689     65690
     65686     65711     65712     65687
.
.
.
.
     70634     70654     70655     70635
     70653     70666     70667     70654
     70654     70667     70668     70655
*SET_SEGMENT_TITLE
R9-9
$      sid       da1       da2       da3       da4
        19
$       N1        N2        N3        N4
     70672     70671     70670     70669
     70678     70677     70671     70672
     70671     70722     70721     70670
.
.
.
```

```
.
     75824     75864     75862     75821
     75862     75888     75886     75860
     75864     75890     75888     75862
*SET_SEGMENT_TITLE
R10
$      sid       da1       da2       da3       da4
        20
$       N1        N2        N3        N4
     72181     72182     72183     72184
     72184     72183     72185     72186
     72182     72207     72208     72183
.
.
.
.
     78485     78505     78506     78486
     78486     78506     78507     78487
     78505     78518     78519     78506
     78506     78519     78520     78507
*SET_SEGMENT_TITLE
R10-10
$      sid       da1       da2       da3       da4
        21
$       N1        N2        N3        N4
     78524     78523     78522     78521
     78530     78529     78523     78524
     78523     78574     78573     78522
.
.
.
.
     84919     84959     84957     84916
     84957     84983     84981     84955
     84959     84985     84983     84957
*SET_SEGMENT_TITLE
SEGMENT SET_30
$      sid       da1       da2       da3       da4
        30
$       N1        N2        N3        N4
         1        14       253       240
        14        27       266       253
        27        40       279       266
        40        46       285       279
        46        52       291       285
        52        58       297       291
        58        64       303       297
        64        70       309       303
        70        76       315       309
        76        82       321       315
        82        88       327       321
        88       101       340       327
       101       114       353       340
       114       127       366       353
.
.
.
.
     86196     86202     86328     86322
     86202     86208     86334     86328
```

```
     86208     86214     86340     86334
     86214     86234     86360     86340
*SET_SEGMENT_TITLE
CF1
$      sid       da1       da2       da3       da4
        35
$       N1        N2        N3        N4
      8079      8080      8082      8081
      8080      8083      8084      8082
      8099      8101      8102      8100
      8101      8103      8104      8102
.
.
.
.
     72053     72054     72180     72179
     72168     72169     72295     72294
     72169     72170     72296     72295
     72178     72179     72305     72304
     72179     72180     72306     72305
*SET_SEGMENT_TITLE
CF1-1
$      sid       da1       da2       da3       da4
        36
$       N1        N2        N3        N4
      9494      9491      9495      9498
      9500      9494      9498      9502
      9536      9532      9534      9538
      9540      9536      9538      9542
.
.
.
.
     74939     74936     75175     75178
     74941     74939     75178     75180
     74959     74957     75196     75198
     74961     74959     75198     75200
*SET_SEGMENT_TITLE
CF2
$      sid       da1       da2       da3       da4
        37
$       N1        N2        N3        N4
       227       228       467       466
       228       229       468       467
       237       238       477       476
.
.
.
.
     81376     81377     81616     81615
     81377     81378     81617     81616
     81386     81387     81626     81625
     81387     81388     81627     81626
*SET_SEGMENT_TITLE
CF2-2
$      sid       da1       da2       da3       da4
        38
$       N1        N2        N3        N4
      3111      3108      3112      3115
      3117      3111      3115      3119
```

```
      3153      3149      3151      3155
.
.
.
.
     84043     84041     84280     84282
     84260     84257     84496     84499
     84262     84260     84499     84501
     84280     84278     84517     84519
     84282     84280     84519     84521
*SET_SEGMENT_TITLE
CF3
$      sid       da1       da2       da3       da4
        39
$       N1        N2        N3        N4
      9943      9944      9946      9945
      9944      9947      9948      9946
      9963      9965      9966      9964
      9965      9967      9968      9966
.
.
.
.
     75162     75163     75402     75401
     75163     75164     75403     75402
     75172     75173     75412     75411
     75173     75174     75413     75412
*SET_SEGMENT_TITLE
CF3-3
$      sid       da1       da2       da3       da4
        40
$       N1        N2        N3        N4
     12601     12598     12602     12605
     12607     12601     12605     12609
     12643     12639     12641     12645
.
.
.
.
     78048     78046     78285     78287
     78066     78064     78303     78305
     78068     78066     78305     78307
*SET_SEGMENT_TITLE
CF4
$      sid       da1       da2       da3       da4
        41
$       N1        N2        N3        N4
      3560      3561      3563      3562
      3561      3564      3565      3563
      3580      3582      3583      3581
      3582      3584      3585      3583
.
.
.
.
     84484     84485     84724     84723
     84493     84494     84733     84732
     84494     84495     84734     84733
*SET_SEGMENT_TITLE
CF4-4
```

```
$      sid       da1       da2       da3       da4
        42
$       N1        N2        N3        N4
      6218      6215      6219      6222
      6224      6218      6222      6226
      6260      6256      6258      6262
      6264      6260      6262      6266
.
.
.
.
     86018     86016     86142     86144
     86020     86018     86144     86146
     86124     86121     86247     86250
     86126     86124     86250     86252
     86144     86142     86268     86270
     86146     86144     86270     86272
$---+----1----+----2----+----3----+----4----+----5----+----6----+----7----+----8
*BOUNDARY_SPC_SET_ID
$       id
         1bottom
$     nsid       cid      dofx      dofy      dofz     dofrx     dofry     dofrz
        21         0         1         1         1         0         0         0
*BOUNDARY_SPC_SET_ID
$       id
         2top
$     nsid       cid      dofx      dofy      dofz     dofrx     dofry     dofrz
        22         0         1         1         1         0         0         0
$---+----1----+----2----+----3----+----4----+----5----+----6----+----7----+----8
*CONTACT_AUTOMATIC_SURFACE_TO_SURFACE_TIEBREAK_ID
$      cid
         1ROW 1
$     ssid      msid     sstyp     mstyp    sboxid    mboxid       spr       mpr
         3         2         0         0         0         0         0         0
$       fs        fd        dc        vc       vdc    penchk        bt        dt
   0.60000   0.40000   0.35000       0.0       0.0         0       0.0 .1000E+21
$      sfs       sfm       sst       mst      sfst      sfmt       fsf       vsf
     1.000     1.000       0.0       0.0     1.000     1.000     1.000     1.000
$   option      nfls      sfls     param    eraten    erates     ct2cn
         6   0.45000   0.63000    10.100       0.0       0.0     1.000
$     soft    sofscl    lcidab    maxpar     sbopt     depth     bsort    frcfrq
         0   0.10000         0     1.025       0.0         2        10         1
$   penmax    thkopt    shlthk     snlog      isym     i2d3d    sldthk    sldstf
       0.0         0         0         0         0         0    10.000       0.0
$     igap    ignore    dprfac    dtstif     blank     blank    flangl
         1         0       0.0       0.0                           0.0
*CONTACT_AUTOMATIC_SURFACE_TO_SURFACE_TIEBREAK_ID
$      cid
         2ROW 2
$     ssid      msid     sstyp     mstyp    sboxid    mboxid       spr       mpr
         5         4         0         0         0         0         0         0
$       fs        fd        dc        vc       vdc    penchk        bt        dt
   0.60000   0.40000   0.35000       0.0       0.0         0       0.0 .1000E+21
$      sfs       sfm       sst       mst      sfst      sfmt       fsf       vsf
     1.000     1.000       0.0       0.0     1.000     1.000     1.000     1.000
$   option      nfls      sfls     param    eraten    erates     ct2cn
         6   0.45000   0.63000    10.100       0.0       0.0     1.000
$     soft    sofscl    lcidab    maxpar     sbopt     depth     bsort    frcfrq
         0   0.10000         0     1.025       0.0         2        10         1
$   penmax    thkopt    shlthk     snlog      isym     i2d3d    sldthk    sldstf
```

```
       0.0         0         0         0         0         0    10.000       0.0
$     igap    ignore    dprfac    dtstif     blank     blank    flangl
         1         0       0.0       0.0                           0.0
*CONTACT_AUTOMATIC_SURFACE_TO_SURFACE_TIEBREAK_ID
$      cid
         3ROW 3
$     ssid      msid     sstyp     mstyp    sboxid    mboxid       spr       mpr
         7         6         0         0         0         0         0         0
$       fs        fd        dc        vc       vdc    penchk        bt        dt
   0.60000   0.40000   0.35000       0.0       0.0         0       0.0 .1000E+21
$      sfs       sfm       sst       mst      sfst      sfmt       fsf       vsf
     1.000     1.000       0.0       0.0     1.000     1.000     1.000     1.000
$   option      nfls      sfls     param    eraten    erates     ct2cn
         6   0.45000   0.63000    10.100       0.0       0.0     1.000
$     soft    sofscl    lcidab    maxpar     sbopt     depth     bsort    frcfrq
         0   0.10000         0     1.025       0.0         2        10         1
$   penmax    thkopt    shlthk     snlog      isym     i2d3d    sldthk    sldstf
       0.0         0         0         0         0         0    10.000       0.0
$     igap    ignore    dprfac    dtstif     blank     blank    flangl
         1         0       0.0       0.0                           0.0
*CONTACT_AUTOMATIC_SURFACE_TO_SURFACE_TIEBREAK_ID
$      cid
         4ROW 4
$     ssid      msid     sstyp     mstyp    sboxid    mboxid       spr       mpr
         9         8         0         0         0         0         0         0
$       fs        fd        dc        vc       vdc    penchk        bt        dt
   0.60000   0.40000   0.35000       0.0       0.0         0       0.0 .1000E+21
$      sfs       sfm       sst       mst      sfst      sfmt       fsf       vsf
     1.000     1.000       0.0       0.0     1.000     1.000     1.000     1.000
$   option      nfls      sfls     param    eraten    erates     ct2cn
         6   0.45000   0.63000    10.100       0.0       0.0     1.000
$     soft    sofscl    lcidab    maxpar     sbopt     depth     bsort    frcfrq
         0   0.10000         0     1.025       0.0         2        10         1
$   penmax    thkopt    shlthk     snlog      isym     i2d3d    sldthk    sldstf
       0.0         0         0         0         0         0    10.000       0.0
$     igap    ignore    dprfac    dtstif     blank     blank    flangl
         1         0       0.0       0.0                           0.0
*CONTACT_AUTOMATIC_SURFACE_TO_SURFACE_TIEBREAK_ID
$      cid
         5ROW 5
$     ssid      msid     sstyp     mstyp    sboxid    mboxid       spr       mpr
        11        10         0         0         0         0         0         0
$       fs        fd        dc        vc       vdc    penchk        bt        dt
   0.60000   0.40000   0.35000       0.0       0.0         0       0.0 .1000E+21
$      sfs       sfm       sst       mst      sfst      sfmt       fsf       vsf
     1.000     1.000       0.0       0.0     1.000     1.000     1.000     1.000
$   option      nfls      sfls     param    eraten    erates     ct2cn
         6   0.45000   0.63000    10.100       0.0       0.0     1.000
$     soft    sofscl    lcidab    maxpar     sbopt     depth     bsort    frcfrq
         0   0.10000         0     1.025       0.0         2        10         1
$   penmax    thkopt    shlthk     snlog      isym     i2d3d    sldthk    sldstf
       0.0         0         0         0         0         0    10.000       0.0
$     igap    ignore    dprfac    dtstif     blank     blank    flangl
         1         0       0.0       0.0                           0.0
*CONTACT_AUTOMATIC_SURFACE_TO_SURFACE_TIEBREAK_ID
$      cid
         6ROW 6
$     ssid      msid     sstyp     mstyp    sboxid    mboxid       spr       mpr
        13        12         0         0         0         0         0         0
$       fs        fd        dc        vc       vdc    penchk        bt        dt
```

```
   0.60000   0.40000   0.35000       0.0       0.0         0       0.0 .1000E+21
$      sfs       sfm       sst       mst      sfst      sfmt       fsf       vsf
     1.000     1.000       0.0       0.0     1.000     1.000     1.000     1.000
$   option      nfls      sfls     param    eraten    erates     ct2cn
          6   0.45000   0.63000    10.100       0.0       0.0     1.000
$     soft    sofscl    lcidab    maxpar     sbopt     depth     bsort    frcfrq
          0   0.10000         0     1.025       0.0         2        10         1
$   penmax    thkopt    shlthk     snlog      isym     i2d3d    sldthk    sldstf
       0.0         0         0         0         0         0    10.000       0.0
$     igap    ignore    dprfac    dtstif     blank     blank    flangl
          1         0       0.0       0.0                           0.0
*CONTACT_AUTOMATIC_SURFACE_TO_SURFACE_TIEBREAK_ID
$      cid
         7ROW 7
$     ssid      msid     sstyp     mstyp    sboxid    mboxid       spr       mpr
         15        14         0         0         0         0         0         0
$       fs        fd        dc        vc       vdc    penchk        bt        dt
   0.60000   0.40000   0.35000       0.0       0.0         0       0.0 .1000E+21
$      sfs       sfm       sst       mst      sfst      sfmt       fsf       vsf
     1.000     1.000       0.0       0.0     1.000     1.000     1.000     1.000
$   option      nfls      sfls     param    eraten    erates     ct2cn
          6   0.45000   0.63000    10.100       0.0       0.0     1.000
$     soft    sofscl    lcidab    maxpar     sbopt     depth     bsort    frcfrq
          0   0.10000         0     1.025       0.0         2        10         1
$   penmax    thkopt    shlthk     snlog      isym     i2d3d    sldthk    sldstf
       0.0         0         0         0         0         0    10.000       0.0
$     igap    ignore    dprfac    dtstif     blank     blank    flangl
          1         0       0.0       0.0                           0.0
*CONTACT_AUTOMATIC_SURFACE_TO_SURFACE_TIEBREAK_ID
$      cid
         8ROW 8
$     ssid      msid     sstyp     mstyp    sboxid    mboxid       spr       mpr
         17        16         0         0         0         0         0         0
$       fs        fd        dc        vc       vdc    penchk        bt        dt
   0.60000   0.40000   0.35000       0.0       0.0         0       0.0 .1000E+21
$      sfs       sfm       sst       mst      sfst      sfmt       fsf       vsf
     1.000     1.000       0.0       0.0     1.000     1.000     1.000     1.000
$   option      nfls      sfls     param    eraten    erates     ct2cn
          6   0.45000   0.63000    10.100       0.0       0.0     1.000
$     soft    sofscl    lcidab    maxpar     sbopt     depth     bsort    frcfrq
          0   0.10000         0     1.025       0.0         2        10         1
$   penmax    thkopt    shlthk     snlog      isym     i2d3d    sldthk    sldstf
       0.0         0         0         0         0         0    10.000       0.0
$     igap    ignore    dprfac    dtstif     blank     blank    flangl
          1         0       0.0       0.0                           0.0
*CONTACT_AUTOMATIC_SURFACE_TO_SURFACE_TIEBREAK_ID
$      cid
         9ROW 9
$     ssid      msid     sstyp     mstyp    sboxid    mboxid       spr       mpr
         19        18         0         0         0         0         0         0
$       fs        fd        dc        vc       vdc    penchk        bt        dt
   0.60000   0.40000   0.35000       0.0       0.0         0       0.0 .1000E+21
$      sfs       sfm       sst       mst      sfst      sfmt       fsf       vsf
     1.000     1.000       0.0       0.0     1.000     1.000     1.000     1.000
$   option      nfls      sfls     param    eraten    erates     ct2cn
          6   0.45000   0.63000    10.100       0.0       0.0     1.000
$     soft    sofscl    lcidab    maxpar     sbopt     depth     bsort    frcfrq
          0   0.10000         0     1.025       0.0         2        10         1
$   penmax    thkopt    shlthk     snlog      isym     i2d3d    sldthk    sldstf
       0.0         0         0         0         0         0    10.000       0.0
```

```
$     igap    ignore    dprfac    dtstif     blank     blank    flangl
         1         0       0.0       0.0                         0.0
*CONTACT_AUTOMATIC_SURFACE_TO_SURFACE_TIEBREAK_ID
$      cid
        10ROW 10
$     ssid      msid     sstyp     mstyp    sboxid    mboxid       spr       mpr
        21        20         0         0         0         0         0         0
$       fs        fd        dc        vc       vdc    penchk        bt        dt
   0.60000   0.40000   0.35000       0.0       0.0         0       0.0 .1000E+21
$      sfs       sfm       sst       mst      sfst      sfmt       fsf       vsf
     1.000     1.000       0.0       0.0     1.000     1.000     1.000     1.000
$   option      nfls      sfls     param    eraten    erates     ct2cn
         6   0.45000   0.63000    10.100       0.0       0.0     1.000
$     soft    sofscl    lcidab    maxpar     sbopt     depth     bsort    frcfrq
         0   0.10000         0     1.025       0.0         2        10         1
$   penmax    thkopt    shlthk     snlog      isym     i2d3d    sldthk    sldstf
       0.0         0         0         0         0         0    10.000       0.0
$     igap    ignore    dprfac    dtstif     blank     blank    flangl
         1         0       0.0       0.0                         0.0
*CONTACT_AUTOMATIC_SURFACE_TO_SURFACE_TIEBREAK_ID
$      cid
        11COLUMN 1
$     ssid      msid     sstyp     mstyp    sboxid    mboxid       spr       mpr
        36        35         0         0         0         0         0         0
$       fs        fd        dc        vc       vdc    penchk        bt        dt
   0.60000   0.40000   0.35000       0.0       0.0         0       0.0 .1000E+21
$      sfs       sfm       sst       mst      sfst      sfmt       fsf       vsf
     1.000     1.000       0.0       0.0     1.000     1.000     1.000     1.000
$   option      nfls      sfls     param    eraten    erates     ct2cn
         6   0.45000   0.63000    10.100       0.0       0.0     1.000
$     soft    sofscl    lcidab    maxpar     sbopt     depth     bsort    frcfrq
         0   0.10000         0     1.025       0.0         2        10         1
$   penmax    thkopt    shlthk     snlog      isym     i2d3d    sldthk    sldstf
       0.0         0         0         0         0         0    10.000       0.0
$     igap    ignore    dprfac    dtstif     blank     blank    flangl
         1         0       0.0       0.0                         0.0
*CONTACT_AUTOMATIC_SURFACE_TO_SURFACE_TIEBREAK_ID
$      cid
        12COLUMN 2
$     ssid      msid     sstyp     mstyp    sboxid    mboxid       spr       mpr
        38        37         0         0         0         0         0         0
$       fs        fd        dc        vc       vdc    penchk        bt        dt
   0.60000   0.40000   0.35000       0.0       0.0         0       0.0 .1000E+21
$      sfs       sfm       sst       mst      sfst      sfmt       fsf       vsf
     1.000     1.000       0.0       0.0     1.000     1.000     1.000     1.000
$   option      nfls      sfls     param    eraten    erates     ct2cn
         6   0.45000   0.63000    10.100       0.0       0.0     1.000
$     soft    sofscl    lcidab    maxpar     sbopt     depth     bsort    frcfrq
         0   0.10000         0     1.025       0.0         2        10         1
$   penmax    thkopt    shlthk     snlog      isym     i2d3d    sldthk    sldstf
       0.0         0         0         0         0         0    10.000       0.0
$     igap    ignore    dprfac    dtstif     blank     blank    flangl
         1         0       0.0       0.0                         0.0
*CONTACT_AUTOMATIC_SURFACE_TO_SURFACE_TIEBREAK_ID
$      cid
        13COLUMN 3
$     ssid      msid     sstyp     mstyp    sboxid    mboxid       spr       mpr
        40        39         0         0         0         0         0         0
$       fs        fd        dc        vc       vdc    penchk        bt        dt
   0.60000   0.40000   0.35000       0.0       0.0         0       0.0 .1000E+21
```

```
$      sfs       sfm       sst       mst      sfst      sfmt       fsf       vsf
     1.000     1.000       0.0       0.0     1.000     1.000     1.000     1.000
$   option      nfls      sfls     param    eraten    erates     ct2cn
          6   0.45000   0.63000    10.100       0.0       0.0     1.000
$     soft    sofscl    lcidab    maxpar     sbopt     depth     bsort    frcfrq
          0   0.10000         0     1.025       0.0         2        10         1
$   penmax    thkopt    shlthk     snlog      isym     i2d3d    sldthk    sldstf
       0.0         0         0         0         0         0    10.000       0.0
$     igap    ignore    dprfac    dtstif     blank     blank    flangl
          1         0       0.0       0.0                           0.0
*CONTACT_AUTOMATIC_SURFACE_TO_SURFACE_TIEBREAK_ID
$      cid
        14COLUMN 4
$     ssid      msid     sstyp     mstyp    sboxid    mboxid       spr       mpr
        42        41         0         0         0         0         0         0
$       fs        fd        dc        vc       vdc    penchk        bt        dt
   0.60000   0.40000   0.35000       0.0       0.0         0       0.0 .1000E+21
$      sfs       sfm       sst       mst      sfst      sfmt       fsf       vsf
     1.000     1.000       0.0       0.0     1.000     1.000     1.000     1.000
$   option      nfls      sfls     param    eraten    erates     ct2cn
          6   0.45000   0.63000    10.100       0.0       0.0     1.000
$     soft    sofscl    lcidab    maxpar     sbopt     depth     bsort    frcfrq
          0   0.10000         0     1.025       0.0         2        10         1
$   penmax    thkopt    shlthk     snlog      isym     i2d3d    sldthk    sldstf
       0.0         0         0         0         0         0    10.000       0.0
$     igap    ignore    dprfac    dtstif     blank     blank    flangl
          1         0       0.0       0.0                           0.0
$---+----1----+----2----+----3----+----4----+----5----+----6----+----7----+----8
*LOAD_BLAST
$      wgt       xbo       ybo       zbo       tbo     iunit     isurf
   0.08000   497.500 -15000.00       0.0       0.0         5         1
$      cfm       cfl       cft       cfp
  2204.620   0.00328  1000.000   145.040
$---+----1----+----2----+----3----+----4----+----5----+----6----+----7----+----8
*LOAD_BODY_Z
$     lcid        sf    lciddr        xc        yc        zc       cid
         1  9810.000         0       0.0       0.0       0.0         0
$---+----1----+----2----+----3----+----4----+----5----+----6----+----7----+----8
*LOAD_SEGMENT_SET_ID
$       id
         1
$     ssid      lcid        sf        at        dt
        30        -2     1.000       0.0       0.0
$---+----1----+----2----+----3----+----4----+----5----+----6----+----7----+----8
*DEFINE_CURVE_TITLE
LCur_1_Gravity
$     lcid      sidr       sfa       sfo      offa      offo    dattyp
         1         0     1.000     1.000       0.0       0.0         0
$    abscissa (time)    ordinate (value)
    0.0000000000E+00    0.1000000000E+01
    0.1000000000E+04    0.1000000000E+01
*DEFINE_CURVE_TITLE
LCur_2
$     lcid      sidr       sfa       sfo      offa      offo    dattyp
         2         0     1.000     1.000       0.0       0.0         0
$    abscissa (time)    ordinate (value)
    0.0000000000E+00    0.0000000000E+00
    0.1000000000E+01    0.1000000000E+01
$---+----1----+----2----+----3----+----4----+----5----+----6----+----7----+----8
*NODE
```

```
$    nid               x               y               z      tc      rc
       1 0.000000000E+00 0.000000000E+00 0.000000000E+00
       2 0.000000000E+00 1.583334255E+01 0.000000000E+00
       3 0.000000000E+00 3.166667557E+01 0.000000000E+00
       4 0.000000000E+00 4.750000763E+01 0.000000000E+00
       5 0.000000000E+00 6.333333969E+01 0.000000000E+00
       6 0.000000000E+00 7.916667175E+01 0.000000000E+00
       7 0.000000000E+00 9.500000763E+01 0.000000000E+00
       8 0.000000000E+00 1.108333435E+02 0.000000000E+00
       9 0.000000000E+00 1.266666794E+02 0.000000000E+00
      10 0.000000000E+00 1.425000153E+02 0.000000000E+00
      11 0.000000000E+00 1.583333435E+02 0.000000000E+00
      12 0.000000000E+00 1.741666718E+02 0.000000000E+00
      13 0.000000000E+00 1.900000000E+02 0.000000000E+00
      14 1.500000000E+01 0.000000000E+00 0.000000000E+00
      15 1.500000095E+01 1.583334255E+01 0.000000000E+00
.
.
.
.
   94912 9.647143555E+02 2.200000000E+02 2.190000000E+03
   94913 9.797852783E+02 1.900000000E+02 2.190000000E+03
   94914 9.797855225E+02 2.050000000E+02 2.190000000E+03
   94915 9.797857666E+02 2.200000000E+02 2.190000000E+03
   94916 9.948566895E+02 1.900000000E+02 2.190000000E+03
   94917 9.948569336E+02 2.050000000E+02 2.190000000E+03
   94918 9.948571777E+02 2.200000000E+02 2.190000000E+03
   94919 1.009928162E+03 1.900000000E+02 2.190000000E+03
   94920 1.009928345E+03 2.049999847E+02 2.190000000E+03
   94921 1.009928589E+03 2.200000000E+02 2.190000000E+03
   94922 1.025000000E+03 1.900000000E+02 2.190000000E+03
   94923 1.025000000E+03 2.050000000E+02 2.190000000E+03
   94924 1.025000000E+03 2.200000000E+02 2.190000000E+03
$---+----1----+----2----+----3----+----4----+----5----+----6----+----7----+----8
*ELEMENT_SOLID
$    eid     pid      n1      n2      n3      n4      n5      n6      n7      n8
       1       1       1      14      15       2     240     253     254     241
       2       1       2      15      16       3     241     254     255     242
       3       1       3      16      17       4     242     255     256     243
       4       1       4      17      18       5     243     256     257     244
       5       1       5      18      19       6     244     257     258     245
       6       1       6      19      20       7     245     258     259     246
       7       1       7      20      21       8     246     259     260     247
       8       1       8      21      22       9     247     260     261     248
       9       1       9      22      23      10     248     261     262     249
      10       1      10      23      24      11     249     262     263     250
      11       1      11      24      25      12     250     263     264     251
      12       1      12      25      26      13     251     264     265     252
      13       1      14      27      28      15     253     266     267     254
      14       1      15      28      29      16     254     267     268     255
      15       1      16      29      30      17     255     268     269     256
.
.
.
.
   60467       2   94666   94672   94673   94667   94901   94904   94905   94902
   60468       2   94667   94673   94675   94669   94902   94905   94906   94903
   60469       2   94672   94678   94679   94673   94904   94907   94908   94905
   60470       2   94673   94679   94681   94675   94905   94908   94909   94906
   60471       2   94678   94684   94685   94679   94907   94910   94911   94908
```

```
   60472       2   94679   94685   94687   94681   94908   94911   94912   94909
   60473       2   94684   94690   94691   94685   94910   94913   94914   94911
   60474       2   94685   94691   94693   94687   94911   94914   94915   94912
   60475       2   94690   94696   94697   94691   94913   94916   94917   94914
   60476       2   94691   94697   94699   94693   94914   94917   94918   94915
   60477       2   94696   94702   94703   94697   94916   94919   94920   94917
   60478       2   94697   94703   94705   94699   94917   94920   94921   94918
   60479       2   94702   94708   94709   94703   94919   94922   94923   94920
   60480       2   94703   94709   94711   94705   94920   94923   94924   94921
$---+----1----+----2----+----3----+----4----+----5----+----6----+----7----+----8
*END
```